Melt-Rock Interaction and Refertilization of Oceanic Lithosphere – a Highly Siderophile Element and Os Isotope Study, Totalp Massif, Switzerland

David van Acken

Freie Universität Berlin

Dissertation zur Erlangung des akademischen Grades
Doktor der Naturwissenschaften
- Dr. rer. nat. -
eingereicht im Fachbereich Geowissenschaften
an der Freien Universität Berlin

Berlin, im November 2008

Hiermit versichere ich, daß ich die vorliegende Arbeit selbständig verfaßt und keine anderen als die angegebenen Hilfsmittel benutzt habe. Die Stellen der Arbeit, die anderen Werken wörtlich oder inhaltlich entnommen sind, wurden durch entsprechende Angaben der Quellen kenntlich gemacht.

Diese Arbeit hat in gleicher oder ähnlicher Form noch keiner Prüfungsbehörde vorgelegen

David van Acken, Berlin, den 27.11.2008

Vortrag und Disputation am 27.01.2009

Gutachter:

1. Prof. Dr. H. Becker, Freie Universität Berlin
   Institut für Geologische Wissenschaften
   AB Geochemie
   Malteserstr. 74 – 100, Haus B
   12249 Berlin, Germany

2. Prof. R. J. Walker, PhD
   Department of Geology
   University of Maryland
   College Park, Maryland 20742, USA

Contents

List of Figures and Tables

Figures

Tables

Chapter 1

Preface

1.1 Structure of the Thesis

The thesis comprises three parts: (1) A general outline of the scientific framework of the thesis, including a brief introduction into HSE geochemistry and melt-rock interaction in the mantle; (2) Three scientific manuscripts documenting and discussing the work that has been undertaken; (3) A concluding chapter summarizing the principal outcome of the study and giving a brief outlook. In order to condense the thesis, sections covering geological setting, sample descriptions and methods were cut from each manuscript and attached as appendices along with two overview tables reporting measured and volatile-content corrected major element data.

1.2 Scientific manuscripts

The main part of this thesis is formed by three scientific papers. The first paper is published; the other two are to be submitted in international, peer-reviewed scientific journals. Each author's contribution to the individual manuscript will be outlined in the following section. All manuscripts were based on a proposal (NSF grant EAR 0309810) by H. Becker and R.J. Walker, who provided the basic ideas for the research carried out. Samples were collected by H. Becker.

Chapter 3: Formation of pyroxenite layers in the Totalp ultramafic massif (Swiss Alps) – insights from highly siderophile elements and Os isotopes, by D. van Acken, H. Becker, R.J. Walker, W.F. McDonough, F. Wombacher, R.D. Ash and P.M. Piccoli. D. van Acken, H. Becker and F. Wombacher are affiliated with the Freie Universität Berlin; R.J. Walker, W.F.

McDonough, R.D. Ash and P.M. Piccoli are affiliated with the University of Maryland. This manuscript is intended to be submitted, in slightly modified form, to Geochimica et Cosmochimica Acta. D. van Acken, H. Becker and F. Wombacher were responsible for data collection at the Freie Universität Berlin. R.J. Walker provided laboratory assistance during stays of D. van Acken at the University of Maryland for TIMS measurements. W.F. McDonough and R.D. Ash provided laboratory assistance during stays of D. van Acken at the University of Maryland for ICP-MS and LA-ICP-MS measurements. P.M. Piccoli provided laboratory assistance during stays of D. van Acken at the University of Maryland for electron microprobe measurements. D. van Acken wrote preliminary and final versions of the manuscript. H. Becker, R.J. Walker, W.F. McDonough and F. Wombacher contributed to discussions on the topics and edited and improved readability, focus and clarity of the manuscript. The chapter focuses on websterite and pyroxenite formation via melt-rock interaction and possible melt sources within the mantle, and deals with the issue of possible presence of pyroxenite layers in plume-related basalt melt sources to account for observed ^{186}Os-^{187}Os systematics.

Chapter 4: Refertilization of Jurassic oceanic peridotites from the Tethys Ocean – implications for the Re-Os systematics of the upper mantle, by D. van Acken, H. Becker and R.J. Walker. D. van Acken and H. Becker are affiliated with the Freie Universität Berlin; R.J. Walker is affiliated with the University of Maryland, Department of Geology. Additionally, D. van Acken is listed as affiliated with the University of Maryland for all three manuscripts to give proper credit to UMD for the laboratory work done there during his two stays in 2005 and 2006. The manuscript was published in Earth and Planetary Science Letters (2008; Vol. 268, pp. 171 – 181).

D. van Acken and H. Becker were responsible for scientific content, sample preparation and data collection. Preliminary versions of the manuscript written by D. van Acken were improved in respect to focus, clarity and readability in discussion with H. Becker and R.J. Walker. Furthermore, R.J. Walker provided laboratory assistance during stays of D. van Acken at the University of Maryland. The paper focuses on the influence of refertilization on the Re-Os isotopic system in oceanic upper mantle peridotites. Throughout the thesis, this chapter will be referenced as van Acken et al. (2008)

Chapter 5: The influence of refertilization on abundances of highly siderophile elements in peridotites - a case study from the Totalp ultramafic body, eastern Swiss Alps, by D. van Acken, H. Becker, R.J. Walker and F. Wombacher. D. van Acken, H. Becker and F. Wombacher are affiliated with the Freie Universität Berlin; R.J. Walker is affiliated with the University of Maryland. This manuscript is intended to be submitted in a revised form to Geochimica et Cosmochimica Acta. D. van Acken, H. Becker and F. Wombacher were responsible for data collection at the Freie Universität Berlin. R.J. Walker provided laboratory assistance during stays of D. van Acken at the University of Maryland. Preliminary versions of this manuscript were written by D. van Acken. H. Becker, R.J. Walker and F. Wombacher contributed to discussion and improved focus and clarity. This chapter focuses on HSE distribution between melt and residual peridotite and possible mechanisms of refertilization.

Chapter 2

Introduction

2.1 Abstract

Mantle peridotites have long been interpreted as residues of partial melting and extraction of basaltic melt. Over the past decades, evidence has accumulated for refertilization of depleted peridotites by interaction with migrating mafic melt. In order to study fundamental processes relevant for the understanding of melt transport, element fluxes and recycling in the suboceanic mantle, a detailed highly siderophile element (HSE; Os, Ir, Ru, Pt, Pd and Re) and Re-Os isotope study was conducted on lherzolites and associated pyroxenite layers from the Jurassic oceanic Totalp ultramafic massif, eastern Switzerland.

The present thesis presents evidence for significant HSE fractionation and redistribution during melt-rock interaction near the asthenosphere-lithosphere boundary in the convecting upper mantle. Earlier episodes of partial melting and melt depletion as well as late accretion or core-mantle interaction are overprinted and effectively obscured during refertilization. Totalp pyroxenite layers, which are interpreted as cumulates from migrating mafic melt, have high Pt, Pd and Re concentrations coupled with highly radiogenic $^{187}Os/^{188}Os$. Suprachondritic Pt/Ir, Pd/Ir and Re/Os in pyroxenites likely reflect the highly fractionated HSE signature of the melt. Coprecipitation of sulfides along cumulate precipitation of pyroxenes in an open system, with limited or no contribution from host peridotite is a suitable explanation for observed HSE signatures in Totalp pyroxenites.

Radiogenic initial $^{187}Os/^{188}Os$ in pyroxenites indicates a melt source with a long-term enrichment in Re/Os. Recycled oceanic crust present as tectonically emplaced eclogite slivers not equilibrated with their host peridotite within a 'marble-cake mantle' as melt source is consistent with the data presented.

Composite pyroxenite – peridotite samples show textural evidence of material transport from websteritic layers into associated lherzolite by pyroxene-rich veins, indicating possible imprint of melt signatures onto peridotite host rocks. Totalp fertile lherzolites show chondritic to suprachondritic Pt/Ir, Pd/Ir and Re/Os, along with subchondritic to slightly suprachondritic $^{187}Os/^{188}Os$. These signatures are inconsistent with an origin as simple melt residues or mixtures between melt and wall rock, but may be explained by addition of melt-derived sulfide to refertilized Totalp lherzolites during melt-rock interaction, resulting in preferential addition of incompatible HSE (Pt, Pd and Re) over compatible HSE (Os, Ir and Ru). Totalp lherzolites can thus be considered refertilization products influenced by smaller amounts of melt, while pyroxenites represent melt-dominated systems.

Because of their lower liquidus, pyroxenite layers contribute extensively to melt generation from a layered peridotite-pyroxenite mantle and thus contribute extensively to oceanic basaltic volcanism. Fractionated HSE and radiogenic Os isotope signatures from oceanic basalts may be understood as pyroxenite-derived signatures. Pyroxenite layers in the lower oceanic lithosphere constitute a high-Re reservoir in the convecting mantle, thus accounting for 'missing' Re estimated by mass balance calculations. Furthermore, suggestions of pyroxenites as the source for high ^{186}Os-^{187}Os signatures observed in plume-related basalts, as opposed to core-mantle interaction, is not supported, as Totalp pyroxenites contain too little Os and have too low Pt/Re to account for observed radiogenic $^{186}Os/^{188}Os$ signatures.

2.2. Kurzfassung

Mantelperidotite wurden lange als Residuen von partieller Aufschmelzung und Schmelzextraktion betrachtet. In den letzten Jahren mehren sich Hinweise auf Refertilisierung verarmter Peridotite durch Interaktion mit mafischem Magma. Peridotite und Pyroxenite aus dem jurassichen Totalpmassiv (Graubünden) wurden im Rahmen dieser Studie auf hochsiderophile Spurenelemente (HSE) und Os-Isotopie analysiert, um besseres Verständnis für Magmentransport, Elementflüsse und Recycling ozeanischer Kruste in der tieferen ozeanischen Lithosphäre zu erlangen.

Die vorliegende Arbeit zeigt signifikante Fraktionierung und Umverteilung von HSE nahe des Lithosphären-Asthenosphärenübergangs im konvektierenden Mantel. In Peridotiten können durch Refertilisierung geochemische Signaturen früherer Aufschmelzung und Schmelzextraktion, Akkretion und Kern-Mantel-Interaktion bis zur Unkenntlichkeit überlagert werden.

Pyroxenitlagen im Totalpmassiv, die als Pyroxenkumulate von migrierenden Schmelzen interpretiert werden, weisen hohe Konzentrationen von Pt, Pd und Re auf, zusammen mit extrem radiogenem $^{187}Os/^{188}Os$. Suprachondritisches Pt/Ir, Pd/Ir, Re/Os and $^{187}Os/^{188}Os$ reflektieren die fraktionierte HSE-Signatur der Schmelze. Präzipitation von Sulfiden während der Bildung von Pyroxenkumulaten in einem offenen System mit geringer Interaktion mit Peridotit kann die beobachteten HSE-Signaturen erzeugen.

Radiogenes $^{187}Os/^{188}Os$ in den Pyroxeniten deutet auf eine Magmenquelle mit hohem Re/Os und langer Isolationszeit im Mantel. Subduzierte ozeanische Kruste, die nicht equilibriert in Form von Eklogitlinsen in einem 'marble-cake mantle' vorliegt, stellt eine solche potentielle Magmenquelle dar.

Mit Websteritlagen assoziierte Peridotite weisen Anzeichen von Schmelztransport durch pyroxenitreiche Adern in Peridotit hinein auf. Die stark fraktionierte HSE-Signatur der Schmelze, angereichert an Pt, Pd, Re und radiogenem $^{187}Os/^{188}Os$ wurde dabei teilweise auf den Peridotit übertragen, erkennbar an chondritischen bis suprachondritischen Verhältnissen von Pt/Ir, Pd/Ir und Re/Os in Lherzoliten, verbunden mit sub- bis suprachondritische $^{187}Os/^{188}Os$. Diese Signaturen sind nicht durch einfache Schmelzextraktion oder Mischung

von Schmelze und Peridotit zu erklären, weisen aber auf erhebliche Umverteilung von HSE durch Refertilisierung hin. Inkompatible HSE (Pt, Pd, Re) werden dabei im Vergleich zu kompatiblen HSE (Os, Ir, Ru) angereichert. Lherzolite können folglich im Zuge von Interaktion von verarmtem Peridotit mit relativ geringen Mengen an Schmelze entstehen, während Pyroxenite schmelzdominierte Systeme dastellen.

Die Anwesenheit von Pyroxenitlagen in der tiefen ozeanischen Lithosphäre zieht eine Reihe von Implikationen für Basaltgenese und HSE-Verteilung im Mantel nach sich. Aufgrund ihrer niedrigeren Liquidustemperatur tragen Pyroxenite überproportional zur Schmelzbildung aus einer Peridotit-Pyroxenit-Mantelquelle bei. Fraktionierte HSE-Muster und radiogene Os-Isotopie in Basalten können als Signatur von Pyroxenit in der Magmenquelle interpretiert werden. Pyroxenite stellen weiterhin ein Re-reiches Reservoir dar, in dem ein Teil des 'fehlenden' Re enthalten sein könnte. Vermutungen, daß Pyroxenite (als Alternative zu Kern-Mantle-Interaktion) Ursache der radiogenen $^{186}Os/^{187}Os$-Signatur von 'plume'-assoziierten Basalten sind, können nicht bestätigt werden.

2.3 Introduction and Scientific Framework

The following section aims to provide an introduction into the main subjects covered by this thesis. The scientific framework of lherzolite and pyroxenite formation is briefly discussed along with some elementary aspects of highly siderophile element (HSE) geochemistry.

Mantle peridotites are widely considered residues of partial melting, whereas basalts are interpreted as their complementary partial melts (e.g. Johnson et al., 1990; Johnson and Dick, 1992; Kinzler and Grove, 1992; Kinzler, 1997). Lherzolites represent residues of small degrees of melting, while harzburgites have experienced larger degrees of melt extraction. However, evidence is accumulating that such a simple melt-residue relationship is not the entire story, and that episodes of partial mantle melting are succeeded by melt-rock interaction events, which may significantly affect not only trace element and isotopic compositions, but also the modal mineralogy and thus major elements.

Based on elevated Na concentrations in abyssal peridotites, Elthon (1992) suggested 'refertilization' of depleted harzburgitic mantle by addition of basaltic melt after episodes of partial melting and melt extraction. A considerable number of studies from other continental and oceanic localities suggest addition of basaltic components in terms of minerals modes or trace elements to depleted peridotite to explain geochemical peridotite signatures (e.g. Menzies et al., 1985; Kelemen, 1990; Cannat et al., 1990; Godard et al., 1995; Takazawa et al., 1996; Rampone et al., 1997; 2004; Baker and Beckett, 1999; Lenoir et al., 2000; Beccaluva et al., 2001; 2004; Dawson, 2002; Ionov et al., 2002; Santos et al., 2002; Hellebrand and Snow, 2003; Bodinier et al., 2004; Beyer et al., 2006; Piccardo et al., 2007). Recently, Le Roux et al. (2007) showed that lherzolites from the type locality, the Lherz ultramafic massif must have formed from harzburgites by interaction with asthenospheric melts.

Interaction of mantle peridotites with infiltrated melt may produce a variety of outcomes, dependent on pressure, melt composition and melt/rock ratio. Dunites, harzburgites or refractory spinel peridotites may be formed by reactive porous melt flow and precipitation of

olivine and orthopyroxene at the expense of clinopyroxene (Kelemen et al., 1992; 1997; Niu, 1997; Asimov, 1999; Rampone et al., 2004; 2005; Rampone and Borghini, 2008). Refertilization sensu stricto occurs by infiltration and solidification of melt in the lithosphere at lower melt/rock ratios, and results in 'fertile' or 'modally metasomatized' lherzolites (e.g. Nicolas and Dupuy, 1984; Bodinier et al., 1988; Takazawa et al., 1992; Rampone et al., 1994; 1997; Van der Wal and Bodinier, 1996; Saal et al., 2001; Lenoir et al., 2001; Bodinier and Godard, 2003; Rampone and Borghini, 2008). 'Modal' mantle metasomatism occurs by precipitation of new minerals, mostly pyroxene, amphibole and aluminous phases, from infiltrating melt (Bodinier and Godard, 2003, and references therein). In contrast, 'cryptic metasomatism' refers to incompatible trace element enrichment without visible modal changes in mineralogy (Bodinier et al., 1990; 2004; Woodland et al., 1996). The range of geochemical signatures exhibited by peridotites affected by interaction with melt is, understandably, diverse (Bodinier and Godard, 2003).

Lherzolites from ultramafic massifs, among abyssal peridotites and mantle xenoliths, have been used to constrain compositional models of the primitive mantle and early Earth processes. Some early studies have assumed fertile lherzolites to represent pristine mantle, having undergone little or no melt extraction and thus potentially preserving geochemical signatures such as core formation, core-mantle interaction or late accretion. As many studies on peridotites suggest, lherzolites from both oceanic and continental lithosphere may not represent pristine mantle, but rather the product of episodes of melt depletion and melt-rock interaction.

In order to study mantle composition and development, scales and preservation of mantle heterogeneities, late accretion or core-mantle exchange processes with lherzolite samples, the extent of secondary overprint by later episodes of melt-rock interaction needs to be understood. A pivotal role for the understanding of melt-rock interaction processes may be played by pyroxenite layers, which are estimated to comprise 1-5% of ultramafic massifs. Pyroxenites have been studied in orogenic and ophiolitic ultramafic massifs worldwide (e.g. Kornprobst, 1969; Suen and Frey, 1987; Bodinier et al., 1987; 1990; 2008; Kornprobst et al., 1990; Shervais and Mukasa, 1991; Becker 1996a; Fabriès et al., 1998; Henry et al., 1998; Garrido and Bodinier, 1999; Garrido et al., 2000; Pearson and Nowell, 2004; Becker et al.,

2004; Luguet et al., 2008), as well as in xenoliths derived from the subcontinental lithospheric mantle (SCLM; e.g. Irving, 1974; Witt-Eickschen et al., 1993; 1998; 2003; Vaselli et al., 1995) and, rarely, in abyssal peridotites (e.g. Dantas et al., 2007).

The origin of pyroxenite layers is still subject to debate. In the 'marble-cake mantle' model suggested by Allègre and coworkers (Polvé and Allègre, 1980; Loubet and Allègre, 1982; Allègre and Turcotte, 1986), pyroxenite layers represent thinned and stretched recycled oceanic crust or its melting residue (Loubet and Allègre, 1982; Blichert-Toft et al., 1999). The majority of studies interpret pyroxenite layers as high-pressure crystal precipitates in former magma conduits (e.g. Bodinier et al., 1987; Pearson et al., 1993; Rivalenti et al., 1995; Garrido and Bodinier, 1999; Takazawa et al., 1999). Pyroxenites thus represent zones of high melt/rock ratios, and may be uniquely suited to study the melts that interact with mantle peridotite.

As peridotite massifs may have contributed to the formation of basalts erupted in the past, preferential melting of pyroxenite layers at high pressures may cause distinct isotopic and trace element signatures in erupted basalts (e.g. Hirschmann and Stolper, 1996; Lassiter and Hauri, 1998; Lassiter et al., 2000; Ito and Mahoney, 2005; Sobolev et al., 2005). A combined study of petrography, major element, trace element and isotopic composition of mafic layers in association with host mantle peridotite may provide information on the scale of mantle heterogeneities, element fluxes in the mantle and during recycling of oceanic crust and the nature of various basalt source regions.

Highly siderophile elements (HSE) have gained importance as geochemical tracers with the advent of improved analytical methods. This group of elements comprises Ru, Rh, Pd, Re, Os, Ir, Pt and Au. Because of their siderophile and chalcophile affinity (Chou, 1978; Mitchell and Keays, 1981; Morgan and Baedeker, 1983; Morgan, 1986; Peach et al., 1990; Fleet et al., 1991; 1996; Bezmen et al., 1994; Sattari et al., 2002), the HSE have emerged as a powerful geochemical tool for the study of metal-silicate, sulfide-silicate and solid metal-liquid metal partitioning processes. During core formation, HSE are supposed to have quantitatively been extracted into the metal core because of metal/silicate partition coefficients > 10000 (e.g. O'Neill et al., 1995). Analyses of mantle rocks show that all HSE are overabundant in the

silicate mantle by a factor of ~ 100 compared to estimates from metal/silicate partitioning of a chondritic Earth and are present in approximately chondritic proportions. This has led to a number of suggestions about the control of the HSE budget of the mantle. Among the processes brought forth are inefficient formation of the core and retention and subsequent oxidation of metal droplets in the mantle (Jones and Drake, 1986) or core-mantle interaction (e.g. Brandon et al., 1996; Snow and Schmidt, 1998). Lower metal/silicate partition coefficients at high pressures have been suggested by several studies (Murthy, 1991; Righter and Drake, 1997; Murthy and Karato, 1997). The model currently favored is that of a chondritic 'late veneer' of late meteoritic influx making up <0.5 % of the Earth's final mass. This model serves to explain both the approximately chondritic relative HSE concentrations and their apparent overabundance in the mantle in respect to metal-silicate partitioning during core formation (e.g. Kimura et al., 1974; Chou, 1978; Morgan, 1986; Holzheid et al., 2000; Righter et al., 2000; Morgan et al., 2001).

Based on their abundances in basalt and in residual peridotites, Os, Ir, Ru, Rh, Pt and Pd are considered compatible, while Re and Au are incompatible (Morgan and Lovering, 1967, Hertogen et al., 1980, Barnes et al., 1985; Morgan et al., 1981; Morgan, 1986). Despite these abundance differences in crustal and mantle rocks pointing at large HSE fractionation during partial mantle melting, detailed HSE partitioning behaviour between mantle phases is not well understood; and may be controlled by complex interplay of sulfide solid – sulfide melt – silicate melt – silicate minerals (olivine, pyroxene, spinel, garnet) – metal phase equilibria (Peach et al., 1990; Righter et al., 2000; 2004; Walter et al., 2000; Ballhaus et al., 2001; 2006; Bockrath et al., 2004; Mallmann and O'Neill, 2007).

The HSE include the long-lived ^{187}Re – ^{187}Os and ^{190}Pt – ^{186}Os isotope systems (^{190}Pt, 0.0129% relative abundance, $\lambda = 1.542 \times 10^{-12} a^{-1}$; ^{187}Re, 62.60% relative abundance, $\lambda = 1.6668 \times 10^{-11} a^{-1}$; Begemann et al., 2001; Selby et al., 2007). In contrast to lithophile isotope systems like Rb-Sr and Sm-Nd, where both element pairs are lithophile and incompatible during mantle melting, the Re-Os system consists of a moderately incompatible mother element and a compatible daughter element, which may lead to rapid ingrowth of radiogenic ^{187}Os over comparatively short periods of time. The Re-Os isotope system has been used to date melt extraction in lithospheric peridotites, either by model ages (τ_{RD} and τ_{MA}, for

definition see Shirey and Walker, 1998) or aluminochron methods, wherein Al is used as a proxy for similarly incompatible Re (Reisberg and Lorand, 1995). Apparent Re-Os model ages and HSE abundances, however, may be influenced by secondary processes in the mantle.

Redistribution of HSE during melt-rock interaction within the mantle is not well understood. Early studies considered the HSE little susceptible to redistribution during melt-interaction (e.g. Gueddari et al., 1996; Handler and Bennett, 1999). More recent studies however, noted considerable redistribution of HSE during melt-rock interaction. Addition of melt-derived sulfides bearing fractionated HSE signatures to peridotite wall rock was suggested by multiple studies (Lorand et al., 1993; 2003; Rehkämper et al., 1999a; Alard et al., 2000; Lorand and Alard, 2001; Schmidt et al., 2003; Luguet et al., 2003; 2004; Pearson et al., 2004; Pearson and Nowell, 2004). This may occur by coprecipitation of sulfides during pyroxene crystallization, either as cumulates or melt-rock reaction products at the expense of olivine, at low melt/rock ratios in an open system of melt channels or during porous flow (e.g. Rehkämper et al., 1999a; Alard et al., 2000; Lorand and Alard, 2001; Luguet et al., 2003; Lorand et al., 2003; Pearson and Nowell, 2004). Other studies suggested segregation of dense sulfide melts from upwelling asthenospheric silicate melt followed by downward percolation, resulting in sulfide addition to peridotites near the asthenosphere-lithosphere boundary (Lorand et al., 1993). At high melt/rock ratios, formation of replacive dunites and harzburgites is accompanied by dissolution of sulfides from peridotite wall rock in sulfide undersaturated melt and removal of HSE from peridotite wall rock (Lorand and Alard, 2001; Becker et al., 2001; Büchl et al., 2002; 2004; Reisberg et al., 2005).

Redistribution of Re and Os in peridotites may influence Os isotopic composition, and, by inference, Re-Os model ages. Addition of Re results in young or even future model ages (Shirey and Walker, 1998). Although the majority of fertile lherzolites bear chondritic or nearly chondritic HSE signatures, partial melting removes HSE, leading to non-chondritic compositions. Addition of HSE during melt-rock interaction may also be expressed by non-chondritic HSE ratios (e.g. Pattou et al., 1996; Rehkämper et al., 1999a; Lorand et al., 1999). In order use fertile lherzolites to gain a better understanding of the HSE budget of the mantle and HSE fluxes within the mantle and between mantle and crust, redistribution of HSE and

possible disturbances of the Re-Os isotope system during melt-rock interaction need to be better constrained.

The Re-Os and Pt-Os decay systems are at the center of a current debate about core-mantle interaction. Coupled suprachondritic $^{186}Os/^{188}Os$ – $^{187}Os/^{188}Os$ in Hawaiian and Siberian basalts supposedly related to mantle plumes were interpreted as the result of mixing of small amounts of outer core material into upwelling mantle plumes at the core-mantle boundary (Brandon et al., 1996; 1998; 1999; 2003; 2006; 2007; Brandon and Walker, 2005). Other geochemical and geophysical studies are difficult to reconcile with significant core-mantle interaction, showing that some specific conditions have to be met (Scherstén et al., 2003; Smith, 2003; Carlson, 2005; Lassiter, 2006; Van Orman et al., 2008). An alternative explanation for these Os isotopic data has been proposed via mixing of sulfide derived from pyroxenites or eclogites derived from subduction of oceanic crust with depleted mantle (Luguet et al., 2008), reducing the need of core contribution to radiogenic Os isotope signatures in basalts.

The manuscripts comprising this thesis deal with various aspects of HSE geochemistry and melt-rock interaction in the deep oceanic lithosphere as represented by the Jurassic Totalp ultramafic massif. The Totalp massif in eastern Switzerland represents a deep section of oceanic lithosphere, with final equilibration conditions in the spinel lherzolite facies followed by rapid uplift prior to emplacement on the Jurassic Piedmont-Liguria ocean floor. The presence of pyroxenite layers in the Totalp massif, which are mostly absent from abyssal peridotites, and petrographic indicators of melt-rock interaction suggests that refertilization processes may be significant in the lower oceanic lithosphere as well. The Totalp massif may thus provide the scarce opportunity to study mantle refertilization processes in deeper sections of oceanic lithosphere not sampled by abyssal peridotites.

Chapter 3 studies pyroxenite formation, HSE fractionation during partial melting, potential sources for mafic melts as refertilizing agents and pyroxenites in the source of oceanic basalts as an explanation for high ^{186}Os-^{187}Os signatures of plume-related basalts. Chapters 4 and 5 focus on the distribution of HSE and Os isotopic systematics in lherzolites affected by melt-rock interaction. Chapter 4 emphasizes the impact of melt-rock interaction on the Re-Os

isotopic systematics of lherzolites by addition of Re and radiogenic Os to peridotite wall rock. Chapter 5 deals with behaviour of HSE during fertile lherzolite melting and HSE addition to depleted peridotite by cumulate precipitation of sulfides. Chapter 6 summarizes the main conclusions and gives a brief outlook. Geological setting, sample descriptions and methods are described in the appendix chapter 7 and 8.

Chapter 3

Formation of pyroxenite layers in the Totalp ultramafic massif (Swiss Alps) – insights from highly siderophile elements and Os isotopes

David van Acken[a,b,*], Harry Becker[a], Richard J. Walker[b], William F. McDonough[b], Frank Wombacher[a], Richard D. Ash[b], Phil M. Piccoli[b]

a) Institut für Geologische Wissenschaften, AB Geochemie, Freie Universität Berlin, Malteserstr. 74 – 100, Haus B, D-12249 Berlin, Germany, Phone: +49 30 838 70200 Fax: +49 30 838 70170

b) University of Maryland, Department of Geology, College Park, Maryland 20742, USA

*Corresponding author

E-mail addresses: dvana@zedat.fu-berlin.de (D. van Acken), hbecker@zedat.fu-berlin.de (H. Becker), rjwalker@geol.umd.edu (R.J. Walker), fwo@zedat.fu-berlin.de (F. Wombacher), mcdonoug@geol.umd.edu (W.F. McDonough), rdash@geol.umd.edu (R.D. Ash), piccoli@geol.umd.edu (P.M. Piccoli)

3.1 Abstract

Understanding the formation of mantle pyroxenites is crucial to assessing their role in the genesis of mantle-derived melts, as well as the chemical and isotopic evolution of the mantle. In this work, the role of spinel and spinel-garnet pyroxenites in refertilization of a Jurassic spinel lherzolite body (Totalp, eastern Switzerland) is examined via major element and highly siderophile element (HSE; Ru, Pd, Re, Os, Ir, Pt) abundances, and $^{187}Os/^{188}Os$ data.

Aluminum-poor pyroxenites (websterites) tend to have chondritic to suprachondritic initial γ_{Os} (160 Ma) of -1.7 to +27.4, Os/Ir and Ru/Ir similar to mantle lherzolites, and suprachondritic Pt/Ir, Pd/Ir and Re/Ir. Aluminum-rich pyroxenites (clinopyroxenites) have highly radiogenic $^{187}Os/^{188}Os$ with initial γ_{Os} (160 Ma) of up to +1700, and are depleted in Os, Ir and Ru, while showing moderate to strong enrichments in Pt, Pd and Re, relative to associated peridotites, resulting in extremely high Pd/Ir (46 x CI chondrite) and Re/Ir (250 x CI chondrite).

In situ analyses of pentlandites and godlevskites from two websterites by laser ablation ICP-MS reveal highly variable Ru, Pd and Re on the thin section scale, possibly reflecting formation during multiple events of melt-rock interaction and sulfide precipitation. Uniformity in the major element compositions of sulfides contrasts with major HSE heterogeneities within and among individual samples. However, within the overall suite, bulk compositions are in broad accordance with average sulfide compositions for Os/Ir, Pd/Ir and Re/Ir, but significantly lower for Ru/Ir. The compositional heterogeneity of HSE within sulfides, combined with extreme HSE composition variations among sulfides precludes meaningful mass balance calculations.

Our new data indicate the presence of mafic components in the exposed lower lithosphere associated with a Jurassic, oceanic slow-spreading environment, that are enriched in Pd, Re (and to a lesser extent Pt), and highly radiogenic Os, relative to associated peridotites. Pyroxenite layers in other ultramafic massifs have been interpreted to be high-pressure cumulates that formed in melt conduits, as residues from melting of subducted eclogitic crust, or as melt-rock reaction products. The HSE and Os isotopic data for the Totalp pyroxenites

are inconsistent with their forming as residues. Instead they appear to have formed by melt-rock interaction between mantle peridotite, with a long-term depletion history, and multiple batches of mafic melt that were derived from Re and Pd enriched materials with highly radiogenic $^{187}Os/^{188}Os$. Partial melting of subducted, old oceanic crust in the asthenosphere is a likely source for such melts.

Pyroxenites from the Totalp massif are generally enriched in Pt and Re, and thus, with time evolve both excess radiogenic ^{187}O and ^{186}Os, compared to ambient mantle. These rocks, however, are much more strongly enriched in Re than in Pt, and thus, do not possess the requisite Pt/Re to account for the coupled suprachondritic ^{186}Os-^{187}Os signatures observed in some Hawaiian picrites, Gorgona komatiites, or the Siberian plume.

Keywords: pyroxenite; websterite; highly siderophile elements; osmium isotopes; melt-rock interaction; partial melting

3.2 Introduction

Pyroxenites and websterites occur as layers or dykes in peridotite massifs, mantle tectonites associated with ophiolites, and mantle xenoliths. They comprise about 1-5% of peridotite massifs (e.g. Kornprobst, 1969; Kumar et al., 1996; Pearson and Nowell, 2004), but are rarely found in association with abyssal peridotites (Elthon, 1992; Seyler and Bonatti, 1997; Hellebrand et al., 2001; 2002; Luguet et al., 2003; Harvey et al., 2006; Dantas et al., 2007). Past studies have suggested that pyroxenite layers in the mantle may play an important role during the genesis of basaltic magmas in mid-ocean ridges (Hirschmann and Stolper, 1996) and intra-plate settings (Lassiter et al., 2000; Hirschmann et al., 2003; Sobolev et al., 2005; 2007; Luguet et al., 2008). In order to understand the influence pyroxenites may have on basalt genesis and upper mantle refertilization, the processes by which pyroxenite layers form must to be better understood. Multiple processes have been suggested that might lead to the formation of pyroxenites in the mantle including: a) formation as tectonically emplaced slices of subducted eclogitic crust, or residues of in situ partial melting of such eclogites

(Loubet and Allègre, 1982; Polvé and Allègre, 1982; Allègre and Turcotte, 1986; Blichert-Toft et al., 1999; Morishita et al., 2003), b) crystal accumulation at high pressures from asthenosphere-derived magmas passing through the lithosphere (Obata, 1980; Sinigoi et al., 1983; Bodinier et al., 1987; 1990; Takahashi, 1992; Vaselli et al., 1995; Becker, 1996a; Kumar et al., 1996; Garrido and Bodinier, 1999), c) crystal segregation from magmas generated by partial melting of subducted crust (Davies et al., 1993; Pearson et al., 1993), d) in situ metamorphic segregation of pyroxene from the host peridotite (Dick and Sinton, 1979), e) melt-rock reaction between existing pyroxenite, host peridotite and percolating melt (Garrido and Bodinier, 1999), and f) reaction of melt derived from subducted eclogitic oceanic crust with peridotite in the asthenosphere (Sobolev et al., 2005; 2007).

The purpose of this work is to study the composition and formation processes of pyroxenite layers and their relation to host lherzolites from the Jurassic Totalp peridotite massif, eastern Switzerland, using a combined major element, highly siderophile element (HSE; Os, Ir, Ru, Pt, Pd and Re) and Re-Os isotope approach. Field and petrographic observations combined with major element and Re-Os isotopic data for the host peridotites have provided evidence for refertilization of the host spinel lherzolites by melts derived from spatially associated pyroxenite layers (Müntener et al., 2004; van Acken et al., 2008). The refertilization may have occurred in the spinel lherzolite - spinel-garnet pyroxenite facies of the former oceanic lithosphere beneath the Tethys ocean basin in a regime transitional between lithosphere and asthenosphere.

HSE may be suited to distinguish between different formation models of pyroxenites as residues or melts of partial mantle melting because of their wide range of compatibility during partial melting, and the resulting large difference in HSE signature. Within the upper mantle, HSE are normally strongly chalcophile. Sulfide–silicate partition coefficients are >1000 for HSE under typical mantle conditions, so the amount of HSE entering silicate phases is small relative to that hosted in sulfides (Fleet et al., 1999; Sattari et al., 2002). Fractionation of the HSE from one another may occur within the mantle by partitioning between monosulfide solid solution (mss) and sulfide melts. Osmium, Ir and Ru are retained in the solid residual mss, while Pt and Pd enter the melt preferentially (Bockrath et al., 2004; Mungall et al., 2005; Ballhaus et al., 2006). Rhenium partitioning during partial melting is likely to be partially

controlled by silicate phases (Righter and Hauri, 1998; Fonseca et al., 2007), resulting in moderately incompatible behaviour during mantle melting (e.g. Hertogen et al., 1980; Morgan, 1986; Walker et al., 1989; Hauri and Hart, 1997; Shirey and Walker, 1998).

Because of the large Re-Os fractionation that occurs between melt and residue during the partial melting of peridotite (Allègre and Luck, 1980, Hertogen et al., 1980; Morgan et al., 1981), the rapid in-growth of radiogenic ^{187}Os from ^{187}Re in subducted mafic crust, and the large differences in Os concentrations and Os isotopic composition typical between peridotites and pyroxenite layers (Reisberg et al., 1991; Carlson and Irving, 1994; Roy-Barman et al., 1996; Kumar et al., 1996; Saal et al., 2001; Becker et al., 2004; Pearson and Nowell, 2004), Os isotopes, along with abundances of other HSE might provide important new insights to pyroxenite formation, mantle heterogeneity and magma provenance in deep lithospheric settings.

Pyroxenites commonly are characterized by $^{187}Os/^{188}Os$ that are considerably more radiogenic than the ambient mantle. They are also typically characterized by low abundances of Os and Ir compared to mantle peridotites, yet are normally enriched in Re (Reisberg et al., 1991; Kumar et al., 1996; Becker et al., 2004; Pearson and Nowell, 2004; Luguet et al., 2008). Pyroxenite data for Ru, Pt and Pd are scarce, but existing data hint at variable enrichments for Pt and Pd, while Ru behaves similarly to Ir (Grieco et al., 2004, Luguet et al., 2008).

Consequently, pyroxenites with suprachondritic Pt/Os and Re/Os develop radiogenic $^{186}Os/^{188}Os$ and $^{187}Os/^{188}Os$ over time. The presence of such pyroxenites as products of crust-mantle interaction in the oceanic mantle has been suggested as an alternative explanation to core-mantle interaction to explain coupled suprachondritic ^{186}Os-^{187}Os in oceanic basalts (Lassiter et al., 2000; Luguet et al., 2008). A comprehensive study of HSE and Os isotopic composition from a suite of oceanic pyroxenites may, therefore, shed further light on this issue.

3.3 Results

3.3.1 Whole rock compositions

Volatile-free calculated major element and HSE abundances are listed in Table 3.1. The original analytical results and loss on ignition values are included in the appendix. Major element, Os and Re abundances as well as isotopic compositions of samples TA11A2, TA13B, TA13D and TA61 have previously been reported by van Acken et al. (2008). In the subsequent discussion, volatile-free calculated major element data are used.

Al_2O_3-contents in websterites and wehrlite sample TA54A range from 7.01 wt. % to 9.18 wt. % compared to 11.0 to 13.6 wt. % in the clinopyroxenites. Correlations between major elements are generally poor. Al_2O_3 shows a broad positive correlation with CaO and a negative correlation with MgO, extending trends observed for associated peridotites (van Acken et al., 2008). No clear correlation exists between Na_2O and Al_2O_3, while MgO shows a negative correlation with Na_2O, also extending the trend observed for Totalp peridotites (not shown). Major element concentrations for Totalp samples are within the range reported for websterites and clinopyroxenites from massifs and xenoliths worldwide (Bodinier et al., 1987; Piccardo et al., 1988; Pearson et al., 1993; Becker, 1996a; Santos et al., 2002; Xu, 2002).

Totalp clinopyroxenites range to higher Pd and Re, similar Pt and lower Os, Ir and Ru concentrations than the websterites (Table 3.1), similar to previously published HSE data for pyroxenites (Beni Bousera, Kumar et al., 1996; Pearson and Nowell, 2004; Luguet et al., 2008; Lower Austria, Becker et al., 2004). Both websterites and clinopyroxenites have lower concentrations of Os, Ir and Ru and higher concentrations of Pt, Pd and Re than typical fertile lherzolites reported in studies of massifs and xenoliths worldwide (e. g., Lorand et al., 1999; 2000; Becker et al., 2006).

The HSE contents of Totalp samples generally correlate positively with each other (Figure 3.1). Good correlations exist between Os, Ir and Ru (not shown). Correlations between Re and the other HSE are less clear. Totalp websterites and clinopyroxenites define two different trends in a Re-Ir diagram (Figure 3.1a). Rhenium contents in Al-poor pyroxenites correlate

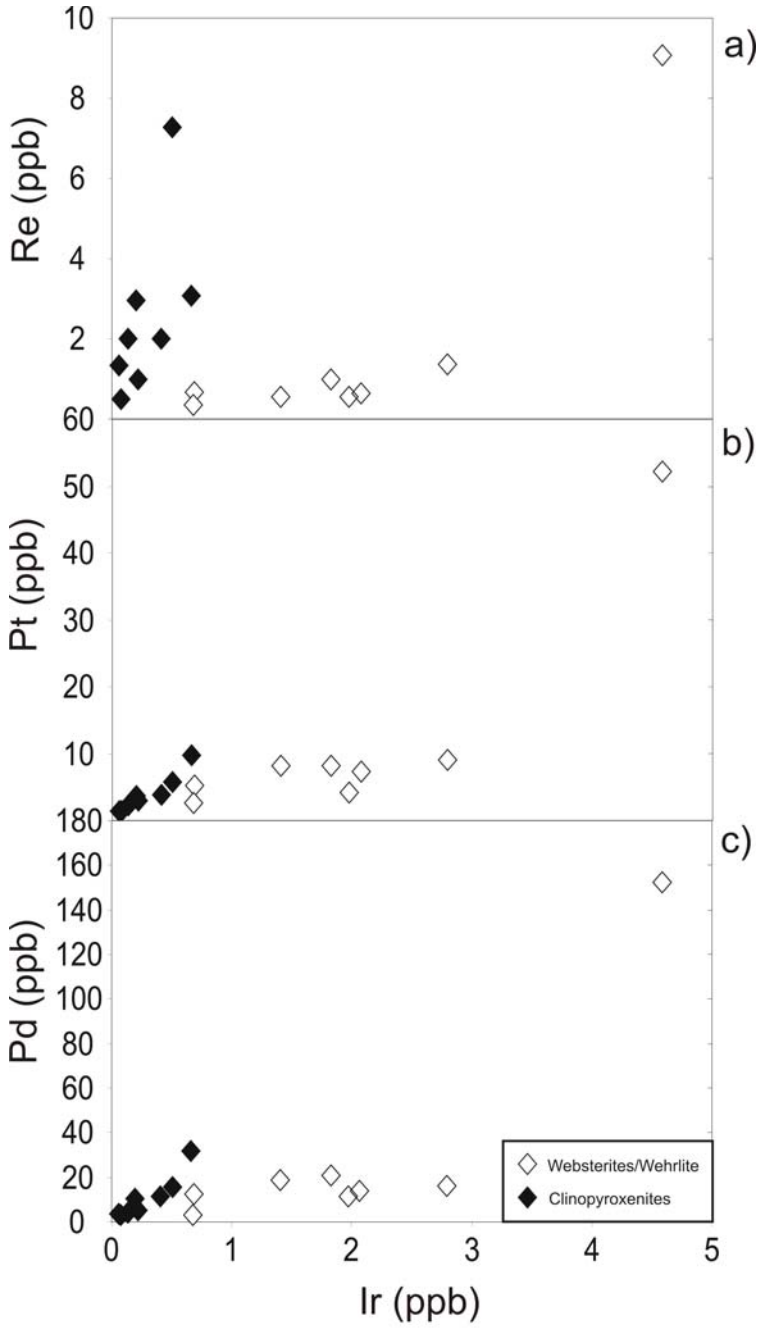

Figure 3.1: a) Re (ppb) vs. Ir (ppb), open symbols: Al-poor pyroxenites (websterites and wehrlite TA54A), filled symbols: Al-rich clinopyroxenites (see Table 1) b) Ir (ppb) vs. Pd (ppb), c) Ir (ppb) vs. Pt (ppb)

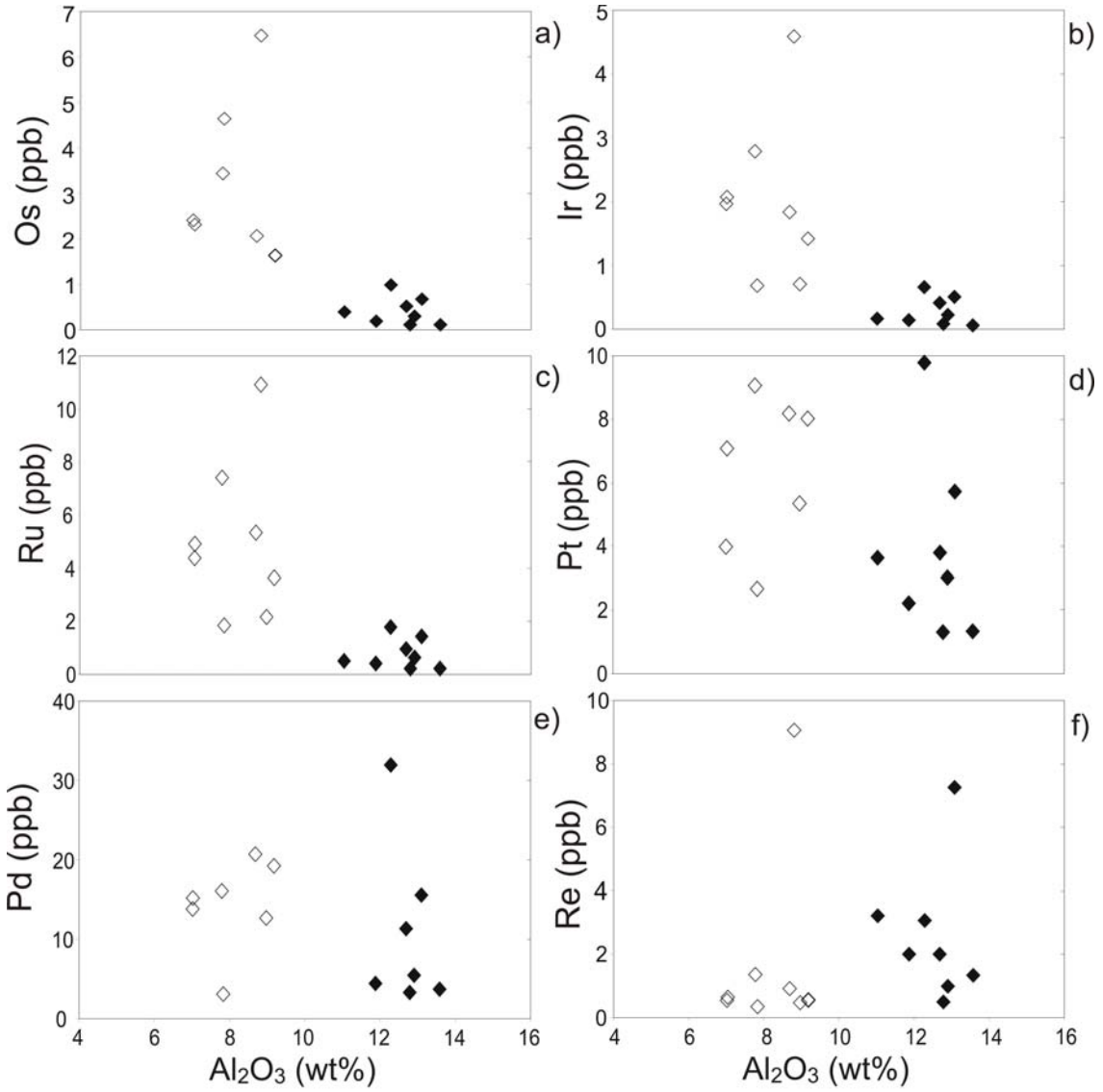

Figure 3.2: HSE abundances (ppb) vs. Al_2O_3 (wt%), a) Os; b); Ir; c) Ru; d) Pt; e) Pd; f) Re; open and filled symbols as in Figure 3.1a; Pd and Pt values for TA54A not plotted for scale reasons

with Ir contents with a shallow positive slope, whereas Al-rich pyroxenites define a positive trend with a steep slope. Palladium and Pt show moderate positive correlations with Ir. Wehrlite sample TA54A is characterized by very high concentrations of all HSE, while the spatially associated clinopyroxenite samples TA54B through D are comparatively poor in HSE, possibly reflecting an enhanced presence of sulfide in TA54A. HSE ratios, however, are

similar throughout the TA54 sample suite, regardless of concentration. Sample TA36A has very high Os coupled with normal concentrations of the other HSE (Table 3.1), resulting in abnormal HSE ratios involving Os.

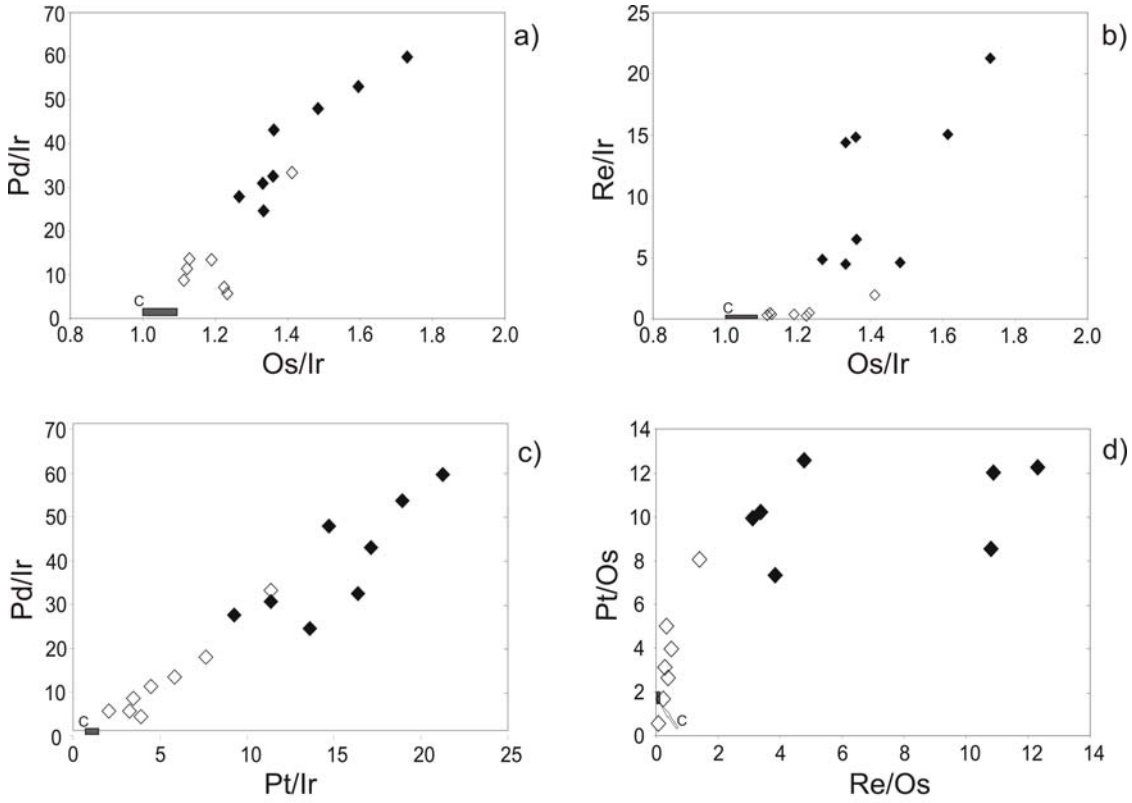

Figure 3.3: HSE ratio plots a) Pd/Ir vs. Os/Ir; b) Re/Ir vs. Os/Ir; c) Pd/Ir vs. Pt/Ir; d) Pt/Os vs. Re/Os; open and filled symbols as in Figure 3.1; C: chondrite area (Horan et al., 2003) TA36A not plotted in a) and b) for scale reasons

Broad negative covariations exist between Al_2O_3 and Os, Ir, Ru and Pt for websterites and clinopyroxenites. Palladium shows no covariation with Al_2O_3 in the Totalp pyroxenites, while Re displays a moderate, positive correlation with Al_2O_3 (Figure 3.2). As in Figure 3.1, samples TA36A and TA54A stand out for their low and high HSE concentrations, respectively, compared to samples with similar major Al_2O_3. In addition sample TA54B is characterized by very high Pt, and TA54C3 is characterized by high Re concentrations for a given Al_2O_3, plotting off the trend defined by the majority of samples.

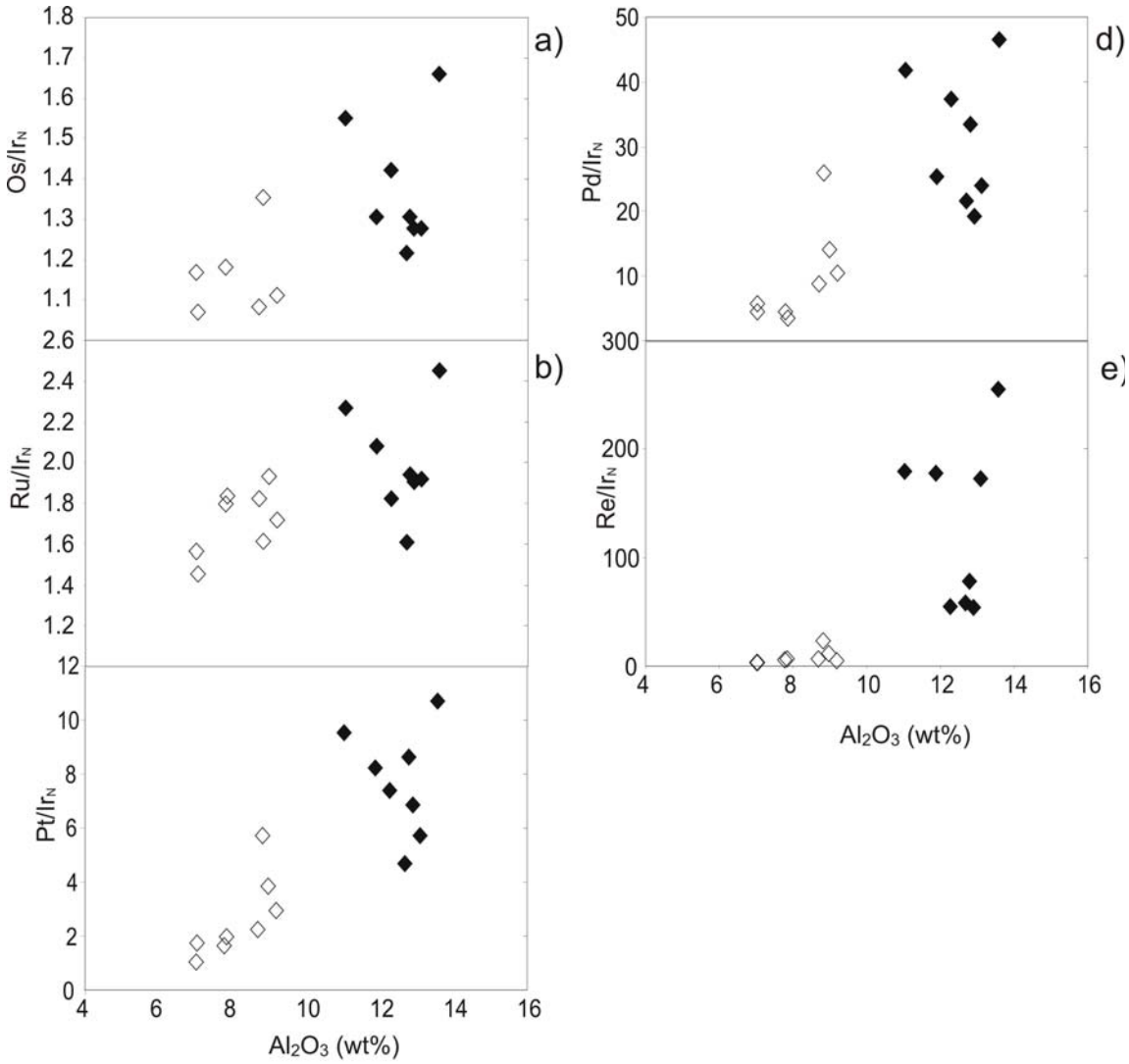

Figure 3.4: CI chondrite normalized HSE ratios vs. Al_2O_3 contents of the pyroxenites. The CI chondrite values in all figures are those of Horan et al. (2003). a) Os/Ir_N b) Ru/Ir_N; c) Pt/Ir_N; d) Pd/Ir_N e) Re/Ir_N ; open and filled symbols as in Figure 3.1. TA36A not plotted in a) for scale reasons

The pyroxenites have chondritic to slightly suprachondritic Os/Ir and Ru/Ir with websterites closer to chondritic values and clinopyroxenites displaying more often suprachondritic values. Owing to the high Os abundance, TA36A shows a highly suprachondritic Os/Ir. Pt/Ir, Pd/Ir and Re/Ir in the pyroxenites are mostly suprachondritic, and show increasing variance from Pt/Ir to Re/Ir. Clinopyroxenites show the highest values

for these ratios, and the greatest variance. Ratios of incompatible HSE in the pyroxenites show good correlations with each other, and fair correlations with ratios of compatible HSE, such as Os/Ir (Fig. 3.3). CI-normalized HSE ratios in the pyroxenites show broad positive correlations with Al_2O_3, with increasing scatter towards the Al-rich clinopyroxenites (Figure 3.4).

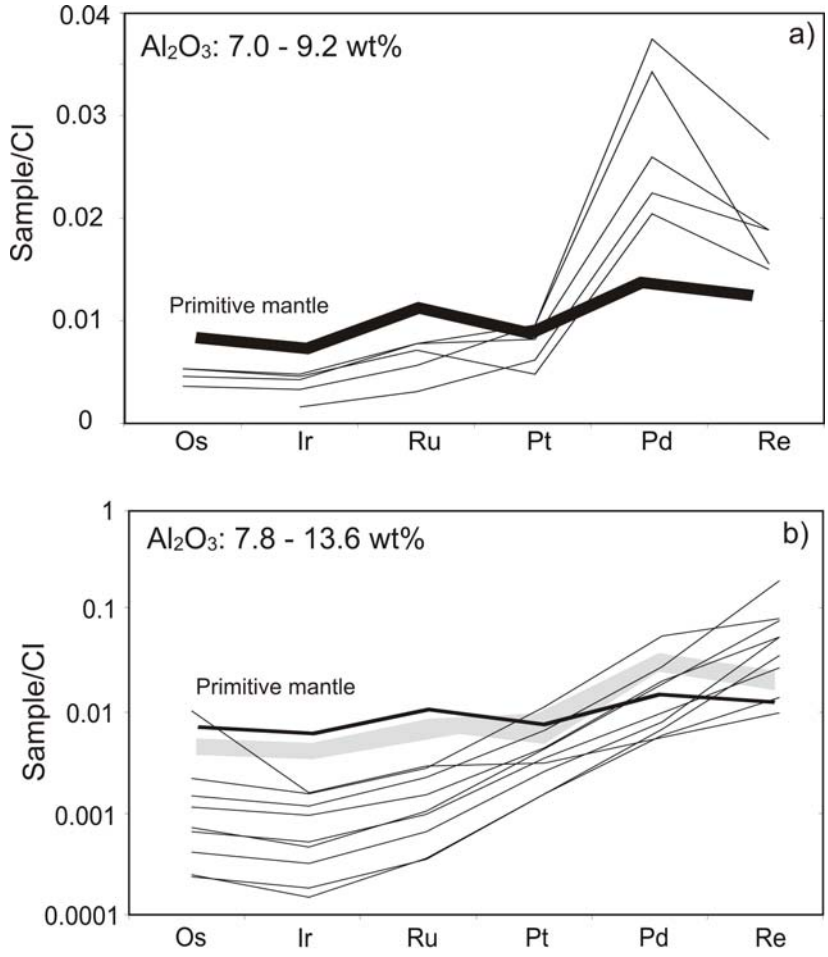

Figure 3.5: a) CI-normalized HSE patterns for type A Totalp pyroxenites, primitive mantle (PM) model composition after Becker et al. (2006); b) CI-normalized HSE patterns for type B Totalp pyroxenites, shaded area: type A pyroxenites from Figure 3.4a). Note the different scales in a) and b).

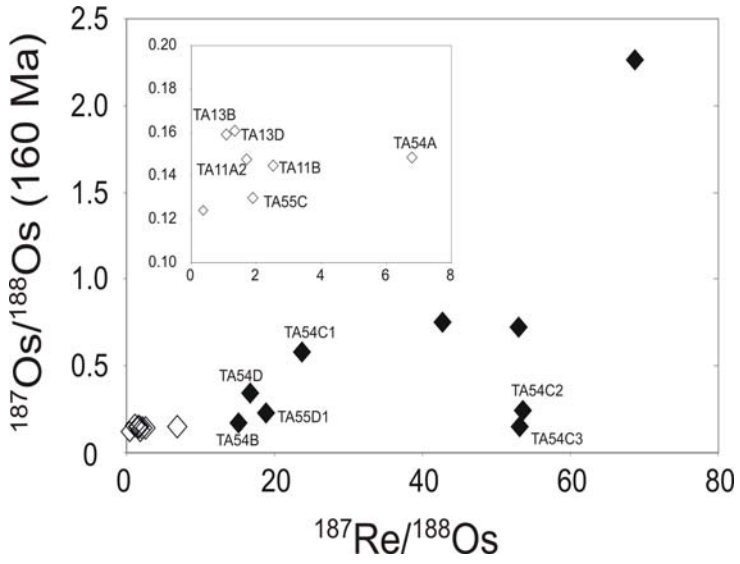

Figure 3.6: a) $^{187}Os/^{188}Os$ (160 Ma) vs. $^{187}Re/^{188}Os$; open and filled symbols as in Figure 3.1; regression of the pyroxenites, excluding two samples at the bottom right (TA54C1 and TA54C2), yields an apparent age of 1740 ± 370 Ma with initial $^{187}Os/^{188}Os$ of 0.01± 0.15, strongly indicating non-isochronous relationship of Totalp pyroxenites

Totalp pyroxenites show two distinct types of HSE patterns, termed A and B, with a gradual transition between the two types. Type A patterns, mostly websterites, have high Pd/Re, resulting in a sometimes strong, positive Pd peak in the pattern (Figure 3.5a), similar, but more extreme, than the Pd excess found in some fertile lherzolites (e.g., Becker et al., 2006). Type B patterns include all garnet-bearing samples, and are predominantly clinopyroxenites, but include websterites. They have low Pd/Re, reflecting a more "melt-like" HSE pattern (Figure 3.5 b). Intermediate patterns, with almost flat slopes between Pd and Re, include websterite samples TA54A (not plotted for scale reasons) and TA55C.

Measured $^{187}Os/^{188}Os$ range from 0.1250 to 2.4. Corrections for radiogenic ingrowth after formation are significant due to the high Re/Os for most samples. Initial $^{187}Os/^{188}Os$ calculated for a formation time of 160 Ma range from subchondritic 0.1240 to extremely radiogenic 2.265, corresponding to γ_{Os} (160 Ma) values (% deviation from chondritic values, Walker et al., 1989) of -1.7 to +1700. A good correlation exists between γ_{Os} (160 Ma) and $^{187}Re/^{188}Os$ (Figure 3.6), with samples TA54C2 and TA54C3 offset to lower γ_{Os} (160 Ma). A

general positive trend is apparent for γ_{Os} (160 Ma) versus Al_2O_3, with large scatter for the high-Al samples (Figure 3.7).

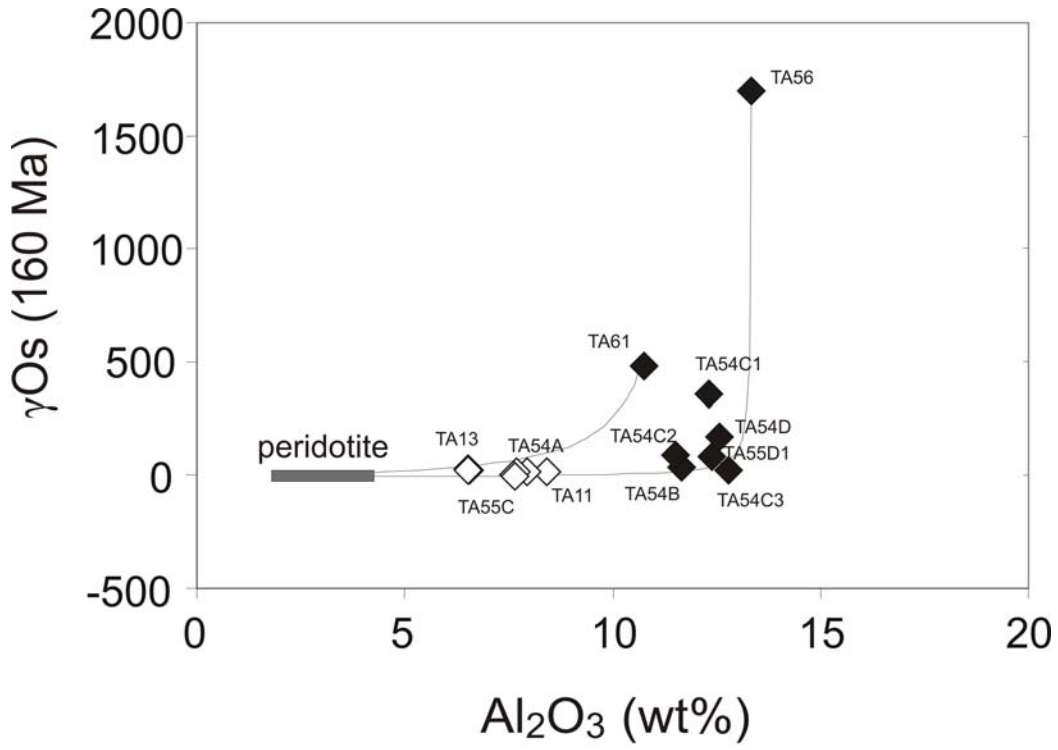

Figure 3.7: γ_{Os} (160 Ma) vs. Al_2O_3; open and filled symbols as in Figure 3.1. Mixing curves denote binary mixing between depleted peridotite with subchondritic γ_{Os} (160 Ma) and the most radiogenic pyroxenites from our dataset as approximations of melt composition (TA56, TA61), isotopic estimates for pyroxenites are at the lower end compared to γ_{Os} reported in pyroxenites from other locations, (Beni Bousera, Kumar et al. (1996); Luguet et al. (2008); open and filled symbols as in Figure 3.1.

3.3.2 Sulfide compositions

The major element composition of sulfides from one websterite and one wehrlite sample is remarkably homogeneous both on thick section and grain scale (Table 2). Sulfide grains are found mostly on silicate grain boundaries. They are anhedral and range in size from a few μm to 150 μm. Fe-bearing alteration phases such as magnetite and hematite occur along with sulfides in both thin sections.

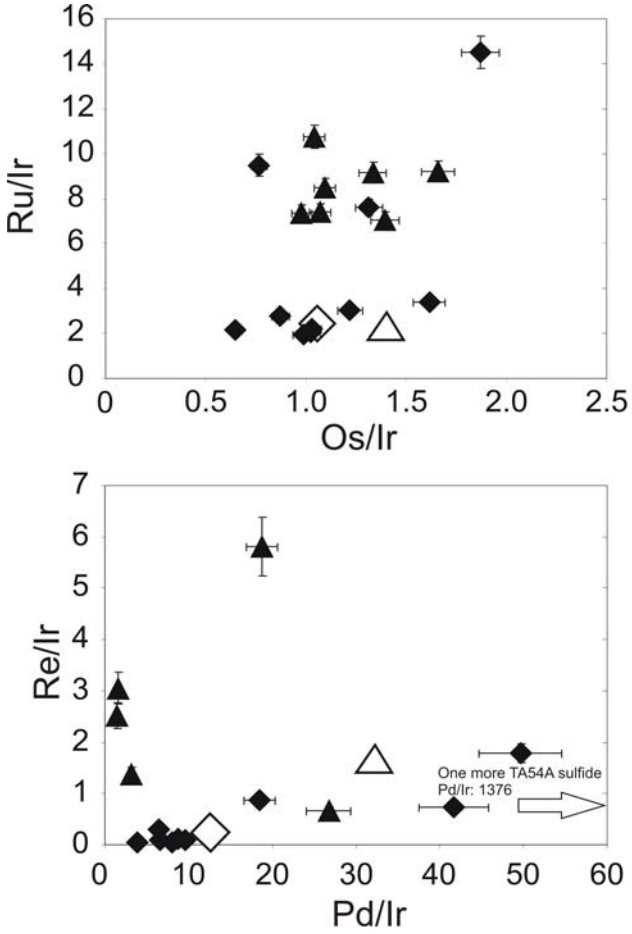

Figure 3.8: inter-element HSE ratios for sulfides from TA11A2 and TA54A; a) Ru/Ir vs. Os/Ir; b) Re/Ir vs. Pd/Ir; diamonds: TA11A2, triangles: TA54A, closed symbols: sulfide individual measurements, open symbols: corresponding bulk rock. One sulfide sample from TA54A not plotted in b) for scale reasons: (Pd/Ir: 1376; Re/Ir 0.98)

Sulfides in websterite sample TA11A2 are almost exclusively pentlandite, with S contents ranging from 55.2 at% to 59.1 at %. Nickel and iron are in the range of 17.8 at % to 21.5 at%, and 20.2 at% and 26.4 at%, respectively. Copper contents are below 0.25 at%, Co contents below 1.4 at%. Sulfides in the wehrlite TA54A consist of pentlandite and godlevskite ((Fe,Ni,Co)S) intergrown with native copper in anhedral grains crosscut by serpentinite veins. The godlevskites and pentlandites contain 43.9 to 49.9 at% S. Iron contents in the pentlandites present in TA11A2 range from 19.7 to 28.5%, with corresponding Ni concentrations ranging from 16.7 to 21.5%. Godlevskites and pentlandites in TA54A contain 0.10 to 1.37 % Fe and

51 to 53 % Ni. For both samples, Cu and Co contents are less than 1.75 at% in all sulfides, with the exception of one Fe-poor, Co-and Cu-rich grain. Native copper grains in sample TA54A contain up to 5 at% of Ni, but are devoid of significant Fe and Co.

Sulfide grains in thick sections from TA11A2 and TA54A were analyzed for HSE by LA-ICP-MS (Table 3.3). Except for Pt, the HSE are about three orders of magnitude more abundant in sulfides than in whole rocks. While major elements in sulfides are homogeneously distributed on the grain scale, this does not hold true for the HSE. Within section TA11A2, Re and Pd concentration in sulfides shows little variation, concentrations of Os, Ir and Ru vary over about an order of magnitude. In TA54A, all HSE are heterogeneously distributed, with the range spanning over two orders of magnitude. While some sulfide grains show enrichment of all HSE determined, other grains show extreme enrichment of only Pd. HSE in sulfides show no systematic correlation with sulfide major elements.

Two grains of native copper were sampled in TA54A. Because of the small grain sizes of native copper, smaller beam diameters had to be used and thus, lower signal intensities were achieved. Abundances of Os, Re and Ru are lower than in pentlandites, while Ir is in a similar range.

None of the sulfides or native copper grains yielded Pt signals resolvable from backgrounds. Calculated values are maximum values based on detection limits. Platinum has been shown to exsolve into micronuggets under subsolidus conditions (Luguet et al., 2001; 2003; 2007; Lorand et al., 2008). Subsequent BSE scans of the thick sections failed to detect any Pt-rich minerals in the section plane.

Os/Ir ratios in sulfides from both samples often lie within the chondritic range, with moderately subchondritic and suprachondritic values occurring as well. Ru/Ir is moderately to highly suprachondritic in TA11A2 and highly suprachondritic in TA54A, with values from 1.96 to 14.5 and 7.4 to 10.8, respectively. The extreme Ru/Ir values of these sulfides seem to play only minor roles in the whole rock mass balance, because the whole rock Ru/Ir values of these pyroxenites (2.3 and 2.7) are at the lower end of the compositional spectrum of the sulfides, and are very similar to “canonical” lherzolite values (Becker et al., 2006).

Pd/Ir is very heterogeneous with values ranging from 6.5 to 49.6 in TA11A2 and from 1.47 to 1380 in TA54A. Most sulfides in these samples have a lower Pd/Ir than the corresponding

whole rock ratios of 13.6 and 33.3, thus balancing a few grains with extremely high Pd/Ir, which reflect high Pd, very low Ir abundances, or both. Re/Ir varies from 0.05 to 1.78 in TA11A2 and from 0.67 to 5.81 in TA54A scattering around the whole rock ratio of 0.40 and 1.98, respectively (Figure 3.8).

The websterites are devoid of chalcopyrite, which has been observed to be a prominent sulfide and host of Pd in previous studies of mantle peridotites (Lorand, 1989; Alard et al., 2000; 2002; Luguet et al., 2001; 2003; 2007). This is unexpected in the context of the high Pd contents observed in Totalp pyroxenites. The presence of native copper, godlevskite and pyrite in sample TA54A suggests secondary redistribution and transformation of sulfides on the grain-scale, presumably during serpentinization.

3.4 Discussion

3.4.1. Pyroxenite Formation and Refertilization

In the following section, we review several formation processes proposed to generate pyroxenites in a variety of geological settings. We then consider data for Totalp pyroxenite layers to distinguish between plausible models.

Pyroxenites have been interpreted to represent residues of melting of eclogitic layers of recycled oceanic crust that are mechanically thinned and reworked in the convecting mantle (Polvé and Allègre, 1980; Loubet and Allègre, 1982; Allègre and Turcotte, 1986; Blichert-Toft et al., 1999). This interpretation, proposed for some pyroxenites from Beni Bousera, Horoman and Ronda, is supported by old Os model ages (Reisberg et al., 1991; Saal et al., 2001; Pearson and Nowell, 2004) and Lu-Hf ages (Blichert-Toft et al., 1999). Eu anomalies possibly indicating oceanic crust in the pyroxenite source are present in some pyroxenites from these locales (Loubet and Allègre, 1982; Kornprobst et al., 1990; Garrido and Bodinier, 1999), but are absent in others (Bodinier et al., 1987; Bodinier, 1988; Garrido and Bodinier, 1999; Downes, 2007).

Other models consider pyroxenites to represent melt, rather than residual compositions. In situ formation models from partial melts of host peridotites which did not segregate fully (Sinigoi et al., 1983; Voshage et al., 1988) have been excluded for the majority of pyroxenites based on major and trace element compositions of mafic layers from several localities, which do not match with peridotite partial melt compositions (Suen and Frey, 1987; Takazawa et al., 1999, Garrido and Bodinier, 1999). The most common formation models suggest that pyroxenites formed by crystal accumulation in the lower lithosphere from mafic asthenospheric magmas infiltrating into variously depleted peridotite (Obata, 1980; Sinigoi et al., 1983; Suen and Frey, 1987; Pearson et al., 1993; Davies et al., 1993; Becker, 1996a; Kumar et al., 1996; Witt-Eickschen and Kramm., 1998; Garrido and Bodinier, 1999; Xu, 2002).

Because of its lower melting temperature and higher melt productivity compared to fertile mantle peridotite, recycled oceanic crust in the form of eclogite has been suggested as the most likely source for this type of melt in the asthenosphere (Yasuda et al., 1994; Hirschmann and Stolper, 1996; Yaxley and Green, 1998; Kogiso and Hirschmann, 2001; Xu, 2002; Pertermann and Hirschmann, 2003; Kogiso et al., 2003; 2004). Andesitic to basaltic partial melts of eclogitic layers may react with depleted peridotite in the immediate vicinity to form pyroxenite layers (e. g. Yaxley and Green, 1998; Pertermann and Hirschmann, 2003; Sobolev et al., 2005). Remelting of these pyroxenite layers has been suggested to contribute extensively to oceanic basaltic volcanism (Hirschmann and Stolper, 1996; Kogiso and Hirschmann, 2001; Kogiso et al., 2003).

In a closed system, complete crystallization of the melt would result in mixing of mantle host rock and mafic melt for porous melt flow, and in formation of mafic mantle veins for melt flow in conduits. In open systems where the melt passes through surrounding peridotites, melt-rock interaction along cumulate mineral precipitation and possibly the retention of some melt in pore space may generate pyroxenites at low melt/rock ratio (Garrido and Bodinier, 1999) or replacive harzburgites and dunites at high melt/rock ratio (Quick, 1981; Kelemen et al., 1992; 1997). Pyroxenite formation by cumulate precipitation or melt-rock reaction during percolative melt flow is supported by field and petrographic observations (e.g. Ronda, Garrido and Bodinier, 1999; Lherz, Le Roux et al., 2007) and major and lithophile trace

element geochemistry (e.g. Irving, 1974; Bodinier et al., 1987; Dawson and Smith, 1992; Pearson et al., 1993; Becker, 1996a; Witt-Eickschen and Kramm, 1998; Garrido and Bodinier, 1999; Xu, 2002).

3.4.2 Modeling Totalp pyroxenite formation with HSE

Totalp pyroxenites display broadly linear major element covariations for pyroxenites and associated peridotites, suggesting a common igneous process for their formation (van Acken et al., 2008). The pyroxenites are also characterized by fractionation of HSE relative to both chondrites and primitive mantle estimates (Figure 3.5). Enrichments of Pt, Pd and Re, relative to Os, Ir and Ru reflect both lowered IPGE concentrations and high PPGE and Re concentrations, compared to PUM. These characteristics of the Totalp pyroxenites are similar to those observed in pyroxenites from other ultramafic massifs. Most samples are also characterized by suprachondritic initial $^{187}Os/^{188}Os$. Two samples are characterized by a heterogeneous HSE distribution on the thin section scale, possibly indicating the presence of multiple sulfide generations.

Of possible formation models, we discount the possibility of formation of the pyroxenites by in situ crystallization of partial melts of the host peridotite, as suggested for some pyroxenites from the Balmuccia peridotite body (Sinigoi et al., 1983; Voshage et al., 1988). Large differences in initial γ_{Os} between Totalp peridotites and pyroxenites (Table 3.1; van Acken et al., 2008) preclude a simple melt-residue relationship at any time during the Phanerozoic.

In light of the Os isotopic and HSE abundance characteristics, we more closely consider other two models for Totalp pyroxenite formation: a) formation as residues of partial melting of eclogitic oceanic crust (Dick and Sinton, 1979; Polvé and Allègre, 1980; Allègre and Turcotte, 1986; Blichert-Toft et al., 1999), b) formation as products of melt-rock interaction, either as cumulate precipitates or melt-rock reaction products, between depleted mantle peridotite and mafic melt (e.g. Obata, 1980; Sinigoi et al., 1983; Suen and Frey, 1987; Becker, 1996a; Takazawa et al., 1999;).

Derivation of the pyroxenites from recycled oceanic crust with high Re/Os (Roy-Barman and Allègre, 1994; Escrig et al., 2005; Gannoun et al., 2007), either as residues of partial melting or as partial melts, is consistent with the radiogenic initial γ_{Os} in most Totalp pyroxenites as well as some associated peridotites (van Acken et al., 2008). Residues of partial melting should be characterized by enrichment in compatible HSE, such as Os, Ir and Ru over their precursor material, and accompanied by depletions in incompatible HSE, such as Pd or Re. In contrast, partial melts would be expected to be enriched in Pd and Re, and if the pyroxenites are products of interactions between mafic melts, produced by partial melting of recycled crust, and peridotite, the HSE signature of the resulting rocks to some degree should reflect the mixed HSE characteristics of the mafic melt and affected peridotite. Estimates of the HSE characteristics of such hybrid mixtures are presently subject to considerable uncertainty.

In order to distinguish between the two models of pyroxenite genesis, we model HSE abundances in both a melt and a residue resulting from the partial melting of a basic rock with an original HSE composition similar to that of subducted MORB. A representative HSE composition of subducted oceanic crust was calculated from datasets of HSE abundances in MORB of Rehkämper et al. (1999a), Bézos et al. (2005), Escrig et al. (2005) and Gannoun et al. (2007). HSE abundances reported for lower oceanic crust, represented by gabbros or gabbroic eclogites, with higher Os abundances and similar Re abundances compared to MORB, were also taken into account (Blusztajn et al., 2000; Dale et al., 2007). As HSE concentrations in MORB vary by as much as two orders of magnitude (Schiano et al., 1997; Rehkämper et al., 1999a; Escrig et al., 2005; Bézos et al., 2005; Gannoun et al. 2007), the choice of starting composition for the model strongly influences the model outcome (Figure 3.9). The starting model MORB composition we use is listed in Table 3.4.

Another factor which might influence the starting condition for melting models using basaltic sources may be Re loss during oceanic crust recycling. Becker (2000) suggested that up to 60% of Re might be lost from altered oceanic crust during subduction, then transferred into the overlying mantle wedge. On the other hand, Re might be added to oceanic crust from

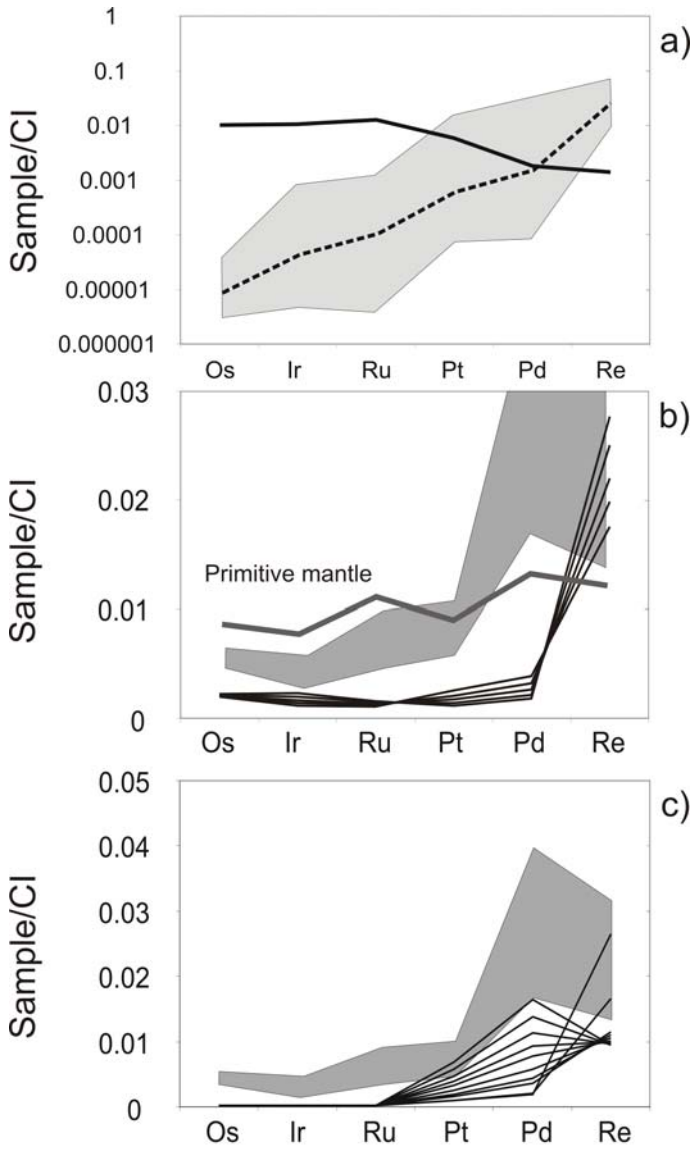

Figure 3.9: CI-normalized HSE patterns for a) typical mid-ocean ridge (dashed), peridotite samples TA22A2 and 64-3 (thick), shaded area: range of MORB composition reported worldwide depleted peridotite: 4.5 ppb Os, 4.5. ppb Ir, 8 ppb Ru, 4 ppb Pt, 1 ppb Pd and 0.05 ppb Re MORB: 0.01 ppb Os; 0.03 ppb Ir, 0.04 ppb Ru, 0.5 ppb Pt, 0.9 ppb Pd, 1 ppb Re; b) composition of residues for 1 to 50 % fractional melting of subducted MORB; gray line: Primitive mantle composition c) corresponding partial melts. MORB HSE data compiled from Rehkämper et al. (1999); Bézos et al. (2005); Escrig et al. (2005); Schiano et al. (2005); Dale et al. (2007); Gannoun et al. (2007). Equations for melting taken from Shaw (1970).

For partial melting calculations involving solid-liquid sulfide equilibria we used the following mss – sulfide melt partition coefficients: D^{Os} = 7 (Fleet et al., 1993; Brenan, 2002; Ballhaus et al., 2006), D^{Ir} = 8 (Li et al., 1996; Ballhaus et al., 2001; Bockrath et al., 2004; Mungall et al., 2005), D^{Ru} = 9 (Ballhaus et al., 2001; Bockrath et al., 2004; Mungall et al., 2005), D^{Pt} = 0.15 (Fleet et al., 1993; Li et al., 1996; Ballhaus et al., 2001; 2006; Bockrath et al., 2004; Mungall et al., 2005), D^{Pd} = 0.15 (Fleet et al., 1993; Li et al., 1996; Ballhaus et al., 2001; 2006; Bockrath et al., 2004; Mungall et al., 2005), D^{Re} = 3 (Brenan, 2002; Ballhaus et al., 2006)

seawater, leading to increased Re by a factor of up to three for upper oceanic crust (Reisberg et al., 2008).

Both batch and fractional melting of MORB were modeled using equations derived by Shaw (1970). We will limit discussion to the fractional melting model, as batch and fractional melting produce similar results for these elements, due to their compatible to moderately incompatible behaviour.

As noted above, the HSE are strongly chalcophile under upper mantle conditions (Garuti et al., 1984; Peach et al., 1990; 1994; Barnes, 1993; Bezmen et al., 1994; Fleet et al., 1999; Sattari et al., 2002). Consequently, in the following models sulfides are the dominant control on the behavior of HSE, and silicate-sulfide partitioning of HSE is assumed to be negligible (although Re will be reconsidered separately below).

For the first step of our models only the mss-sulfide melt equilibria are, therefore, considered. Partitioning data between monosulfide solid solution (mss) and sulfide melt normally indicate that Pd and Pt partition preferably into sulfide melt, whereas the other HSE remain in the solid mss (Fleet et al., 1993; Ballhaus et al., 2001; 2006; Brenan, 2002; Bockrath et al., 2004; Mungall et al., 2005). Subsequent separation of sulfide melt from residual mss can result in fractionated patterns in both melt and residual sulfide (Bockrath et al., 2004; Ballhaus et al., 2006). While Os, Ir, Ru and possibly Re are compatible in mss during partial melting with $D_{mss/melt}$ of about 2 to 10, Pt and Pd are incompatible with $D_{mss/melt}$ of ~0.1 to 0.25 (Brenan, 2002; 2008; Bockrath et al., 2004; Ballhaus et al., 2006).

A model concerning only mss–sulfide liquid partitioning is likely oversimplified. Correlations of several HSE and Os isotopes with lithophile elements such as Al (Figure 2, 4, 9; also seen in peridotites, e.g., Reisberg and Lorand, 1995; Peslier et al., 2000; Schmidt and Snow, 2002; Lorand et al., 2003) suggest that the sulfide system may not always be regarded as completely decoupled from the silicate system. This holds especially true for Re, which is the most lithophile element among the HSE and, under some conditions, may be incorporated in silicate minerals (Righter and Hauri, 1998; Mallmann and O'Neill, 2007). Recent studies report a strong dependence of Re partitioning behaviour on oxygen and sulfur fugacities (Amossé et al., 2000; Fonseca et al., 2007; Mallmann and O'Neill, 2007; Brenan, 2008),

suggesting that Re behavior is controlled by both the redox state of Re and sulfur speciation in the mantle.

Experimentally determined sulfide–silicate partition coefficients for Re may vary over three orders of magnitude, depending on experimental conditions (Fleet et al., 1999; Sattari et al., 2002; Fonseca et al., 2007; Brenan, 2008). Typical experiments have been run at temperatures ranging from 1200 to 1350 °C, and pressures ranging from atmospheric to 1.5 GPa, lower than the likely pressure of both partial melting and crystallization. Extrapolating these partitioning data to higher pressure melting processes is challenging, given the strong influence of pressure on S solubility in silicate melts (Mavrogenes and O'Neill, 1999; Holzheid and Grove, 2002; O'Neill and Mavrogenes, 2002), which in turn may significantly affect Re partitioning (Brenan, 2008).

For typical lower oceanic lithosphere redox conditions of log fO_2 values of -1 relative to the QFM buffer, sulfide-silicate melt partition coefficient D_{Re} may be as low as 300, compared to $D^{Re} > 1000$ at more reducing conditions, thus, resulting in a significant proportion of Re hosted in silicate minerals. More oxidizing conditions during mantle melting may result in even lower D^{Re} (Roy-Barman et al., 1998; Fonseca et al., 2007; Brenan, 2008), but are likely not applicable for convecting oceanic mantle, which has estimated redox conditions of QFM -3 to -1 (e.g., Lee et al., 2003).

With lower $D^{Re}_{sulfide/silicate}$ under these conditions, a significant part of Re will be hosted in garnet (Righter and Hauri, 1998; Mallmann and O'Neill, 2007) and clinopyroxene (Mallmann and O'Neill, 2007). During melting of an eclogitic source, bulk partitioning of Re will, thus, be controlled by complex sulfide solid–sulfide melt–garnet–clinopyroxene–silicate melt partitioning, the solubility of sulfide in silicate melt, and sulfide exhaustion in the source (Ertel et al., 2001). In order to take into account the possible lithophile behaviour of Re, we used a revised bulk partition coefficient for Re at QFM -1 of 0.7 based on literature data for Re partitioning and garnet stability field melting phase relations (Hauri and Hart, 1997; Righter and Hauri, 1998; Pertermann and Hirschmann, 2003; Hirschmann et al., 2003; Mallmann and O'Neill, 2007; Brenan, 2008). A second model considers this complex partitioning behaviour of Re, while still assuming that other HSE are controlled by mss-sulfide melt partitioning during partial melting.

Sulfur content and sulfur solubility in silicate melts at the pressure and temperature of partial melting are also important factors to consider. In order for the sulfide melt–mss fractionation to occur, the sulfide melt and sulfide liquid must coexist throughout the melting process. Sulfur saturation of silicate melt is influenced by temperature, pressure, fO_2, fS_2 and FeO content (Haughton et al., 1974, and references therein). While fO_2, fS_2 and temperature have minor effects, FeO content and pressure exert a strong effect on sulfur solubility of silicate melts (Wendlandt, 1982; Wallace and Carmichael, 1992; Mavrogenes and O'Neill, 1999; Holzheid and Grove, 2002; O'Neill and Mavrogenes, 2002; Liu et al., 2007). Sulfur solubility increases with decreasing pressure by a factor of 2 from garnet peridotite facies conditions to surface conditions (Mavrogenes and O'Neill, 1999; Holzheid and Grove, 2002). Using typical S concentrations in eclogites (Greau et al., 2008), sulfide phases should be present throughout the melting process considered here, making the HSE fractionation model suggested by Bockrath et al. (2004) and Ballhaus et al. (2006) applicable.

Experimental studies of partial sulfide melting and HSE equilibria between sulfide melt and mss have been conducted with a variety of sulfide compositions. HSE partition coefficients have been determined for sulfide with 40 – 60 wt% Fe, 1 – 20 wt% Ni, 0 – 7 wt% Cu and 30 – 40 wt% S (Li et al., 1996; Fleet et al., 1999; Mungall et al., 2005; Ballhaus et al., 2006). These compositions are similar to sulfide compositions observed in MORB and eclogites (Desborough and Czamanske, 1973; Roy-Barman et al., 1998; Richardson et al., 2001). In contrast, sulfides present in lherzolites typically have higher Ni, but lower Fe concentrations than experimental conditions explored, and broadly overlap for Cu and S content (Luguet et al., 2004). HSE partitioning has been shown to be independent of Ni content for a wide range of compositions for mss–sulfide melt and sulfide–silicate partitioning (Fleet et al., 1993; 1999). Similarly, Ballhaus et al. (2001) showed an insensitivity of HSE distribution towards S content for HSE present in trace abundances. The experimentally determined partition coefficients for mss–sulfide melt systems (Fleet et al., 1993; Li et al., 1996; Bockrath et al., 2004; Mungall et al., 2005; Ballhaus et al., 2006) should, thus, be valid for melting of eclogite sulfides.

It is important to note that sulfide liquidus temperatures are lower than liquidus temperatures for mantle peridotite; thus, the degrees of melting inferred for sulfides may not

correspond to similar degrees of melting for bulk lithologies. Complete consumption of sulfide during partial melting is estimated to occur after 15–20% melting of peridotite (e.g. Ballhaus et al., 2001). Mafic mantle lithologies possess lower melting temperatures in comparison to peridotite (Yasuda et al., 1994; Hirschmann and Stolper, 1996; Pertermann and Hirschmann, 2003), so for equivalent conditions, partial melting of peridotite normally would correspond with much higher degrees of partial melting of eclogite (Yasuda et al., 1994; Yaxley and Green, 1998; Pertermann and Hirschmann, 2003). The degree of sulfide melting and melting of bulk eclogite are, thus, likely much more similar than for sulfide-peridotite.

Modeling results for 1 to 50 % melting suggest that residues from partial melting of MORB-type material would be depleted in all elements except for Re (Figure 3.9b), compared to primitive mantle. While Re concentrations in model residues are within the same range as those of Totalp websterites, the concentrations of all other HSE are significantly lower in the model residues. Depletion in Os, Ir and Ru is inherited from the IPGE-poor starting material. Depletions in Pt and Pd result from the incompatibility and preferred partitioning into sulfide melt. The predicted HSE signatures from model residues are in clear contrast to the Pt-, Pd- and Re-enriched signatures observed in Totalp pyroxenites (Figures 3.3 – 3.5). An origin as residues from partial melting of subducted oceanic crust, thus, appears unlikely based on the HSE signatures of the pyroxenites.

Model HSE patterns for partial melts of the MORB source are characterized by PPGE and Re enrichments that are similar to those observed in Totalp pyroxenites. Small degrees of partial melting (1 to 10%) result in enrichment of Pt and Pd over both Ir and Re in the melt, as is observed in the pyroxenites with type A HSE patterns. Increasingly larger degrees of partial melting drive the HSE patterns in the melt towards the pattern of the initial basalt (Figure 3.9). However, because of the low liquidus of basaltic or eclogitic compositions compared to peridotitic lithologies (Yasuda et al., 1994; Pertermann and Hirschmann, 2003), large degrees of melting seem to be more applicable.

If the pyroxenites represent trapped melts, their geochemical composition should be close to that of the melt composition. However, major element compositions of Totalp pyroxenites do not match those of high-pressure partial melts of either mafic mantle lithologies or peridotite (Kogiso et al., 2003; 2004). In addition, most Totalp pyroxenites are too rich in all

HSE except for Re to represent trapped basaltic melts. Coupled with petrographic observation of pyroxene-rich veins extending into adjacent peridotites and pyroxene cumulate textures, an origin via melt-rock interaction is more likely. If the pyroxenites represent products of melt-rock interaction, either as melt-rock reaction products, or as pyroxene cumulates, their geochemical signatures should reflect both depleted peridotite and partial melt components. Interaction of depleted peridotite with mafic melt results in an increase of incompatible major components such as Al_2O_3, CaO and Na_2O, and a decrease in compatible components, such as MgO. At pressures >3 GPa mafic melt precipitates clinopyroxene and garnet as cumulates (O'Hara, 1968; Lundstrom et al., 2000), along with sulfides bearing the HSE signatures of the melt. Using a simple model, we compare the HSE signatures observed in Totalp pyroxenites with mixtures of peridotite and the model compositions of partial melts.

As even the most depleted Totalp samples likely have been affected by refertilization to some extent, a representative depleted mantle composition was chosen as depleted endmember for the mixing model (Table 3.4; Pearson et al., 2004; Luguet et al., 2007). The HSE patterns for the depleted harzburgitic endmember used in the modeling are characterized by pronounced PPGE and Re depletion relative to IPGE.

Results for mixing calculations of these peridotites and partial model melts derived from recycled oceanic crust are shown in Figure 3.10. Although the general trends observed in Totalp pyroxenites are reproduced by partial model melts, neither the type A nor B patterns in Totalp websterites and clinopyroxenites can be reproduced by simple mixing of depleted peridotite with small-degree melts (Figure 3.10a) or larger degree melt (Figure 3.10b) derived from an average MORB-type source. Large degrees of melting, while regarding only mss–sulfide melt partitioning or more limited degrees of partial melting with consideration of lithophile behaviour of Re, and according variation in D_{Re} from compatible behaviour during mss-sulfide melt partitioning to moderately incompatible behaviour, result in similar Re distribution during partial melting, impeding clear discrimination between the two processes (Figure 3.10c). Most Totalp pyroxenites are too enriched in incompatible HSE to be accounted for by simple mixing of peridotite and basalt-derived melt as outlined above.

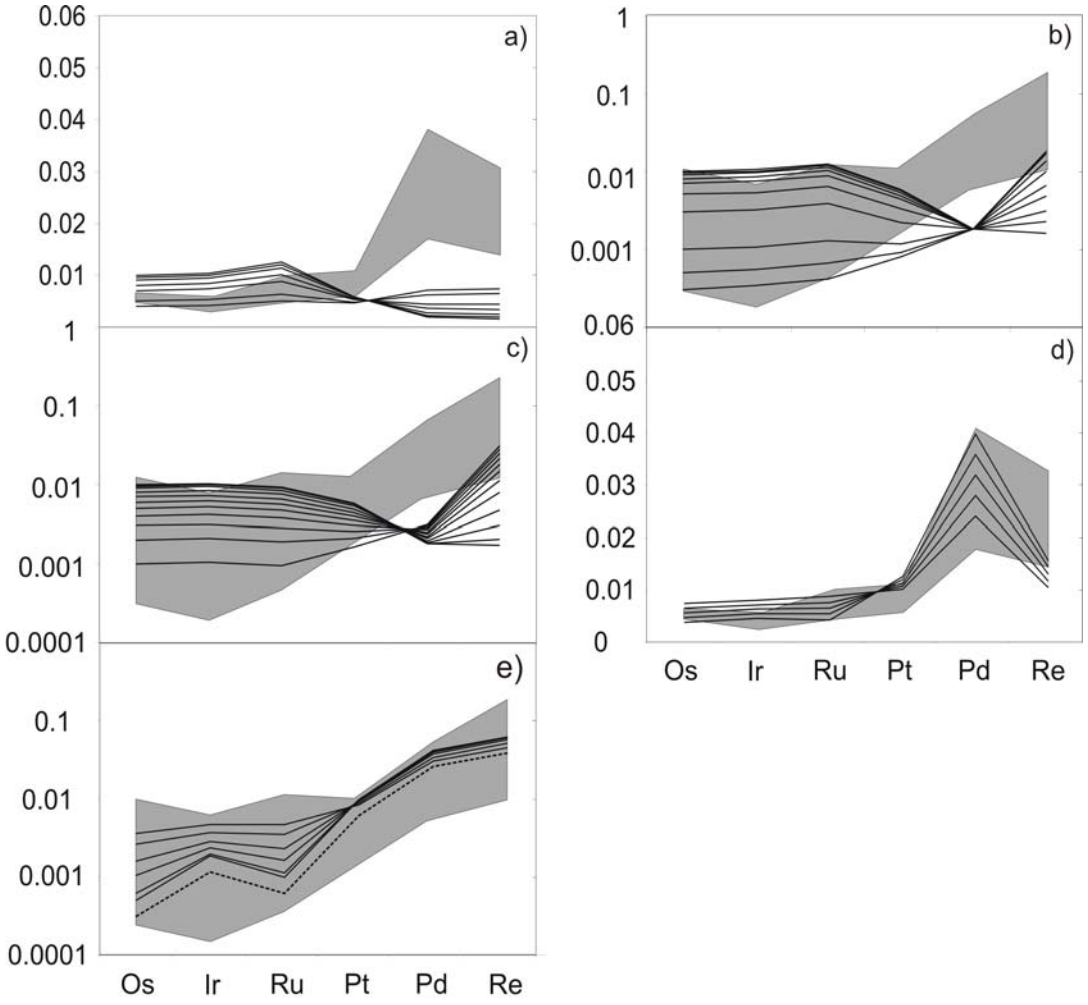

Figure 3.10: a) HSE patterns resulting from addition of partial melt formed by 10 % fractional melting of eclogite to residual peridotite. Chosen peridotite endmembers has 4.5 ppb Os, 4.5. ppb Ir, 8 ppb Ru, 4 ppb Pt, 1 ppb Pd and 0.05 ppb Re a) mixing of a 10% fractional melt with depleted peridotite, b) mixing of 80% fractional melt with depleted peridotite c) mixing of 10% fractional melt with depleted peridotite considering less chalcophile and more incompatible behaviour of Re based on increased incorporation in silicate phases. Patterns from bottom to top reflect mixing with melt fractions of 5%, 10%, 20%, 30%, 50%, 60% and 70% for a) and with melt fractions of 1%, 5%, 10%, 20%, 30%, 40%, 50%, 60%, 70%, 80% and 90% for b) and c).

d) and e) mixing of cumulate sulfide with depleted peridotite sulfide; d) mixing with sulfide from 15 increments of 50% fractional melt of recycled oceanic crust: melt composition: Os: 0.01 ppb; Ir: 0.01 ppb; Ru: 0.01 ppb; Pt: 0.8 ppb; Pd: 1.2 ppb: Re: 0.3 ppb; e) mixing with sulfides from 20 increments of basaltic melt (100% melting of recycled oceanic crust): melt composition Os: 0.01 ppb; Ir: 0.03 ppb, Ru: 0.04 ppb; Pt: 0.5 ppb, Pd: 0.9 ppb, Re: 1 ppb. Lines in d) from top to bottom represent percentages of peridotite derived sulfide of 10, 20, 30, 40 and 50 %. Lines in e) from top to bottom represent percentages of peridotite derived sulfide of 0, 1, 5, 10, 20 and 30%. Dashed line in e) represents sulfide cumulate from 10 increments of melt. Shaded fields represent observed Totalp pyroxenite composition: type A pyroxenites in a) and d); type B pyroxenites in b), c) and e).

A possible mechanism to produce the observed enrichments of PPGE and Re over IPGE may be cumulate precipitation of sulfides from a basaltic melt during multiple episodes of melt-rock interaction in an open system, as outlined by Rehkämper et al. (1999a). As the pyroxenite layers may represent zones of high melt flow, the contribution from peridotite wall rock can expected to be rather small. For modeling sulfide cumulation from basaltic melts, we adopted the model and parameters by Rehkämper et al. (1999a). Multiple batches of basaltic melt were assumed to precipitate 50 ppm of sulfide in equilibrium from each batch of S-saturated melt. Sulfide - silicate partition coefficients for PGE were taken from Fleet et al. (1999; $D^{HSE}_{sulfide/silicate}$: Os: 10000; Ir: 50000; Ru: 7000; Pt: 10000; Pd: 25000). Rhenium was assumed to be chalcophile about one order of magnitude less (Roy-Barman et al., 1998; Fonseca et al., 2007). The $D^{Re}_{sulfide/silicate}$ values are not well constrained, but even lower values have no large influence on the model results.

While mss-sulfide melt partitioning seems to control HSE partitioning during melting of either peridotitic or mafic mantle sources, it likely does not apply to sulfide crystallization from silicate melt. Due to increasing solubility of sulfur in silicate melt with decreasing pressure (Mavrogenes and O'Neill, 1999; Holzheid and Grove, 2002; O'Neill and Mavrogenes, 2002), ascending basaltic melts may become S-undersaturated, even if they were formed under S-saturated conditions. Sulfide saturation of S-undersaturated melts may only be reached after crystallization of some portion of the silicate melt, likely pyroxene cumulates. Sulfide melt forming upon reaching sulfur saturation carries the HSE signature of the melt, as HSE would be controlled by sulfide – silicate partitioning at this point. For the model purpose, it does not matter whether the precipitating sulfides were carried in the infiltrating batch of basaltic melt in an immiscible sulfide liquid, or dissolved in silicate melt and exsolving only upon sulfide saturation due to progressive pyroxene crystallization. Consequently, no sulfide solid – sulfide liquid equilibria were assumed to influence HSE behaviour upon crystallization of sulfide, in accordance with observation on sulfide segregation during MORB differentiation (Rehkämper et al., 1999a,b).

Additionally, sulfides are possibly precipitated from silicate melt in disequilibrium for HSE trace elements (Campbell and Naldrett, 1979), leaving large uncertainties for possible melt compositions. Possible contribution of fractional crystallization of sulfides during Totalp

pyroxenite formation is also difficult to evaluate, because of sulfide major element homogeneity, strong, non-systematic HSE trace element heterogeneity and the presence of serpentinization-associated sulfide minerals (godlevskite, native Cu).

Mixture of cumulates from multiple melt batches with small amounts of peridotite with 640 ppm sulfide (McDonough and Sun, 1995) match the observed type A and B Totalp pyroxenite patterns fairly well, with the possible exception of Pt (Figure 3.10 d), e). Websterites may have formed as mixtures from larger amounts of peridotites with cumulates, while clinopyroxenites contain little or no contribution from peridotite host rock. Formation of pyroxenites as cumulates in zones of high melt/rock ratio is thus consistent with observed HSE signatures (Figure 3.10 d), e).

This is in accordance with in situ data for sulfides from two pyroxenites, which show a larger variability of Pd/Ir and Re/Os, than of Os/Ir and Ru/Ir and, thus, mimic the observations for whole rock samples. Furthermore, the sulfides show a spectrum of compositions that range from "lherzolitic" in Os/Ir and Ru/Ir, to suprachondritic for HSE ratios involving incompatible HSE in the numerator. Clearly, these sulfides cannot be in equilibrium with each other.

While ratios of compatible HSE Os/Ir and Ru/Ir vary little within one section, large variations are observed in Re/Ir and Pd/Ir, as previously described for in situ analyses of sulfides in peridotites (Alard et al., 2000; 2002; Luguet et al., 2001; 2003; 2007; Lorand et al., 2008). The low Pd/Ir and Re/Ir sulfides may be interpreted as a depleted component inherited from the residual peridotite (Alard et al., 2000; 2002; 2005), while the high Pd/Ir and Re/Ir sulfides may have been subsequently added or modified by intruding melt.

These observations imply generation of small-scale HSE heterogeneities resulting from melt-rock interaction processes in the mantle. Given that sulfides sited within 1 cm of each other clearly are in disequilibrium with respect to the HSE, single grain analyses of mantle sulfides may not be representative of the whole rock, especially for the more mobile elements Pd and Re. The heterogeneous distribution of HSE abundances, as well as the difficulty in identifying a Pt carrier phase, testifies to the difficulty of obtaining reliable mass balance constraints for the HSE on the basis of mineral compositions.

3.4.3 Websterite and Clinopyroxenite Formation

As demonstrated above, Totalp pyroxenites likely underwent a complex history of melting and precipitation. Broad correlations of HSE with lithophile elements (Figures 3.2, 3.4) suggest that the HSE and lithophile elements may not be considered totally decoupled from each other. Totalp pyroxenites show both pyroxene macro- and megacryst cumulate textures and remnants of trapped melt, indicating multiple petrogenetic processes during their formation. Petrographic evidence from modally layered pyroxenites of several dm thickness (e. g., samples TA54, TA55) shows that websterites typically occur adjacent to peridotites, sometimes forming a 'boundary' between peridotite and clinopyroxenite.

These observations along with geochemical characteristics are most easily explained by open-system interaction of olivine-undersaturated melt with wall rock peridotite and precipitation of high-Al pyroxene, garnet, and occasionally spinel (O'Hara, 1968) near the garnet-spinel peridotite transition to form pyroxenites. Both websterites and clinopyroxenites would thus represent strongly melt-influenced systems. While websterites represent products of melt-rock interaction at lower melt/peridotite ratio, clinopyroxenites can be considered melt-dominated systems with extremely high melt/peridotite ratios, in accordance with HSE signatures (Figures 3.7, 3.10, 3.11). Variation in initial γ_{Os} in clinopyroxenites suggests the presence of at least two different endmembers with very radiogenic Os isotopic compositions (Figure 3.7). Differences in γ_{Os} may reflect differences in age or Re/Os in the melts that produced the pyroxenites. This is supported by HSE heterogeneity observed in sulfides in samples TA11A2 and TA54A, especially for the mobile HSE Pd and Re.

A petrogenetic model for Totalp pyroxenite formation taking into account cumulate precipitation and interaction of peridotite with multiple melt batches is outlined in Figure 3.11b). Estimated clinopyroxene-spinel or clinopyroxene-garnet cumulate compositions overlap with websterite compositions and may show a wide range of Pd/Re and $^{187}Os/^{188}Os$ over a comparatively narrow range of Al_2O_3, depending on melt composition. Continuous re-reaction of these early precipitates with further batches of mafic, Al-rich melt and ongoing

precipitation of both pyroxene and melt-derived sulfide is assumed to result in the generation of Al-rich clinopyroxenites, in accordance with model calculations above (Figure 3.10).

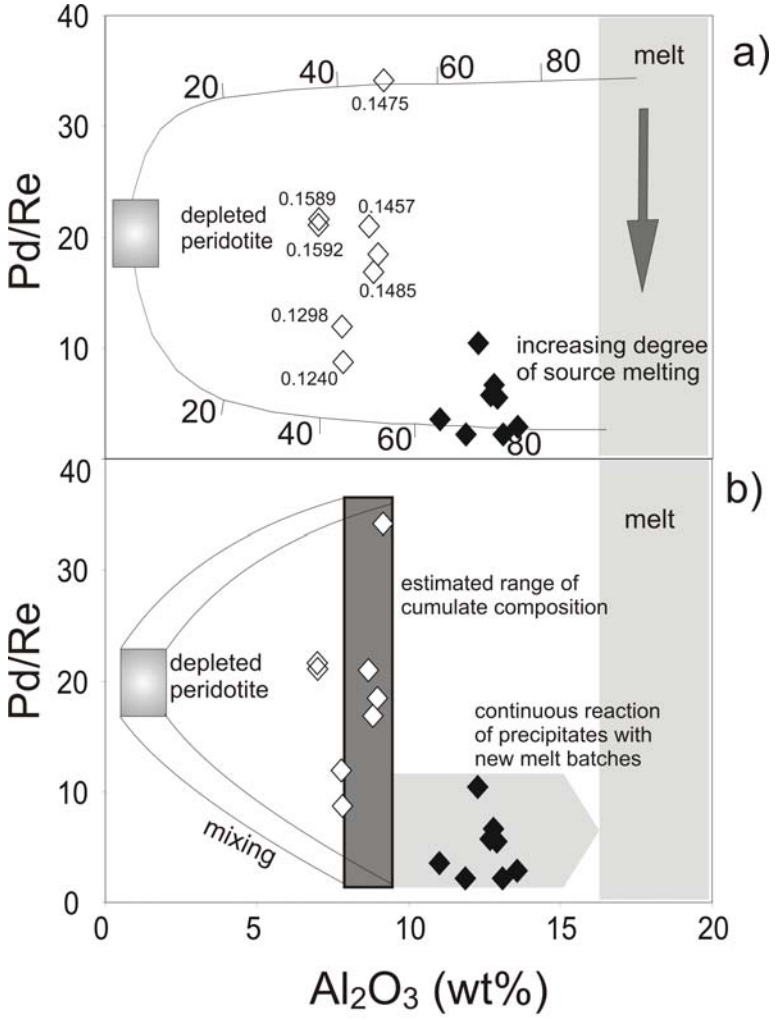

Figure 3.11: Al_2O_3 vs. Pd/Re; symbols as in Figure 1; a) mixing of depleted peridotite and melt formed by different degrees of melting of MORB (shaded area), While Al_2O_3 concentrations and Pd/Re ratios appear consistent with bulk mixing, absolute HSE concentrations in HSE cannot be reproduced (see text for discussion). Petrographic features indicate more complex processes than simple mixing of bulk melt and depleted peridotite; numbers next to open Al-poor pyroxenite symbols refer to the initial $^{187}Os^{188}Os$ isotopic composition of the respective samples; non systematic distribution suggests formation of websterites by multiple batches of melt; b) symbols as in Figure 1; alternative model of websterite and pyroxenite formation: cumulate pyroxene – garnet assemblage continuously reacts with new, Al-rich batches of melt. Pd/Re of melt in equilibrium with cumulate precipitates is difficult to constrain due to poorly constrained Re partitioning behaviour (see text for more detailed discussion).

The exact processes controlling HSE distribution during cumulate precipitation of sulfides are difficult to constrain for a variety of reasons. As sulfides in Totalp pyroxenites are clearly in disequilibrium with each other, melt composition is difficult to estimate. The largest uncertainties concern the behaviour of Re. Sulfide-silicate partitioning coefficients for Re are lower than for all other HSE, and are dependent of O_2 fugacity and silicate phase composition more than other HSE, and may be controlled by silicate phases to a significant amount (Righter and Hauri, 1998; Mallmann and O'Neill, 2007). In addition to fractionation because of less siderophile Re behaviour during sulfide precipitation, observed variation in Pd/Re in pyroxenites (Figure 3.11) may reflect degree of melting in the melt source, primordial heterogeneity between different melt sources or various degrees of depletion in the host peridotite prior to melt infiltration.

In summary, Totalp websterites contain sulfides segregated during cumulate formation from high-degree partial mantle melts of recycled oceanic crust alongside residual sulfide from depleted peridotite wall rock, leading to relatively high Os, Ir and Ru contents as well as the moderately radiogenic initial γ_{Os} (as high as +28), mostly inherited from peridotite. Elevated Pt, Pd and Re contents in both websterites and Al-rich clinopyroxenites require open system cumulate precipitation of sulfides from multiple melt batches. The clinopyroxenites contain less peridotite-derived sulfide and are in turn dominated by the HSE signature of the mafic melts from which they precipitated. This interpretation is also supported by the highly radiogenic initial γ_{Os} values of as high as +1700.

3.4.4 Pyroxenites and the ^{186}Os-^{187}Os systematics of mantle rocks

Coupled suprachondritic $^{187}Os/^{188}Os$ and $^{186}Os/^{188}Os$, have been reported for several mantle-derived systems (Walker et al., 1994; 1997; Brandon et al., 1998; 1999; 2003; Bird et al., 1999; Brandon and Walker, 2005). The isotopic enrichments require long term-isolation of precursor materials with suprachondritic Re/Os and Pt/Os, as required by the long half-

lives of the parent isotopes and their respective abundances (^{190}Pt, 0.0129%, λ = 1.542 x $10^{-12}a^{-1}$; ^{187}Re, 62.60%, λ = 1.6668 10^{-11} a^{-1}; Begemann et al., 2001; Selby et al., 2007). In order to produce the coupled suprachondritic $^{187}Os/^{188}Os$ and $^{186}Os/^{188}Os$ observed in some picrites and komatiites, entrainment of approx. 0.5% of high Re/Os and Pt/Os outer core material into the mantle and its subsequent incorporation into mantle plumes has been proposed (Walker et al., 1997; Brandon et al., 1998; 2006; Bird et al., 1999; Brandon and Walker, 2005). In a recent study Luguet et al. (2008) suggested that pyroxenite-derived sulfides in the mantle sources of some plume-derived lavas show the appropriate Pt-Re fractionations that might explain coupled $^{187}Os/^{188}Os$ - $^{186}Os/^{188}Os$ systematics in some picrites and komatiites. Here, we further assess the feasibility of pyroxenites as contributing sources for plume-derived lavas with suprachondritic ^{186}Os-^{187}Os systematics.

Pyroxenites from the Totalp massif show radiogenic initial $^{187}Os/^{188}Os$ coupled with chondritic to strongly suprachondritic Re/Os between 0.08 and 12.8, and Pt/Os between 0.57 and 15.9. The maxima of both ratios are at the lower end of the range reported for pyroxenites from Beni Bousera reported by Luguet et al. (2008). Pt/Re ratios of the whole rocks range between 0.79 and 14.8, well within the range reported by Luguet et al. (2008) for Beni Bousera pyroxenites. Thus, Totalp pyroxenites have strongly suprachondritic Re/Os and Pt/Os and will, with time, produce elevated $^{187}Os/^{188}Os$ and $^{186}Os/^{188}Os$, relative to chondrites. However, in order to match the coupled suprachondritic $^{187}Os/^{188}Os$–$^{186}Os/^{188}Os$ data observed in picrites from Hawaii, Brandon et al. (1999) calculated a required Pt/Re of ~ 88 – 100. Such high Pt/Re values are reported for only a minority of pyroxenites or pyroxenite hosted sulfides (Figure 3.12 a). The majority of pyroxenite samples studied for HSE will grow to radiogenic $^{187}Os/^{188}Os$ too rapidly (Figure 3.12 b). Mixtures of primitive mantle and these pyroxenites, as suggested to be present in the source of high $^{186}Os/^{188}Os$-basalts, cannot reproduce the observed Hawaiian-Siberian trend defined by Brandon et al. (1999), Walker et al. (1997) and Brandon and Walker (2005). Furthermore, pyroxenites tend to have low Os concentrations. To reproduce radiogenic $^{186}Os/^{188}Os$ observed in picrites by a mixed pyroxenite-peridotite source, the amount of pyroxenite and thus, by inference, recycled crust needs to unreasonably large.

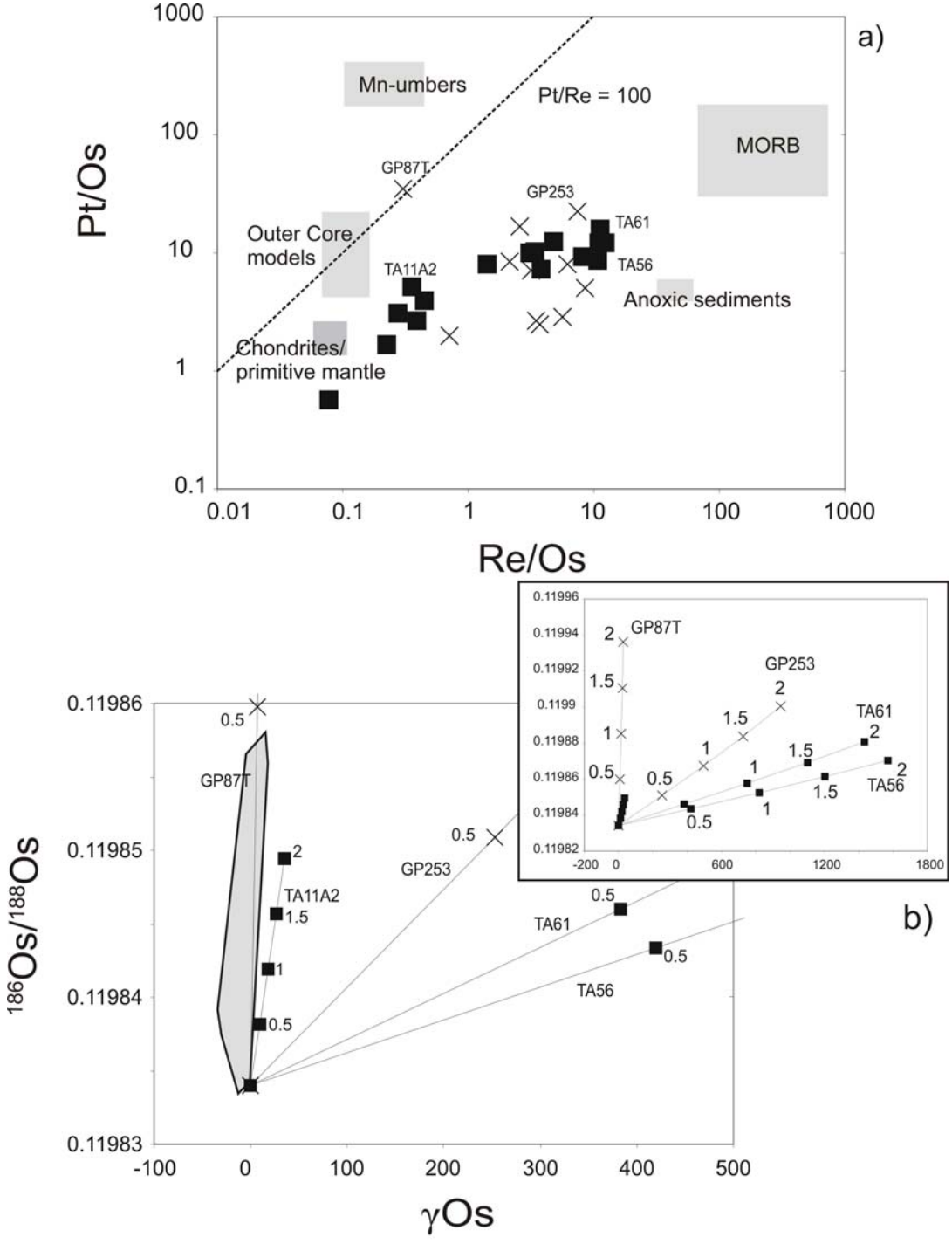
a)
Pt/Os
Re/Os
1000
100
10
1
0.1
0.01
0.1
1
10
100
1000
Mn-umbers
Pt/Re = 100
MORB
GP87T
GP253
TA61
TA56
Outer Core
models
TA11A2
Anoxic sediments
Chondrites/
primitive mantle
b)
$^{186}Os/^{188}Os$
γOs
0.11986
0.11985
0.11984
0.11983
-100
0
100
200
300
400
500
0.5
GP87T
2
TA11A2
1.5
1
0.5
GP253
0.5
TA61
0.5
TA56
0.11996
0.11994
0.11992
0.1199
0.11988
0.11986
0.11984
0.11982
-200
0
600
1200
1800
2
GP87T
1.5
1
0.5
GP253
2
1.5
1
0.5
TA61
2
1.5
1
0.5
TA56
2
1.5
1
0.5

Figure 3.12 (previous page): a) Pt/Os vs. Re/Os; squares: Totalp samples; crosses: Beni Bousera bulk rock pyroxenites from Luguet et al. (2008). Chondrite values from Horan et al. (2003); Primitive mantle from McDonough and Sun (1995); Walker et al. (1997) and Becker et al. (2006); Outer Core models from Brandon et al. (2003); Mn-umbers from Scherstén et al. (2004) and Ravizza et al. (2001); MORB from Escrig et al. (2005) and Bézos et al (2005); Reducing sediments from Ravizza and Pyle (1997) and Poirier (2006); b) $^{186}Os/^{188}Os$ vs. γOs; shaded area: Hawaiian, Gorgona Island and Siberian samples from Brandon et al. (1999; 2003); lines represent isotopic evolution of pyroxenite samples from Totalp and Beni Bousera over time from chondritic values over 2 Ga; dotted lines: development of Beni Bousera samples GP87T and GP253 (Luguet et al., 2008). Most studied pyroxenites have too low Pt/Re and develop radiogenic $^{187}Os/^{188}Os$ too rapidly compared to $^{186}Os/^{188}Os$ to account for observed Os isotopic systematics attributed to core-mantle interaction. Mixing of a source containing these pyroxenites and depleted mantle cannot reproduce the Hawaiian-Siberian trend of Brandon and Walker (2005).

Some base metal sulfides and Pt-rich alloys from eclogite, pyroxenites or ophiolites have the appropriate Pt/Re ratios (Luguet et al., 2008) that could produce the observed coupled $^{187}Os/^{188}Os$–$^{186}Os/^{188}Os$ systematics after sufficient isolation time. How representative such compositions are for samples on the scale of hand specimen or even larger mantle domains, however, remains an important open question. The heterogeneity in sulfide and alloy compositions and the contrasts with bulk rock HSE compositions reported here and in a variety of mantle rocks elsewhere indicate that the mass balance of such phases must be well constrained before extrapolations to whole rock compositions or even larger scale processes are possible.

3.5 Conclusions

Modeling results suggest that pyroxenites of the Totalp ultramafic massif formed as cumulates from melts reacting to various extents with pre-existing peridotite. The Pd and Re rich nature and radiogenic Os isotopic composition of the pyroxenites are consistent with derivation by partial melting of mafic components in the convecting mantle. Multiple melt batches derived from reservoirs with suprachondritic, but disparate Re/Os and $^{187}Os/^{188}Os$ are required to account for the different, radiogenic initial $^{187}Os/^{188}Os$ of the pyroxenites. Sulfide melt–mss partitioning of HSE during partial melting of subducted oceanic crust is capable of generating appropriate HSE fractionations observed in these rocks. Low degree melts carry a high Pd/Re signature similar to that seen in websterites, while higher degree melts have lower Pd/Re as displayed by the clinopyroxenites. Simple mixing of melt- and peridotite-derived

sulfides cannot reproduce the observed HSE patterns from Totalp pyroxenites. Cumulate precipitation of sulfides bearing a melt signature is required to account for the high HSE concentrations and fractionations observed.

While websterites represent addition of comparatively small amounts of melt-derived sulfide, clinopyroxenites may form in a melt-dominated system by reaction of websterites with further batches of pyroxene saturated melt, thus acquiring HSE and radiogenic Os isotope signature of high degree eclogite-derived melts.

Formation of websterites and clinopyroxenites in the Totalp massif can, thus, be attributed to melt-rock interaction; observed geochemical variations are both a function of variable source compositions of the melts, variable degree of melting of these sources, and melt – peridotite interaction. An origin as residues from in situ melting of either peridotite or slices of recycled oceanic crust appears unlikely.

The presence of pyroxenites in the source of high $^{186}Os/^{188}Os$ basalts cannot be confirmed. While some base metal sulfides and Pt-rich alloys have sufficiently high Pt/Re to produce the observed Os isotopic signature over time, small scale HSE heterogeneities cast doubt on the representativeness of these analyses. Analyses of bulk rock pyroxenites from both this study and from Luguet et al. (2008) show that most pyroxenite are too enriched in Re and consequently develop radiogenic $^{187}Os/^{188}Os$ too quickly. The presence of typical pyroxenites in the source of plume-related rocks cannot explain the ^{186}Os-^{187}Os systematics observed in Hawaiian, Gorgona Island and Siberian basalts suites.

Acknowledgements

We thank C. Behr, M. Feth, H. Frohna-Binder, A. Gottsche, K. Hammerschmidt, W. Michaelis, R. Milke, R. Naumann, B. Pracejus and I. Puchtel for technical assistance. Discussions with J.-P. Lorand, S.J. Barnes, V. Le Roux and O. Müntener are gratefully acknowledged. This work was partly funded by NSF grant EAR 0309810 to H. B. and R.J.W., EAR 0739006 to WFM and funds from the Freie Universität Berlin..

Table 3.1: Whole rock major, trace element and Os isotopic composition data for Totalp pyroxenites

Sample	lithology		Al_2O_3	MgO	CaO	Mg#	Os(ppb)	Ir(ppb)	Ru(ppb)	Pt(ppb)	Pd(ppb)	Re(ppb)	$^{187}Re/^{188}Os$	$^{187}Os/^{188}Os$	2 sd	$^{187}Os/^{188}Os$ 160Ma	γ_{Os} 160 Ma
TA-11A1	ol-websterite	b	8.97	26.2	11.7	0.891		0.69	1.90	5.47	12.9	0.93					
TA-11A2	ol-websterite	a	9.18	29.1	9.09	0.890	1.62	1.44	3.95	8.47	20.1	0.57	1.70	0.1521	1	0.1476	16.9
duplicate		b					1.63	1.39	3.20	8.12	19.1	0.55	1.61	0.1518	1	0.1475	16.9
TA-11B	ol-websterite	b	8.69	28.4	9.87	0.888	2.06	1.82	4.36	8.19	20.7	1.07	2.15	0.1514	1	0.1457	15.4
duplicate		b						1.83	4.32	8.32	21.2	0.93			1		
TA-13B	ol-websterite	a	7.01	27.2	9.91	0.890	2.40	1.96	4.14	3.99		0.53	1.07	0.1618	1	0.1589	25.9
duplicate		b						1.97	4.98	4.19	8.97	0.54					
TA-13D	ol-websterite	a	7.04	30.8	6.81	0.894	2.31	2.08	4.46	7.01		0.64	1.34	0.1643	1	0.1607	27.4
duplicate		b						2.13	4.64	6.55	6.23	0.64	1.38	0.1615	1	0.1578	25.1
duplicate		b					2.50	2.16	4.68	6.59	6.10	0.71					
TA-36A	websterite	a	7.84	20.4	15.1	0.903	4.64	0.68	1.84	2.67	3.10	0.36	0.370	0.1250	1	0.1240	-1.7
TA-54A	wehrlite	b	8.81	35.2	5.32	0.874	6.47	4.62	10.8	53.5	160	9.13	6.79	0.1666	1	0.1485	17.7
TA-54B	ol-clinopyroxenite	b	12.3	22.6	14.0	0.875	0.98	0.69	1.77	9.91	32.4	3.07	15.2	0.2156	1	0.1751	39
TA-54C1	ol-clinopyroxenite	b	12.8	22.0	14.0	0.877	0.10	0.08	0.21	1.36	3.34	0.51	24.6	0.647	11	0.581	360
duplicate		b												0.509	18		
TA-54C2	ol-clinopyroxenite	b	11.9	20.4	15.5	0.875	0.18	0.14	0.41	2.25	4.47	2.01	54.3	0.385	6	0.241	91
TA-54C3	ol-clinopyroxenite	b	13.1	18.9	15.8	0.860	0.67	0.51	1.40	5.87	15.7	7.92	53.2	0.294	4	0.152	20.3
duplicate		b												0.2953	1		
TA-54D	ol-clinopyroxenite	b	12.9	17.8	17.3	0.850	0.30	0.22	0.61	3.10	5.52	1.01	16.8	0.389	2	0.344	172
dupicate		b												0.375	2		
TA-55C	ol-websterite	b	7.78	27.5	6.75	0.883	3.44	2.77	7.09	9.09	16.0	1.33	1.89	0.1348	1	0.1298	2.8
TA-55D1	ol-websterite	b	12.7	21.5	12.6	0.867	0.52	0.41	0.94	3.81	11.3	1.96	18.9	0.279	2	0.228	81
TA-56	ol-clinopyroxenite	b	13.6	16.2	17.6	0.850	0.11	0.06	0.22	1.33	3.72	1.31	68.8	2.472	5	2.265	1700
duplicate		b												2.205	8		
TA-61	ol-clinopyroxenite	a	11.0	15.4	18.6	0.831	0.40	0.16	0.51	3.63		3.20	42.8	0.869	1	0.754	498
duplicate		b					0.24	0.16	0.47	3.82	10.5	2.69	62.7	0.884	3	0.725	475

a) measured at UMD, b) measured at FUB

Table 3.2: Sulfide major element compositions in websterites TA11A2 and TA54A

			S		Ni		Fe		Co		Cu	
sample	Grain #	# analyses	at%	2 sd	at%	2 sd	at%	2 sd	at%	2 sd	at%	2 sd
TA11A2	1	5	58.3	0.6	20.5	0.4	20.3	0.4	0.73	0.05	0.08	0.07
	2	3	57.5	0.6	20.1	0.1	21.0	0.5	1.30	0.09	0.11	0.06
	3	5	57.0	3.1	18.8	1.5	23.6	4.6	0.43	0.05	0.11	0.10
	4	4	58.1	0.5	21.1	0.3	20.3	0.2	0.45	0.06	0.07	0.05
	5	2	57.8		21.5		19.7		0.92		0.08	
	6	2	53.9		16.7		28.5		0.69		0.17	
	7	8	58.7	1.2	19.6	1.1	21.1	1.1	0.54	0.30	0.10	0.05
TA54A	1	4	45.1	2.8	51.7	2.9	1.37	3.28	0.13	0.21	1.69	5.29
	nc 2/4	4	0.03	0.0	4.04	1.7	0.38	0.65	0.05	0.07	95.5	1.9
	3	5	46.6	1.6	52.1	1.6	0.27	0.20	0.12	0.06	0.90	1.13
	4	3	46.9	0.0	52.7	0.1	0.10	0.05	0.15	0.03	0.12	0.05
	5	2	46.3		52.7		0.24		0.12		0.70	
	6	8	48.2	2.3	51.1	2.7	0.07	0.07	0.14	0.62	0.49	1.02
	7	10	46.7	1.5	52.3	2.2	0.41	0.60	0.26	1.00	0.29	0.50
	8	1	47.0		51.6		0.56		0.10		0.70	

Table 3.3: Sulfide trace element compositions for websterite TA11A2 and wehrlite TA54A

Sample	Grain	Mineral	Spot Size	**Ru**	**Pd**	**Re**	**Os**	**Ir**	**Pt**	**Os/Ir**	**Pd/Ir**	**Ru/Ir**	**Re/Os**	**Re/Ir**
TA11A2	1	Pn	40	0.81	2.77	0.35	0.10	0.06	<0.04	1.87	49.6	14.5	3.34	1.78
TA11A2	2	Pn	25	2.53	4.94	0.14	0.20	0.27	<0.12	0.77	18.5	9.49	0.67	0.88
TA11A2	2	Pn	25	0.84	4.61	0.14	0.15	0.11	<0.21	1.31	41.7	7.62	0.97	0.74
TA11A2	3	Pn	40	2.34	6.94	0.14	0.70	1.07	<0.07	0.65	6.5	2.18	0.20	0.30
TA11A2	3	Pn	40	3.27	7.80	0.09	1.03	1.19	<0.08	0.87	6.6	2.76	0.08	0.10
TA11A2	3	Pn	40	3.23	8.56	0.07	1.30	1.06	<0.04	1.22	8.1	3.04	0.06	0.05
TA11A2	3	Pn	30	1.72	7.88	0.09	0.84	0.83	<0.08	1.02	9.5	2.08	0.10	0.10
TA11A2	4	Pn	25	1.79	7.97	0.11	0.90	0.91	<0.16	0.99	8.7	1.96	0.12	0.12
TA11A2	5	Pn	30	4.90	5.48	0.20	2.33	1.44	<0.11	1.62	3.80	3.40	0.08	0.05
TA11A2	5	Pn	30	3.09	<0.17	0.11	1.43	1.40	<0.07	1.03	-	2.21	0.08	0.08
TA54A	2	Pn/Gdl	25	0.25	37.3	0.04	0.04	0.03	<0.02	1.66	1376	9.2	1.62	0.98
TA54A	2	Pn/Gdl	25	0.18	0.66	0.02	0.02	0.02	<0.02	0.98	26.7	7.4	0.7	0.67
TA54A	4	Pn/Gdl	25	12.5	4.66	2.23	1.62	1.48	<1.66	1.09	3.1	8.5	1.51	1.38
TA54A	6	Pn/Gdl	40	25.1	4.98	9.14	3.63	3.39	<0.78	1.07	1.5	7.4	2.69	2.52
TA54A	6	Pn/Gdl	40	5.16	0.91	2.30	0.75	0.56	<0.11	1.33	1.6	9.1	4.07	3.05
TA54A	6	Pn/Gdl	25	0.95	1.65	0.53	0.09	0.09	<0.11	1.04	18.7	10.8	6.04	5.81
TA54A	6	Pn/Gdl	25	0.20	<0.25	0.12	0.04	0.03	<0.01	1.40	-	7.0	4.07	2.92
TA54A	2	Cu	6	<2.04	15.9	<0.26	<0.45	1.35	0.07	-	-	-	-	-
TA54A	2	Cu	12	0.30	23.1	<0.05	<0.06	0.18	<2.58	-	-	-	-	-

Pn: pentlandite, Gdl: godlevskite; Cu: native copper

Table 3.4: melting model starting composition and mixing model endmembers

	Al2O3 (wt%)	**MgO (wt%)**	**CaO (wt%)**	**Os (ppb)**	**Ir (ppb)**	**Ru (ppb)**	**Pt (ppb)**	**Pd (ppb)**	**Re (ppb)**
MORB	14	8.5	11.5	0.004	0.05	0.07	0.55	0.9	1
depleted peridotite	1	43	1.4	4.5	4.5	8	4	1	0.05

Chapter 4

Refertilization of Jurassic oceanic peridotites from the Tethys Ocean – implications for the Re-Os systematics of the upper mantle

David van Acken*[a,b], Harry Becker[a] and Richard J. Walker[b]

a) Institut für Geologische Wissenschaften, AB Geochemie, Freie Universität Berlin, Malteserstr. 74 – 100, Haus B, D-12249 Berlin, Germany, Phone: +49 30 838 70200 Fax: +49 30 838 70170

b) University of Maryland, Department of Geology, College Park, Maryland 20742, USA

*Corresponding author

E-mail addresses: dvana@zedat.fu-berlin.de (D. van Acken), hbecker@zedat.fu-berlin.de (H. Becker), rjwalker@geol.umd.edu (R.J. Walker)

4.1 Abstract

The influence of melt migration and solid state mixing of pyroxenites on Re-Os isotopic and major element systematics of oceanic mantle rocks have been studied in serpentinized spinel lherzolites and associated spinel and spinel-garnet pyroxenite layers from the Totalp ultramafic massif near Davos (eastern Swiss Alps). The ultramafic body originally was emplaced and serpentinized on the Jurassic Liguria-Piedmont ocean floor and was little modified during the Alpine orogeny. Field and petrographic observations indicate that refertilization of the peridotites occurred by migration of melt between abundant websterite layers and the peridotites, as well as by mechanical stretching and thinning of websterite layers down to the sub-centimeter scale, thus producing fertile lherzolite compositions.

Osmium concentrations in the peridotites are in the range observed for normal upper mantle peridotites, whereas Re concentrations in some peridotites are substantially higher than typical mantle values (up to 0.76 ppb). Initial Os isotopic compositions and Re/Os ratios in the peridotites range from subchondritic to suprachondritic (γ_{Os} (160 Ma) between -5.5 and +7.2). Re/Os, γ_{Os} (160 Ma) and Re concentrations correlate with fertility indicators such as Al_2O_3 and Na_2O, suggesting limited influence of serpentinization on Re-Os systematics of the peridotites. These correlations extend beyond estimates for primitive upper mantle (PUM) compositions suggesting that depletion by partial melting cannot have been the only process producing the variations.

The pyroxenites generally have higher Re, (up to 3.2 ppb Re) but lower Os concentrations than lherzolites, and suprachondritic initial γ_{Os} (+9.0 to +497). Websterites with suprachondritic γ_{Os} (160 Ma) alternate with peridotites with chondritic or even subchondritic $^{187}Os/^{188}Os$, indicating substantial small-scale Os isotopic heterogeneity. The combined petrographic observations and contrasting compositions of peridotites and pyroxenites indicate that the correlations of γ_{Os} (160 Ma) with fertility indicators reflect mixing of peridotites with a long-term depletion history and Re-enriched Melts. The pyroxenites may represent residues of eclogites that melted during asthenospheric upwelling or could be cumulates which precipitated from asthenospheric melts.

These data provide new evidence that the lower section of the suboceanic lithospheric mantle contains fertile components that are enriched in Re and radiogenic Os. Melt migration evidently does not completely homogenize small scale Os isotopic heterogeneities in the lower lithosphere, thus accounting for the presence of old depleted peridotites in young oceanic lithospheric mantle.

Keywords: Re/Os, mantle, peridotites, pyroxenites, ultramafic massif, refertilization

4.2 Introduction

The ^{187}Re-^{187}Os decay system (λ_{187Re} = 1.666 x 10^{-11} a^{-1}, Smoliar et al., 1996) applied to mantle-derived rocks represents a versatile tracer to constrain processes ranging from late accretion to ancient melt extraction and recycling events in the Earth's mantle (Shirey and Walker 1998, and references therein). In mantle peridotites, Re and Os are mostly concentrated in trace sulfides and platinum group element (PGE) alloys (Morgan and Baedecker, 1983; Hart and Ravizza, 1996; Luguet et al., 2007). During mantle melting, Re behaves as a moderately incompatible element, whereas Os is normally highly compatible (Morgan, 1986; Hauri and Hart, 1997; Shirey and Walker, 1998; Burton et al., 2000). Residual peridotites depleted in Re by partial melting will, thus, evolve to subchondritic $^{187}Os/^{188}Os$. In contrast, crustal rocks with high Re/Os quickly develop highly suprachondritic $^{187}Os/^{188}Os$ (e. g., Roy-Barman and Allègre, 1994; Schiano et al., 1997; Shirey and Walker, 1998).

Early studies of the Re-Os systematics of mantle rocks led to the conclusion that melt extraction is the main control on Re and Os abundances and, consequently, the $^{187}Os/^{188}Os$ of mantle peridotites (Walker et al., 1989; Reisberg and Lorand, 1995; Shirey and Walker, 1998, and references therein). Effects of secondary melt or fluid migration on Re-Os systematics of peridotites were presumed to be minor (e. g., Handler et al., 1997). A number of studies over the last 10 years, however, have changed this picture. Detailed Re-Os work, in combination with other radiogenic isotopes and trace elements has shown that Re and Os abundances and $^{187}Os/^{188}Os$ of mantle peridotites can be significantly affected by at least two different styles

of melt or fluid migration in the mantle. Melt percolation by porous flow at high melt/rock ratios leads to the formation of replacive dunites and harzburgites (Kelemen et al., 1997). This open-system process may produce lower than normal abundances of the compatible Ir group PGE (Os, Ir, Ru), low Re abundances, and often chondritic to suprachondritic $^{187}Os/^{188}Os$ in the modified peridotites. These variations have been most clearly noted in spatially-controlled Re-Os studies of peridotite massifs, and may reflect dissolution of sulfides, along with pyroxenes, in percolating basic melt, and addition of radiogenic Os from such melts (Becker et al., 2001; Büchl et al., 2002; 2004). Similar compositional features, although less clearly documented, occur in peridotite xenoliths (e. g. Handler et al., 1997, 2005; Brandon et al., 1999; Schmidt and Snow, 2002; Pearson et al., 2003; 2004; Reisberg et al., 2005) and possibly in abyssal peridotites (Standish et al., 2002; Harvey et al., 2006).

Melt addition at low melt/rock ratios leads to a very different manifestation of mantle metasomatism. These conditions likely prevail in the lithospheric mantle where cooling magma may precipitate pyroxenes and sulfides, leading to addition of basaltic components to previously depleted peridotites ('refertilization') (see reviews of Bodinier and Godard, 2003; Pearson et al., 2003). Considerable uncertainties remain regarding the behavior of Re, Os and other highly siderophile elements (HSE) during these secondary mantle processes. Since for a number of elements (including the HSE), fertile lherzolites represent the most reliable material to constrain the composition of Earth's primitive upper mantle (PUM; a hypothetical primitive upper mantle reservoir), the influence of melt migration and refertilization on Os isotopes and HSE abundances in lherzolites needs to be better understood.

The purpose of the present work is to investigate the importance melt migration processes on Re-Os systematics of the deeper suboceanic mantle in a detailed study of fertile spinel lherzolites emplaced on the Jurassic Piedmont-Liguria ocean floor, and now exposed in the Totalp ultramafic massif in the Eastern Swiss Alps. The Totalp massif provides a rare opportunity to study the deeper section of suboceanic lithosphere in a very slow-spreading environment not unlike modern occurrences from the Arctic Ocean (Michael et al., 2003). Field and petrographic observations as well as major element compositions of the ultramafic rocks show evidence for melt migration and related refertilization that may have occurred near the transition from asthenosphere to lithosphere. We also discuss the role of pyroxenite

layers as sources of Re and radiogenic Os in the generation of Os isotopic heterogeneities in the convecting mantle.

4.3 Results

Volatile-free calculated major element oxide concentrations and Re-Os data are listed in Table 4.1. The complete set of major element data, including water and C contents, is provided in the electronic supplement table. In the following, volatile-free calculated major element data are used. The Al_2O_3-content of the peridotites ranges from 1.82 to 4.47 wt%, with 20 out of 26 samples between 3 and 4%. In the websterites, Al_2O_3 ranges between 7.01 and 9.18%. Notably, there are no samples within this sample set that would bridge the gap between 4.5 and 7% wt% Al_2O_3. Na_2O in peridotites lies between 0.05 and 0.32%, while values in pyroxenites lie between 0.49 and 0.59%. MgO in the peridotites covers a range from 37.0 to 42.7%. The websterites have lower MgO from 27.2 to 30.8%. The Mg-number (Mg#; $Mg/(Mg+Fe^{2+})$ of the peridotites varies between 0.888 and 0.910, with most samples having Mg# between 0.890 and 0.900; also consistent with a rather homogeneous composition of peridotites in the ultramafic body. Sample TA22A1, a cpx-enriched layer next to a depleted lherzolite domain (TA22A2) shows an unusual composition, it has peridotite-like Al_2O_3 (3.26%), but high Na_2O (0.36%), along with low MgO (34.4%), values in-between those typical for peridotites and websterites. A garnet-bearing clinopyroxenite, TA61, has low Mg (15.40%), but high Al_2O_3 (11.03), and Na_2O (0.96%). Well defined negative correlations exist between MgO and both Al_2O_3 and Na_2O (Figure 4.1), similar to those previously reported for suites of orogenic and ophiolitic peridotites (e.g. Frey et al., 1985; Pearson et al., 1993; Asimov, 1999; Takazawa et al., 2000; Bodinier and Godard, 2003).

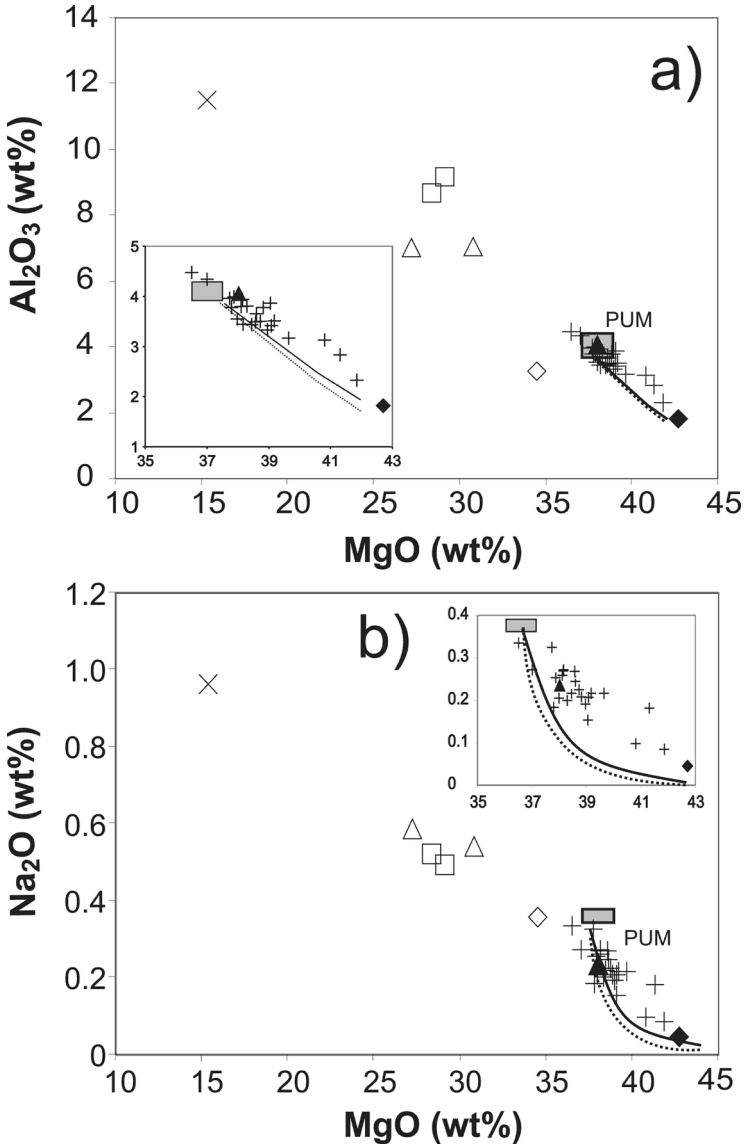

Figure 4.1: a) Al_2O_3 plotted versus MgO b) Na_2O plotted against MgO. box indicates: primitive upper mantle, PUM compositions according to McDonough and Sun (1995), Meisel et al. (2001) and Becker et al. (2006), lines show melting trends according to modeling by Niu (1997) and Baker and Beckett (1999); dashed line: fractional melting, solid line: batch melting. According to Niu (1997) excess olivine is generated during the generation of melt and consumption of pyroxene; see Appendix A from Niu (1997) for details. Baker and Beckett (1999) calculated peridotite compositions from mineral modes and phase compositions, without significant olivine accumulation during mantle melting. A melting trend was fitted to suit the observed data from abyssal peridotites best. Although the proposed mechanisms and reactions from the two references are explicitly different, the resulting melting paths in MgO/Al_2O_3–Na_2O–diagrams are not discernable. Open symbols represent websterites, closed symbols peridotites in composite websterite-peridotite samples; Crosses: peridotite samples, squares: sample TA11, triangles: sample TA13, diamonds: sample TA22, diagonal cross: sample TA61; error bars are symbol size or smaller.

Measured and age-corrected $^{187}Os/^{188}Os$ in the peridotite samples range from subchondritic to moderately suprachondritic values. Differences between measured and age-corrected $^{187}Os/^{188}Os$ are minor (Table 4.1). Age-corrected $^{187}Os/^{188}Os$ values in peridotites range from 0.1200 to 0.1361, corresponding to deviations from a mean chondritic $^{187}Os/^{188}Os$ at 160 Ma (γ_{Os} (160 Ma)) of -5.5 to +7.2 (Shirey and Walker, 1998). Nine samples have γ_{Os} (160 Ma) in the narrow range between -1.5 and +1.5. Osmium abundances in peridotites range from 0.20 ppb to 5.08 ppb, with most samples falling in the range between 3 and 4 ppb Os, typical of lherzolites from massifs and xenoliths worldwide (Reisberg et al., 1991; Meisel et al., 1996; 2001; Saal et al., 2001; Büchl et al., 2002; Pearson et al., 2004; Harvey et al., 2006; Becker et al., 2006). Rhenium abundances vary from 0.009 to 0.712 ppb, with most peridotites showing higher Re abundances than previously reported for lherzolites. (e.g. Saal et al., 2001; Meisel et al., 2001; Büchl et al., 2002; Pearson et al., 2004; Harvey et al., 2006).

Duplicate analyses were conducted on different powder splits in order to check sample homogeneity. The repeat analyses are in good agreement for $^{187}Os/^{188}Os$, with the exception of sample TA38, where the duplicate produced significantly different Os isotopic composition. Duplicate analyses yield similar Os abundances. The reproducibility for Re abundances is rather poor, with significantly different values occurring for duplicates of samples TA 18 and TA38.

Websteritic layers have age-corrected $^{187}Os/^{188}Os$ substantially more radiogenic than peridotites. Ratios range from 0.1384 to 0.1608, corresponding to γ_{Os}(160 Ma) of +9.0 to +26.6. Osmium abundances are relatively high, ranging between 1.62 and 3.12 ppb. The websterites also show relatively high Re abundances between 0.53 and 1.07 ppb. The garnet-clinopyroxenite sample TA61 has an extremely radiogenic $^{187}Os/^{188}Os$ ratio of 0.7544, corresponding to a γ_{Os}(160 Ma) of +494, combined with an Os and Re abundance of 0.40 ppb and 3.20 ppb, respectively. Several composite samples of spinel websterites interlayered with lherzolites were studied. Websteritic samples TA11A2 and TA11B, taken centimeters apart, have moderately high $^{187}Os/^{188}Os$ (γ_{Os} = +14.1 and +16.3) and high, but variable Re (0.545 to 1.068 ppb) abundances. Samples TA13B-C-D have radiogenic websterite layers (TA13B and TA13D, γ_{Os} = +25.2 and +26.6) within a few centimeters of a less radiogenic lherzolite (TA13C, γ_{Os} = +0.6). The websteritic sample TA22A1 (discussed above) forms a 1 cm-wide

cpx-enriched layer located in the most depleted lherzolite of the sample set, TA22A2. This websterite is radiogenic (γ_{Os} = +9.0) and rich in Re (0.555 ppb), while the lherzolite host rock has subchondritic γ_{Os}(160 Ma) of -3.1 and is relatively depleted in Re (0.204 ppb).

Rhenium and Re/Os show rough positive correlations with Al_2O_3 for the peridotites, as well as for the complete peridotite-pyroxenite dataset (Figure 4.2), with less scatter for Re/Os than for Re. The high-Re samples form a positive trend subparallel to the trend defined by the low-Re samples. Peridotites and pyroxenites (Figure 4.2 b) show suprachondritic Re/Os by a factor of up to 2.5 for some peridotites, and up to 7 for websterite layers. Na_2O shows a good positive correlation with Re (Figure 4.2 c).

Peridotites and pyroxenites show a broad positive correlation between γ_{Os}(160 Ma) and $^{187}Re/^{188}Os$, with increasing scatter towards high $^{187}Re/^{188}Os$ (Figure 4.3). $^{187}Re/^{188}Os$ in the peridotites varies between 0.225 and 1.257 (the chondritic ratio averages ~0.4). As expected from their higher Re and Re/Os, the pyroxenites tend to have higher γ_{Os}(160 Ma) compared to the peridotites.

There is no good correlation between γ_{Os} (160 Ma) and Os concentration, although samples with suprachondritic ratios tend to have somewhat lower Os concentrations than samples with chondritic or subchondritic ratios. However, γ_{Os} (160 Ma) correlates well with Al_2O_3, with some samples plotting off the main trend towards higher γ_{Os} (TA14, TA22A1 and TA22A2; Figure 3.4). Overall, Re abundances, Re/Os and γ_{Os} (160 Ma) show increasing scatter with increasing abundances of lithophile elements (Figs. 3.2-3.4).

While many peridotites from the Totalp massif are characterized by $^{187}Os/^{188}Os$ typical for mantle rocks, $^{187}Os/^{188}Os$ in some peridotites is significantly elevated compared to most results from studies of mantle xenoliths and ultramafic massifs which report mostly subchondritic to chondritic ratios (e.g. Reisberg and Lorand, 1995; Meisel et al., 1996; Saal et al., 2001; Pearson et al., 2004).

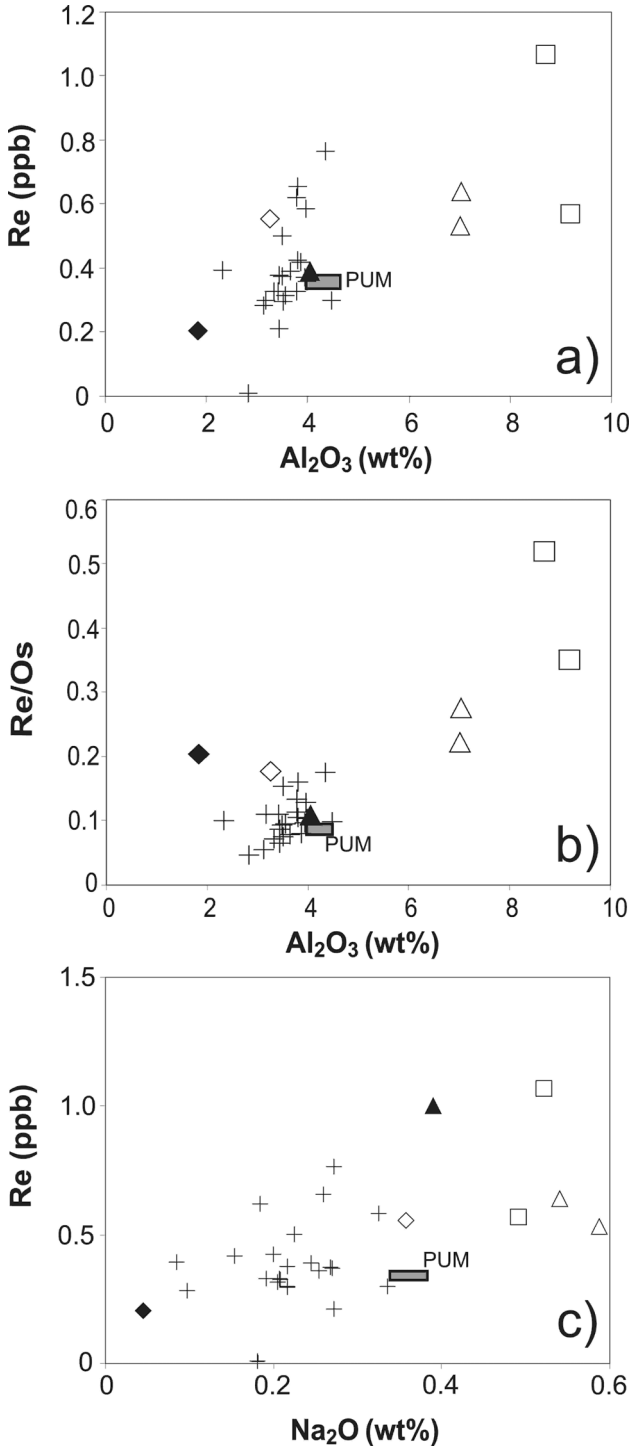

Figure 4.2: a) Re vs. Al_2O_3; b) Re/Os vs. Al_2O_3 c) Re vs. Na_2O; Symbols as in Figure 3.1, error bars are symbol size or smaller. Pyroxenite TA61 plots off the scale of the figure and is not shown.

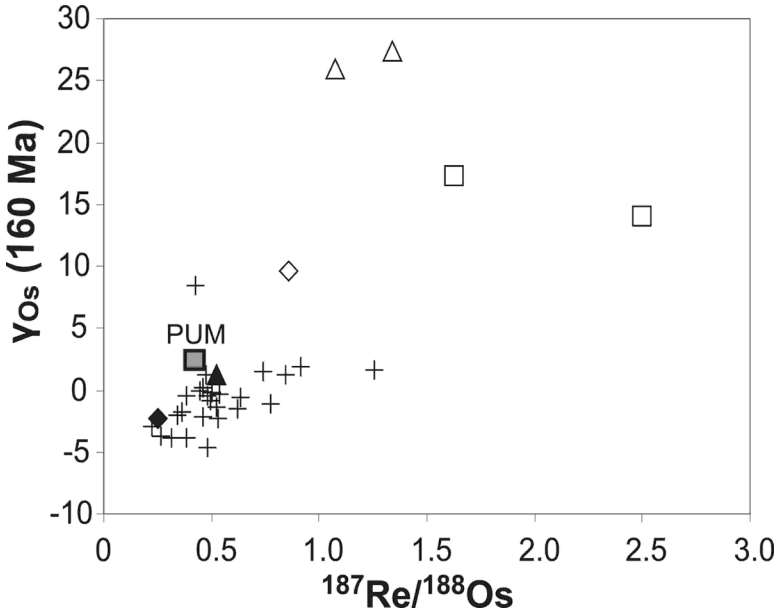

Figure 4.3: γ_{Os}(160 Ma) vs. $^{187}Re/^{188}Os$, Symbols as in Figure 2, error bars are symbol size or smaller. Pyroxenite TA61 plots off the scale of the figure and is not shown.

Several processes have been discussed as possible causes for variations in $^{187}Os/^{188}Os$ and Re abundances in upper mantle peridotites: a) near-surface alteration and serpentinization (Snow and Reisberg, 1995; Walker et al., 1996; Standish et al., 2002); b) melt extraction from a near-primitive lherzolite mantle composition and long-term retardation of ingrowth of radiogenic Os (e.g. Reisberg and Lorand, 1995; Meisel et al. 2001); c) mantle metasomatism by melt infiltration (e.g. Brandon et al., 1996; 1999; Becker et al., 2001; 2006; Büchl et al., 2002; Pearson et al., 2004); d) mantle refertilization by stretching of mafic layers derived from subducted oceanic crust during convective stirring in the mantle (Reisberg et al., 1991; Roy-Barman et al., 1996; Becker et al., 2001; 2006).

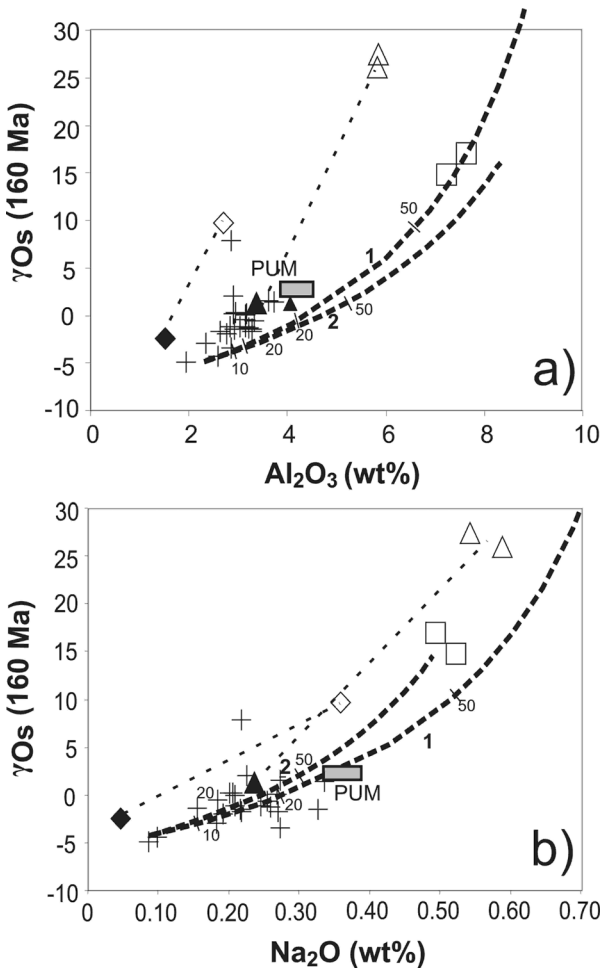

Figure 4.4: a) γ_{Os} (160 Ma) versus Al_2O_3; b) γ_{Os} (160 Ma) versus Na_2O; PUM values from Meisel et al. (2001). Symbols as in Figure 3.1. Thin dashed line connects a depleted peridotite and a websterite layer from samples TA13 (triangles) and TA22A (diamonds). Thick dashed lines denote mixing between typical depleted peridotite (Al_2O_3: 2.3%; Na_2O: 0.1%; γ_{Os} (160 Ma): -5) and 1) a clinopyroxenite (Al_2O_3: 11%; Na_2O: 0.95%; γ_{Os} (160 Ma) 480; e.g. TA61), and 2) a typical websterite (Al_2O_3: 8% ; Na_2O: 0.5%; γ_{Os} (160 Ma): +19; e.g. TA11A2, TA13B, TA13D); Error bars are symbol size or smaller. Pyroxenite TA61 plotting off scale is not shown. Mixing models indicate that bulk mixing between depleted peridotite and reasonable amounts of a single pyroxenite cannot explain the observed correlations.

4.4 Discussion

Among these processes, alteration processes due to weathering or serpentinization can be eliminated as a main cause for the range of Os isotopic variations in the Totalp suite. First, brown crusts that reflect weathering of serpentinite were removed prior to sample processing. Second, correlations between $^{187}Os/^{188}Os$ (160 Ma), Re and fertility indicators such as Al_2O_3 (Figures 3.2 and 3.4) suggest that the observed Re-Os systematics of Totalp peridotites have an igneous origin and that effects of serpentinization are negligible (e. g., Reisberg and Lorand, 1995; Meisel et al., 1996; Reisberg et al. 2005; Becker et al., 2001, 2006). This is further illustrated by the observation that the most radiogenic and Re-rich samples are pyroxenites (TA13B and D, TA11, TA61), which are less altered than the peridotites. The apparently limited mobility of Re and Os in serpentinized peridotites may reflect the reducing conditions during serpentinization (Snow and Schmidt, 1998; Rehkämper et al., 1999a; Büchl et al., 2002).

4.4.1 Partial melting and refertilization of peridotites

In the past, negative correlations of moderately incompatible elements such as Al or Na with MgO in peridotites have been interpreted to reflect varying amounts of melt extraction (Walter, 2003 and references therein). Elthon (1992), however, noticed that linear trends of Na_2O with MgO in suites of abyssal peridotites could not have been produced by fractional melting processes, as Na should be more rapidly depleted by progressive partial melting than observed in peridotites. He suggested that such correlations may originate from refertilization of depleted peridotites by addition of up to 10% of basaltic liquids. The data for Totalp peridotites also display a linear correlation between Na_2O and MgO which lies significantly above curves for both batch and fractional melting of fertile lherzolite (Figure 3.1), but is consistent with precipitation of clinopyroxene from melts during porous melt flow and melt-rock reaction (Müntener et al., 2004). Detailed studies of orogenic peridotites and xenoliths

indicate that many lherzolites have undergone pyroxene addition from percolating melts (Bodinier and Godard, 2003; Pearson et al., 2003).

A spectacular example of refertilization has been reported from the Lherz peridotite massif, where harzburgitic mantle rocks were transformed into lherzolites by influx of LREE depleted melt under conditions of the asthenosphere-lithosphere transition (Le Roux et al., 2007). Bulk compositions and textural evidence suggest that similar processes have affected the lherzolites at Totalp. Transport of material between websterites and lherzolites at Totalp is clearly indicated by networks of pyroxene-rich veins between these lithologies (see Appendix) and irregular patches that show modal enrichment of pyroxenes and spinel. These igneous textures were little affected by subsolidus textural reequilibration, indicating that mass transfer between pyroxenites and peridotites occurred under magmatic conditions. The absence of plagioclase in lherzolites and pyroxenites, the presence of exsolved garnet in some pyroxenites and exsolved megacrystic pyroxenes (up to 10 cm) suggest that the refertilization processes in the Totalp peridotites also occurred at conditions near the asthenosphere-lithosphere transition (1300 – 1400°C, 20 - 25 kbar, Gasparik, 1984). It remains elusive what the original composition of the peridotites might have been. The lherzolite with the lowest Al_2O_3 content (1.8 wt. %, TA22A2) provides a hint that depleted peridotite compositions may have been present prior to refertilization. Two end-member processes for refertilization have been proposed by Bodinier and Godard (2003): a) infiltration of equilibrium partial melt in residual depleted peridotite and b) fractional infiltration along a thermal gradient involving melt-consuming reactions and dissolution of peridotite minerals.

4.4.2 Influence of refertilization on Re-Os systematics

In the past, positive correlations between Al_2O_3, Re/Os and $^{187}Os/^{188}Os$ in peridotites were generally assumed to reflect variable degrees of melt extraction of cogenetic samples (Reisberg and Lorand 1995; Peslier et al. 2000; Meisel et al. 2001; Gao et al. 2002; Reisberg et al. 2005). This assumption led to the interpretation of Os model ages to reflect formation ages of the lithospheric mantle. If the variation of moderately incompatible lithophile elements in peridotites is controlled by mixing of depleted peridotite with mineral precipitates

from melts, this could also affect the Re-Os systematics and the interpretation of Os model ages of peridotites. Rhenium and γ_{Os}(160Ma) in the Totalp lherzolites correlate with Na_2O (Figure 3.2), which suggests that the Re-Os systematics of the peridotites were controlled by the same refertilization processes as the Na_2O abundances. While a positive correlation between initial γ_{Os} and lithophile elements may be consistent with melt extraction in the past, some peridotites from the Totalp massif show $^{187}Os/^{188}Os$, Re/Os, and Re concentrations of up to 0.712 ppb Re (Table 1) that are higher than estimates for the primitive upper mantle (PUM, (Meisel et al., 2001), and thus, can not reflect simple melt extraction. Accordingly, Re depletion model ages of individual peridotite samples (Shirey and Walker 1998) range from 1.32 Ga to future ages.

These data, along with textural observations and the rhenium-enriched nature of the associated pyroxenites, suggest that mixing between rhenium-depleted peridotites and rhenium-enriched pyroxenite-derived components represents the main control on variations of Re abundances, Re/Os and $^{187}Os/^{188}Os$ in the lherzolites at Totalp. Different subparallel trends of Al_2O_3, γ_{Os} (160 Ma) and Re for layered pyroxenite-peridotite samples (Figure 3.2 a) and 3.4 a) may reflect mixing between depleted peridotite and melts with a varying degrees of enrichment in Re and γ_{Os}.

The addition of radiogenic Os, mostly to refractory harzburgites and dunites via melt percolation was suggested by several recent studies (Brandon et al., 1999; Becker et al. 2001; 2004; Saal et al. 2001; Büchl et al. 2002; 2004; Schmidt and Snow, 2002; Pearson et al., 2004). The effect of a migrating mafic melt on the Re and Os budget of residual peridotite is strongly influenced by the degree of sulfur saturation in the melt and its interaction with preexisting residual mantle sulfide grains (Mavrogenes and O'Neill, 1999; Bockrath et al., 2004; Brenan et al., 2005). Sulfur undersaturated melts may remove sulfides and HSE, whereas sulfur saturated melts may precipitate sulfides and add HSE to residual peridotites. On the basis of Os isotopic variations, trace element abundances and lithophile element radiogenic isotope variations, it has been argued that at the high melt/rock ratios and open-system conditions likely associated with replacive dunite-harzburgite rocks, sulfide, Re and Os abundances may be depleted and $^{187}Os/^{188}Os$ of the reacted peridotite will be strongly influenced by the melt composition (Becker et al., 2001; Büchl et al., 2002; 2004). At lower

melt/rock ratios, for instance during melt infiltration and pyroxene precipitation in lherzolites, smaller quantities of radiogenic Os may be added to peridotites, and this may not be detectable (Becker et al., 2001). Correlation of chalcophile elements such as Re with lithophile elements, as in the case in the Totalp rocks suggests coprecipitation of sulfides along with pyroxenes (Becker et al., 2001; Saal et al. 2001).

Substantial Os isotopic contrasts across layered websterite-lherzolite rocks from Totalp indicate that melt infiltration and mineral precipitation apparently did not result in centimeter-scale Os isotopic equilibration. In previous studies of peridotites, substantial differences in Os isotopic composition and PGE patterns of sulfides and PGE alloy inclusions in olivines and spinels have been noted when compared to interstitial grain boundary sulfides, the latter typically showing more radiogenic $^{187}Os/^{188}Os$ and also different major and trace element compositions (Olive et al., 1997; Burton et al., 1999; Chesley et al., 1999; Alard et al., 2000; 2005; Pearson et al., 2002; Reisberg et al., 2005). In all cases melt infiltration has been implicated as a cause for Os isotopic disequilibrium. These results can be explained only, if substantial dissolution of preexisting peridotite minerals in the infiltrating melt did not occur.

4.4.3 Refertilization by ductile stretching of pyroxenites

While material exchange by the transport of melts and mineral-melt equilibria have played a major role in causing the compositional variations in the Totalp rocks, ductile stretching and thinning of websterite layers down to the sub-centimeter scale represents another prominent feature in the Totalp ultramafic massif. Mechanical mixing of peridotites and pyroxenites by ductile stretching and folding has been reported from other peridotite massifs and the creation of mixed lithologies with "enriched" radiogenic isotope signatures has been discussed in previous studies (e.g., Polvé and Allègre, 1980; Allègre and Turcotte, 1986; Becker, 1996b; Toramaru et al., 2001; Becker et al., 2001; Pearson and Nowell, 2004). The extent to which solid state mixing processes may be responsible for some of the chemical variations in Figures 3.1 – 3.4, is difficult to evaluate. The layered sample TA22A may reflect solid state mixing processes, with TA22A1 representing an "atypical" lherzolite composition (low Al_2O_3 of 3.26 and high Na_2O of 0.36, see Table 1) and showing macroscopic evidence for being a

mixture of a disintegrating websterite layer, and the corresponding depleted lherzolite (TA22A2). In contrast, other layered samples, most notably TA11 and TA13 do not show a strong influence of stretching and concurrent recrystallization. The centimeter-scale variations of Os isotopic composition and Re and Os abundances almost certainly reflect mineral-melt equilibria. Binary mixing models between depleted peridotites such as TA2A and the most Ca-Al-rich clinopyroxenite analyzed (TA61) or typical websterites (TA11A2, TA11B, TA13B, TA13D) show that bulk mixing of peridotite with pyroxenite cannot account for the complete range of observed chemical variation of the peridotites (Figure 3.4), indicating the need for mineral-melt equilibria as an additional factor.

4.4.4 Source of the melts and origin of the pyroxenites

The spatial context of peridotites and pyroxenites in the Totalp massif and the enhanced abundances of Re and radiogenic ^{187}Os in the pyroxenites indicate that the pyroxenite layers are the most plausible source of the melts. A closed-system model where the pyroxenites originate by partial melting of the surrounding peridotites appears unlikely. The large differences in γ_{Os} (160 Ma) cannot be easily reconciled with a common origin, not even in the distant past. The cumulate-like compositions of the pyroxenites do not match melt compositions in equilibrium with peridotites. Compositions and occasional modal layering are consistent with the pyroxenites representing reaction products of sublithospheric melts with surrounding peridotites. Alternatively, the pyroxenites may be residues of precursor mafic rocks that have undergone partial melting and reaction with surrounding peridotite. In either case, enhanced Re contents in the pyroxenites may reflect the presence of trapped melt. The occurrence of extremely transposed and isoclinally folded websterites suggests that some of these rocks may have been deformed in the viscous regime of the asthenosphere, where concurrent partial melting may be difficult to avoid.

4.4.5 Rhenium rich components in the convecting mantle?

While HSE abundances and Os isotopic data for fertile peridotites (including the Totalp lherzolites) and Mg-rich lavas such as komatiites tend to indicate a generally chondritic bulk composition of the mantle, most $^{187}Os/^{188}Os$ data for samples from oceanic mantle indicate the presence of Re-depleted reservoirs. Young abyssal peridotites, widely believed to be derived from the convecting suboceanic mantle, display mostly subchondritic $^{187}Os/^{188}Os$ with a mean value near 0.125 (Martin, 1991; Roy-Barman & Allègre, 1994; Snow and Reisberg, 1995; Brandon et al., 2000; Standish et al., 2002; Alard et al., 2005; Harvey et al., 2006). If the $^{187}Os/^{188}Os$ of abyssal peridotites are representative of the convective mantle, a substantial portion of this mantle would have to be long-term depleted in Re, with no reservoir available to balance the missing Re. In contrast to abyssal peridotites, young MORBs are characterized by a range of chondritic to moderately suprachondritic $^{187}Os/^{188}Os$ (0.127 to 0.16; Martin, 1991; Roy-Barman & Allègre, 1994; Schiano et al. 1997; Alard et al., 2005; Escrig et al., 2005). It has been noted that some of the more radiogenic $^{187}Os/^{188}Os$ in MORBs may reflect uptake of seawater-derived Os or ingrowth of radiogenic Os (Roy Barman et al., 1998), while Gannoun et al. (2007) interpret the radiogenic signatures of MORB as inherited from recycled oceanic crust. If the chondrite-like $^{187}Os/^{188}Os$ in MORBs represent the composition of the mantle source, this would indicate little or no Re depletion in the source. This notion is supported by an independent estimate of the $^{187}Os/^{188}Os$ of the modern convecting upper mantle of 0.1281 ± 0.0009 on the basis of Os isotopic data on late Proterozoic to Phanerozoic podiform chromitites (Walker et al. 2002). The rhenium rich pyroxenites in the Totalp ultramafic massif and their geologic context provide fresh evidence for the presence of components with suprachondritic $^{187}Os/^{188}Os$ in the sublithospheric mantle. Whether the pyroxenites are precipitates of sublithospheric melts or melting residues of mafic precursors, in either case, the Re and radiogenic Os would be derived from the asthenosphere.

The discrepancy between the Os isotopic compositions of abyssal peridotites and those of MORBs and chromitites can be resolved if one accepts that: (1) abyssal peridotites may have

lost pyroxene rich components (veins, layers, streaks) during upwelling and melting in the asthenosphere, and (2) these pyroxene rich components have been enriched in Re and, at least regarding Os isotopes, are in isotopic disequilibrium with surrounding harzburgites. This scenario implies that some poorly constrained fraction of the upwelling convecting mantle is comprised of infertile harzburgites and pyroxenitic or eclogitic rocks, the latter possibly representing recycled oceanic crust. The lower melting temperatures of eclogites and pyroxenites (Hirschmann and Stolper, 1996; Yaxley and Green, 1998; Kogiso et al., 2003; Pertermann and Hirschmann, 2003) invariably will lead to deep melting of such fertile components during upwelling. In the distal part of upwelling asthenosphere or in ultra slow spreading environments, melting of fertile peridotite or pyroxene rich components may lead to refertilization of nearby depleted peridotites, as suggested for the Lherz (Le Roux et al., 2007) and Totalp mantle rocks.

4.5 Conclusions

The Totalp lherzolites and pyroxenites provide new evidence for refertilization of oceanic peridotites by infiltration of mafic melts related to nearby residual or cumulate pyroxenites. Although not very common, similar fertile peridotites are known from modern oceanic transform fault settings and from ultra-slow spreading environments. Melt infiltration occurred at conditions of the asthenosphere-lithosphere transition, similar to refertilization processes reported from Lherz (Le Roux et al, 2007). Rhenium and radiogenic Os were added to the peridotites along with lithophile incompatible elements, as indicated by rhenium enriched and suprachondritic $^{187}Os/^{188}Os$ in peridotite samples. Thus, Os isotopic heterogeneity in peridotites occurs not only because of variable age of melt extraction, but also because of variable mixing and addition of Re and radiogenic Os from melts. Centimeter-scale Os isotopic heterogeneities indicate that melt migration did result in incomplete Os isotopic equilibration, consistent with results from previous studies of mantle rocks (Chesley et al., 1999; Burton et al., 1999; Becker et al. 2001; 2004; Büchl et al., 2002). The Totalp ultramafic rocks imply the presence of Re-enriched components associated with melts derived from pyroxene rich lithologies in the asthenosphere.

Acknowledgements

We thank R.D. Ash, M. Feth, H. Frohna-Binder, A. Gottsche, K. Hammerschmidt, R. Naumann, I. Puchtel, and F. Wombacher for technical assistance. Constructive reviews by M. Handler and T. Meisel helped improve the manuscript. We thank R.W. Carlson for editorial handling. This work was partly funded by NSF grant EAR 0309810 to H. B. and R.J.W. and funds from the Freie Universität Berlin.

Table 4.1: Major element, trace element and Os isotope data from peridotite and pyroxenite samples from the Totalp ultramafic massif, eastern Switzerland.

		Remarks	Al_2O_3	Na_2O	MgO	Mg#	Os (ppb)	$^{187}Os/^{188}Os$	Re (ppb)	$^{187}Re/^{188}Os$	$^{187}Os/^{188}Os$ (160 Ma)	γ_{Os} (160 Ma)
	Peridotites											
TA-2A		b) g)	2.32	0.09	41.9	0.889	3.90	0.1213	0.393	0.477	0.1200	-4.9
TA-2B		b) g)	3.44	0.27	38.2	0.899	3.24	0.1227	0.212	0.309	0.1219	-3.4
TA-2C		b) g)	3.51	0.22	39.2	0.895	3.94	0.1252	0.295	0.354	0.1243	-1.5
TA-3		b) g)	3.87	0.15	39.1	0.897	5.27	0.1255	0.419	0.376	0.1245	-1.4
TA-5		b) g)	3.77	0.21	38.8	0.896	2.87	0.1277	0.327	0.539	0.1262	0.0
TA-7		d) g)	3.13	0.10	40.8	0.896	5.20	0.1214	0.283	0.258	0.1207	-4.4
TA-10		c) g)	3.55	0.21	38.0	0.887	3.33	0.1277	0.316	0.449	0.1265	0.2
TA-12		b) g)	3.42	0.21	39.1	0.890	3.00	0.1261	0.329	0.518	0.1247	-1.2
TA-14		d) g)	3.44	0.22	38.5	0.892	4.33	0.1372	0.378	0.413	0.1361	7.9
TA-15		b) g)	4.34	0.27	37.0	0.893	4.34	0.1303	0.764	0.833	0.1281	1.5
a)							3.93	0.1310	0.412	0.496		
a)							4.02	0.1311	0.409	0.481		
TA-16		b) g)	3.99	0.25	37.9	0.893	3.49	0.1267	0.360	0.488	0.1254	-0.6
TA-17		b) g)	3.16	0.22	39.6	0.901	2.71	0.1254	0.300	0.525	0.1240	-1.7
TA-18		d) g)	3.79	0.26	38.1	0.894	4.10	0.1267	0.656	0.757	0.1247	-1.2
dupl									0.412			
TA-19		b) g)	3.81	0.20	38.3	0.894	4.03	0.1277	0.425	0.499	0.1264	0.2
TA-21		b) g)	3.95	0.27	38.1	0.893	3.82	0.1252	0.370	0.458	0.1240	-1.8
TA-23A		d) g)	3.65	0.24	38.6	0.896	5.02	0.1257	0.390	0.368	0.1247	-1.2
TA-23B		b) g)	3.49	0.27	38.6	0.895	4.02	0.1275	0.375	0.442	0.1264	0.1
TA-24A		b) g)	3.78	0.18	37.8	0.889	4.66	0.1273	0.622	0.631	0.1256	-0.5
TA-24B		b) g)	3.50	0.22	38.7	0.898	3.26	0.1306	0.501	0.726	0.1287	2.0
TA-26		c) g)	3.33	0.19	39.0	0.895	4.60	0.1246	0.329	0.338	0.1237	-2.0
TA-31		b) g)	3.96	0.32	37.7	0.894	4.52	0.1260	0.584	0.611	0.1244	-1.5
TA-37		e) f)	2.83	0.18	41.3	0.905	0.201	0.1230	0.009	0.221	0.1224	-3.0
dupl		b) g)					0.204	0.1231				
TA-38		c) h)	4.47	0.34	36.5	0.891	3.05	0.1292	0.299	0.464	0.1279	1.4
dupl		b) g)					2.71	0.1320	0.712	1.24	0.1287	2.0
	Pyroxenites and Composite samples											
TA-11A2	**Websterite**	b) g)	9.18	0.49	29.1	0.890	1.62	0.1521	0.570	1.66	0.1477	17.0
dupl		d) g)					1.63	0.1518	0.545	1.58	0.1476	17.0
TA-11B	**Websterite**	b) g)	8.69	0.52	28.4	0.888	2.06	0.1514	1.07	2.46	0.1449	14.8
TA-13B	**Websterite**	c) f)	7.01	0.59	27.2	0.890	2.40	0.1618	0.533	1.05	0.1590	26.0
TA-13C	**Peridotite**	c) f)	4.05	0.24	38.0	0.899	3.60	0.1292	0.390	0.512	0.1278	1.3
TA-13D	**Websterite**	c) h)	7.04	0.54	30.8	0.894	2.31	0.1643	0.639	1.31	0.1608	27.4
dupl		b) g)					2.50	0.1615	0.711	1.35	0.1579	25.1
dupl									0.640			
TA-22A1	**Websterite**	e) h)	3.26	0.36	34.5	0.910	3.12	0.1406	0.555	0.841	0.1384	9.7
TA-22A2	**Peridotite**	d) g)	1.82	0.05	42.7	0.908	3.97	0.1237	0.204	0.243	0.1230	-2.5
a)							3.41	0.1228	0.171	0.237	0.1222	-3.2
a)							2.88	0.1246	0.170	0.279	0.1239	-1.9
TA-61	**Clinopyroxenit**	c) f)	11.03	0.96	15.4	0.831	0.400	0.8685	3.20	37.8	0.7544	497.8
dupl							0.240	0.8835	2.69	53.0	0.7251	474.6

a) data from samples TA15 and TA22A2 was previously published by Becker et al., 2006
b) measured on Faraday cup at FU Berlin
c) measured on Faraday cup at University of Maryland
d) measured on SEM at FU Berlin
e) measured on SEM at University of Maryland
f) digested in quartz Carius tubes at 345°C
g) digested in Pyrex Carius tubes at 320 °C
h) digested in Pyrex Carius tubes at 230 °C
$^{187}Os/^{188}Os$ fractionation corrected using $^{192}Os/^{188}Os = 3.08271$ (Shirey and Walker, 1998) and O-corrected corrected using $^{18}O/^{16}O$ and $^{17}O/^{16}O$ of 0.00204 and 0.00037, respectively.

Chapter 5

The influence of refertilization on abundances of highly siderophile elements in peridotites - a case study from the Totalp ultramafic body, eastern Swiss Alps

David van Acken [a,b,*], Harry Becker [a], Richard J. Walker [b], Frank Wombacher[a]

a) Institut für Geologische Wissenschaften, AB Geochemie, Freie Universität Berlin, Malteserstr. 74 – 100, Haus B, D-12249 Berlin, Germany, Phone: +49 30 838 70200 Fax: +49 30 838 70170

b) University of Maryland, Department of Geology, College Park, Maryland 20742, USA

*Corresponding author

E-mail addresses: dvana@zedat.fu-berlin.de (D. van Acken), hbecker@zedat.fu-berlin.de (H. Becker), rjwalker@geol.umd.edu (R.J. Walker). fwo@zedat.fu-berlin.de (F. Wombacher)

5.1 Abstract

Understanding the causes of highly siderophile element (HSE) distribution in mantle peridotites is crucial to understand the chemical and isotopic evolution of the mantle and to use the HSE to study mantle processes, core formation or Earth accretion. In the Jurassic Totalp ultramafic body (Davos, Swiss Alps), serpentinized spinel lherzolites are the host rocks of spinel and spinel-garnet pyroxenite layers. The body shows petrographic evidence for melt-migration and associated precipitation of pyroxenes, spinel and sulfides in peridotites and pyroxenites at conditions of the deep lithosphere. HSE and lithophile element abundances and Os isotopic data on peridotites provide insights on how peridotites might change their compositions during these processes.

The lherzolites cover a range from moderately depleted to fertile compositions based on Al_2O_3 contents ranging from 1.8 to 4.9 wt%. Sulfide is a trace phase and is macroscopically visible in many samples. Most of the HSE concentrations are well within the range of previously reported data for samples of similar fertility, except for a notable enrichment in Re relative to Pd in many, though not all, samples. HSE concentrations and element ratios and correlations with each other and with Al_2O_3 are generally inconsistent with an origin as residues of partial melting using sulfide-silicate or monosulfide solid solution-liquid sulfide equilibrium partitioning models. Several samples show Re or Pd enrichment and HSE element ratios exceeding PUM values, along with textural evidence for introduction of HSE into the lherzolite by coprecipitation of sulfides along with clinopyroxenes from migrating melt during episodes of melt-rock interaction. The observed covariations of HSE thus likely reflect a complex multistage history of one or more episodes of partial melting and melt extraction, and late addition of a mafic or ultramafic melt component with a strongly fractionated HSE pattern (high Re/Os, Pd/Ir and Pt/Ir), as supported by the HSE compositions of associated pyroxenites.

HSE element and Os isotope covariations in Totalp lherzolites are consistent with addition of about 5 – 30% of mafic melt component to depleted peridotite. Differences in initial Os

isotopic compositions in Totalp lherzolites and associated pyroxenites suggest several endmember melt compositions with highly radiogenic $^{187}Os/^{188}Os$, possibly high-Re/Os old recycled oceanic crust. Re and Pd were added to depleted peridotite in substantial amounts, whereas Ir, Os, Ru and Pt remain largely unaffected. Consequentially, Pd/Ir or Re/Os are shifted from subchondritic values established by partial melting and melt extraction to chondritic and suprachondritic values, effectively overprinting primary HSE signatures. The observed compositions and variations of HSE and lithophile elements are very similar to compositions of fertile lherzolite around the world.

Keywords: lherzolite; highly siderophile elements; oceanic mantle; melt-rock interaction; refertilization

5.2 Introduction

Past studies have indicated that reaction of mantle melts with depleted mantle peridotites may produce spinel or plagioclase lherzolites, leading to refertilization of depleted mantle domains and effectively obscuring previous episodes of partial melting (Van der Wal and Bodinier, 1996; Rampone et al., 1997; Saal et al., 2001; Piccardo et al., 2004; Müntener et al., 2004; Le Roux et al., 2007). The general importance of such metasomatic processes in determining the major element, trace element and isotopic composition of fertile peridotites, and thus the lithospheric mantle and the implications for compositional models of the mantle is currently debated and will be a major focus of future research (e.g. Beccaluva et al., 2004; Rampone et al., 2004; Reisberg et al., 2005; Becker et al., 2006; Piccardo et al., 2007; Le Roux et al., 2007). Because of some specific geochemical properties, the highly siderophile elements (HSE) Os, Ir, Ru, Pt, Rh, Pd, Re and Au, and the long-lived radioactive decay systems ^{187}Re-^{187}Os and ^{190}Pt-^{186}Os have been playing an increasingly important role in constraining modern and past mantle processes, such as melting and lithosphere formation,

crustal recycling, core-mantle interaction and late accretion (e.g., Kimura et al., 1974; Walker et al., 1997; Brandon et al., 1999; Meibom et al., 2002; Pearson et al., 2004; Sobolev et al., 2005; Becker et al., 2006; Luguet et al., 2008.). Concentrations of the HSE in basalts, komatiites and mantle peridotites have been used to argue that Os, Ir, Ru, Rh, and sometimes Pt behave compatibly during moderate degrees of mantle melting, while Pd, Re and Au are generally considered as moderately incompatible elements and this view is consistent with the long-term variation of $^{187}Os/^{188}Os$ in the crust-mantle system (Morgan and Lovering, 1967; Hertogen et al., 1980; Morgan et al., 1981; Barnes et al., 1985, Shirey and Walker, 1998). Aside from these general observations, however, it must be stated that the detailed chemical behaviour of these elements and their host phases in the mantle and associated partitioning and transport processes remain poorly understood.

Partial mantle melts are enriched in PPGE and Re compared to residua of mantle melting, making HSE a potential tracer for reaction of mafic melt with depleted peridotite. In spite of the increasing quantity of data, possible redistribution of HSE during mantle refertilization needs to be understood in order to accurately understand aforementioned processes.

HSE distribution during melt-rock interaction is not yet fully understood and is influenced by a number of parameters. One important factor to control HSE distribution is melt/rock ratio. Melt flow at high melt rock ratios in conduits or as percolative flow leading to the formation of replacive dunites and harzburgites (Kelemen et al., 1997) may result in removal of sulfide and HSE hosted therein by the melt (Becker et al., 2001; Büchl et al., 2002; 2004). At lower melt rock ratios, refertilization of depleted peridotites seems to occur by addition of a mafic component, either by precipitation of pyroxenes and co-precipitation of HSE-bearing sulfides (e. g., Lorand et al., 1993; Rehkämper et al., 1999a; Becker et al., 2001; Lorand and Alard, 2001; Pearson et al. 2004) or by cryptic metasomatism with minor modal change and trace element enrichment only (e.g. Menzies et al., 1985; Downes and Dupuy, 1987, Bodinier et al., 1990; Woodland et al., 1996; Rampone et al., 2005). As metasomatism has been demonstrated to produce distinct sulfide populations within peridotites (Burton et al., 2002; Alard et al., 2002), refertilized lherzolites should contain a mixture of melt-derived and depleted mantle-derived sulfides.

The present study aims at improving the understanding of lherzolite formation and HSE behaviour during melt-rock interaction and refertilization in the convecting upper mantle. The Jurassic Totalp massif provides a scarce opportunity to study a deeper part of suboceanic lithosphere with preserved igneous relations between lherzolites and pyroxenites. Geochemical as well as field and petrographic evidence suggest a complex history of depletion and refertilization events the massif underwent prior to emplacement on the ocean floor (Lagabrielle and Lemoine, 1997; Desmurs et al., 2002; Müntener et al., 2004; Manatschal et al., 2007). Understanding the HSE distribution processes between residual peridotite and migrating mafic melt, presumably represented by pyroxenitic layers, may further resolve the formation of lherzolite and refertilization of the upper mantle.

While many geochemical and petrological studies on peridotites from the subcontinental lithospheric mantle (SCLM) have shown effects of refertilization and mantle metasomatism, examples from oceanic tectonic settings are much less abundant. Abyssal peridotites are commonly very depleted, with reports for evidence of refertilization in lherzolites mostly restricted to fracture zone settings and some very slow spreading environments (Cannat et al., 1990; Elthon, 1992; Seyler and Bonatti, 1997; Baker and Beckett, 1999; Luguet et al., 2003). Deeper sections of convecting upper mantle, as represented by the Totalp massif, are likely more fertile and may contain pyroxenite layers, which are rarely found in abyssal peridotite (Dantas et al., 2007). These layers and adjacent lherzolites may represent refertilized mantle component which melts preferentially during partial melting (Hirschmann and Stolper, 1996; Lundstrom et al., 2000; Pertermann and Hirschmann, 2003), and thus contributes disproportionately high to basalts.

5.3 Results

Volatile element-free Al_2O_3 and HSE abundances for the peridotite samples are shown in Table 5.1. For additional major element abundances and Os isotopic compositions of the samples see van Acken et al. (2008).

Al_2O_3 content in Totalp lherzolites ranges from 1.82 wt% to 4.92 wt%, covering a range from depleted to fertile lherzolite. Highly siderophile element concentrations of Totalp

lherzolites fall well within the range reported for lherzolites from orogenic massifs worldwide (e.g. Reisberg et al., 1991; Reisberg and Lorand, 1995; Roy-Barman et al., 1996; Rehkämper et al., 1999a; Lorand et al., 1999; 2000; Schmidt et al., 2000; Becker et al., 2001; 2006; Luguet et al., 2004; Pearson et al., 2004).

Iridium in Totalp lherzolites is positively correlated with most HSE. The quality of the correlations with Ir abundances become worse from Ru to Os, Pt and Pd, whereas Re-Ir displays merely scatter (Figure 5.1). Os, Ir and Ru concentrations scatter broadly around PUM estimates, with the exception of sample TA37, which has uniformly low concentrations of all HSE. A few samples have higher HSE concentrations than PUM estimates (Os, Ir, Ru: TA3; TA21; TA23A; TA24A; TA26; Pt: TA3; Pd: TA13C). Several samples plot off HSE-Ir covariations (Os-Ir: TA2B; TA9; TA14: Pt-Ir: TA2A, TA7; TA22A2; Pd-Ir: TA2A; TA7; TA13C; TA17) Rhenium concentrations scatter widely, with about half of the samples having higher Re than PUM estimates.

Indicators of the extent of depletion such as Al_2O_3 show no correlation with Os, Ir, or Ru abundances (Figure 5.2 a)-c). A weak correlation can be seen for Pt, Pd and Re, with some samples offset to high Pd and Re concentrations (e. g., TA13C, TA17, TA26, Figure 3 d -f). The Re-Pd diagram in Figure 5.1 and the variations of these elements with Al_2O_3 content (Figure 5.2) illustrate that in fertile lherzolite compositions, Re and Pd abundances become to some extent decoupled. Concentrations of Os, Ir, and Ru scatter around recent estimates for the primitive upper mantle model (PUM, Meisel et al., 2001; Becker et al., 2006). In contrast, Pt and Pd concentrations are mostly below PUM estimates, while Re abundances of samples with high Al contents are similar or higher than PUM (Figures 5.1, 5.2).

Two different types of HSE patterns can be recognized, with a continuous transition between them. Most samples have Re/Pd_N (index N indicates normalization to CI chondrite, chondrite values from Horan et al., 2003) > 1, whereas a minority of 6 samples have Re/Pd_N < 1, and show patterns similar to primitive mantle estimates (Becker et al., 2006, Figure 5.3). Os/Ir ratios are chondritic to slightly suprachondritic, while Ru/Ir ratios are all suprachondritic, and in some cases slightly higher than PUM estimates. As in other peridotites, these ratios do not correlate with Al_2O_3, (Figure 5.4 a)-b). Pt/Ir and Pd/Ir ratios correlate with Al_2O_3, and extend from PUM like or slightly higher values to subchondritic va-

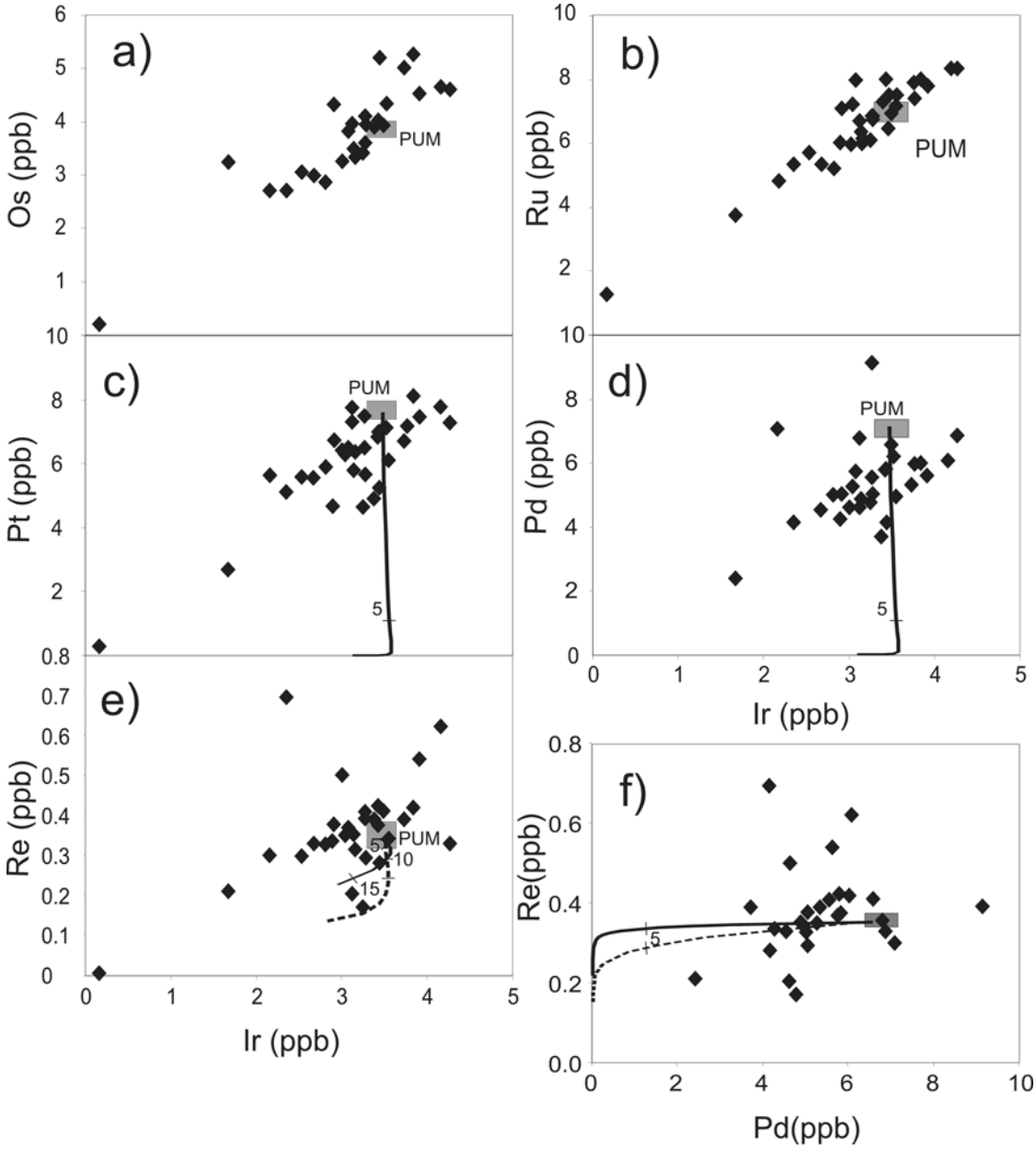
a)
Os (ppb)
PUM
b)
Ru (ppb)
PUM
c)
Pt (ppb)
PUM
5
d)
Pd (ppb)
PUM
5
Ir (ppb)
e)
Re (ppb)
PUM
5
10
15
Ir (ppb)
f)
Re(ppb)
5
Pd(ppb)

Figure 5.1 (previous page): HSE abundances vs. Ir (ppb) for Totalp lherzolites; a) Os (ppb) vs. Ir (ppb); b) Ru (ppb) vs. Ir (ppb); c) Pt (ppb) vs. Ir (ppb); d) Pd (ppb) vs. Ir (ppb); e) Re (ppb) vs. Ir (ppb); shaded box in all figures: Primitive Upper Mantle (PUM, Becker et al., 2006); continuous lines in Figure c) – e): residual peridotite compositions after partial batch melting, assuming monosulfide sold solution (mss) – sulfide melt equilibrium (Bockrath et al., 2004; Mungall et al., 2005; Ballhaus et al., 2006), fractional melting trend is similar (not shown). As the HSE partition preferentially into sulfides under mantle conditions with sulfide – silicate partition coefficients > 1000 (Fleet et al., 1996; Sattari et al., 2002), HSE concentrations may be primarily controlled by mss – sulfide liquid partitioning (Fleet et al., 1993; Brenan, 2002; Ballhaus et al., 2001; 2006; Bockrath et al., 2004); dashed line in e) assumes moderately incompatible bulk partitioning behaviour of Re, as estimated from concentrations in basalts and peridotites (Morgan and Lovering, 1967; Hauri and Hart, 1997; Shirey and Walker, 1998). Neither melting model can account for the observed distribution of Re. Mss – sulfide liquid partition coefficients used D^{Os}: 7; D^{Ir}: 8; D^{Ru}: 9; D^{Pt}: 0.15; D^{Pd}: 0.15; D^{Re}: 2.5; Bulk peridotite-silicate melt partition coefficient used for Re: D^{Re}: 0.13 (Hart and Dunn, 1993; Kelemen et al., 1993; Li et al., 1996; Hauri and Hart, 1997; Brenan, 2002; Bockrath et al., 2004; Mungall et al., 2005; Ballhaus et al., 2006).

lues. Several samples introduce substantial scatter due to high Pt/Ir and Pd/Ir at a given alumina content (Fig. 5.4 c)-d). The Re/Ir- Al_2O_3 diagram shows substantial scatter (Fig. 5.4 e), and Re/Ir values extend from subchondritic to suprachondritic values.

Re/Os is moderately positively correlated with both Pt/Ir and Pd/Ir, with some high Pd samples plotting off the main trend (Figure 5.5 a-d). Associated pyroxenites broadly extend the trend to high Pt/Ir, Pd/Ir and Re/Os values. No correlations exist between $\gamma_{Os\ I}$ and Os/Ir, Ru/Ir and Pd/Re (not shown). In most lherzolite samples, Re is enriched to a higher degree than both Pt and Pd (Figure 5.1, 5.4). No good correlations can be established for initial $^{187}Os/^{188}Os$ and both Pt/Ir and Pd/Ir (Figure 5.5).

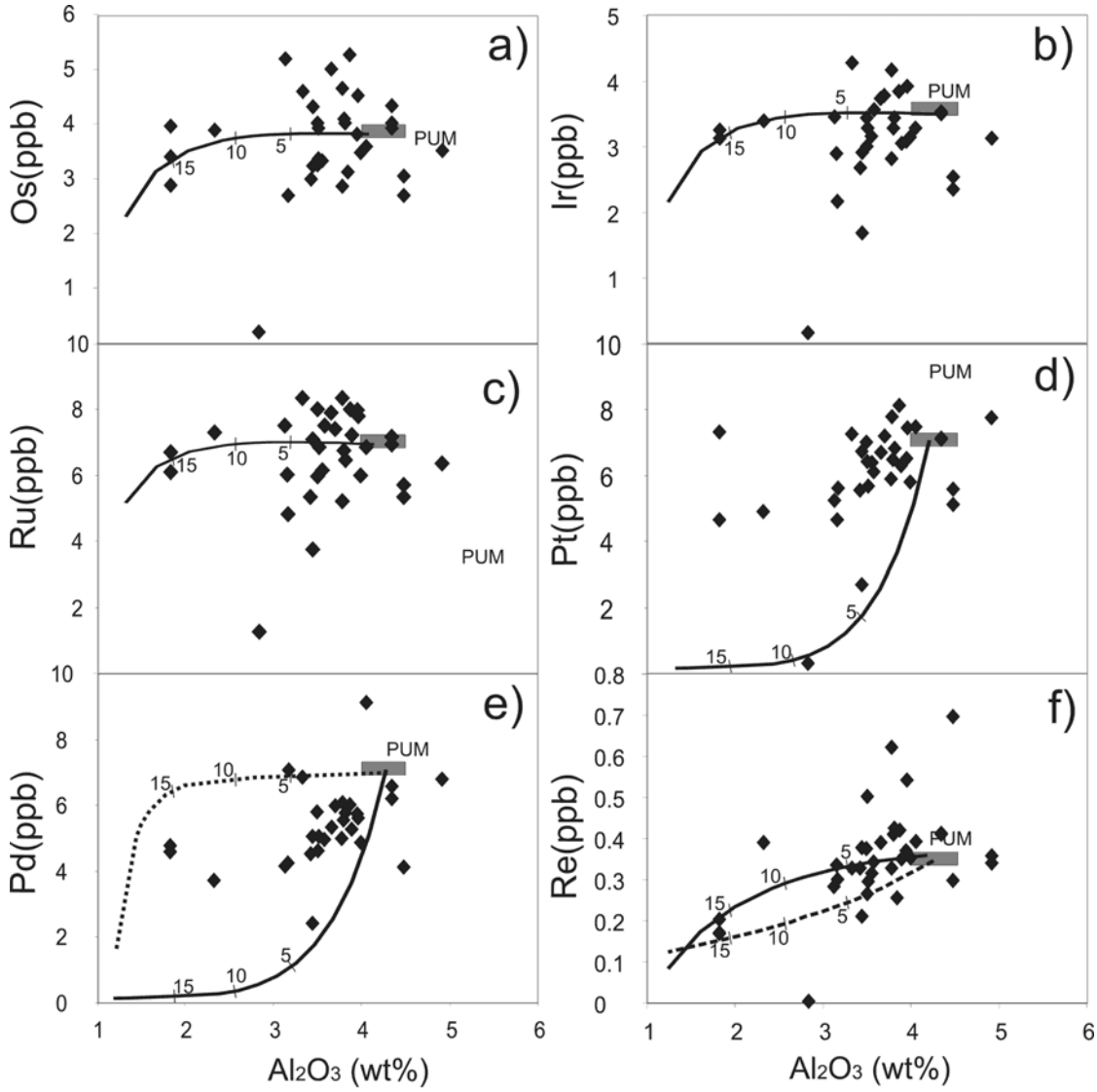

Figure 5.2: HSE vs. Al_2O_3 (wt%) a) Os (ppb); b) Ir (ppb); c) Ru (ppb); d) Pt (ppb); e) Pd (ppb); f) Re (ppb); solid and dashed lines: see Figure 5.1 for details; dotted line in 5.2 e): evolution of residual peridotite during partial melting based on sulfide melt – silicate melt partitioning and dissolution of sulfur in the partial melt (from Lorand et al.; 1999). None of the three melting models presented in Figures 5.1 and 5.3 provide a reasonable fit for the Totalp lherzolites.

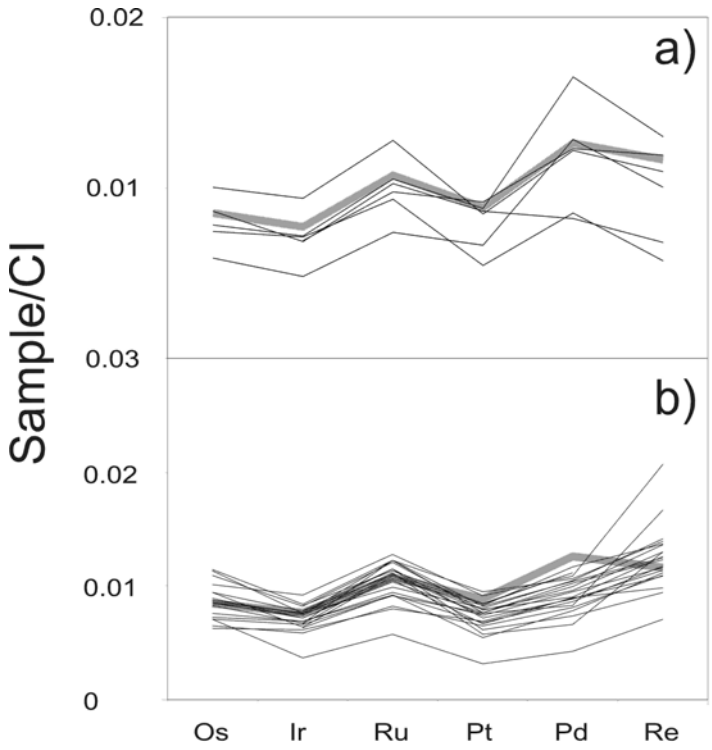

Figure 5.3: CI-chondrite-normalized HSE patterns for Totalp lherzolites; a) Samples with $Pd_N/Re_N < 1$; b) Samples with $Pd_N/Re_N > 1$. The transition between both groups of samples is continuous; shaded area: primitive mantle (Becker et al., 2006); CI values from Horan et al. (2003).

5.4 Discussion

In the following sections, we shall briefly review the effects of serpentinization on the HSE abundances in the peridotites. In order to estimate HSE behaviour during partial mantle melting, observed HSE signatures from Totalp lherzolites are compared with trends predicted by different melting models. The final part of the discussion focuses on lherzolite refertilization and concurrent precipitation of sulfides carrying a basaltic HSE signature and the effects on HSE abundance ratios in mantle peridotites.

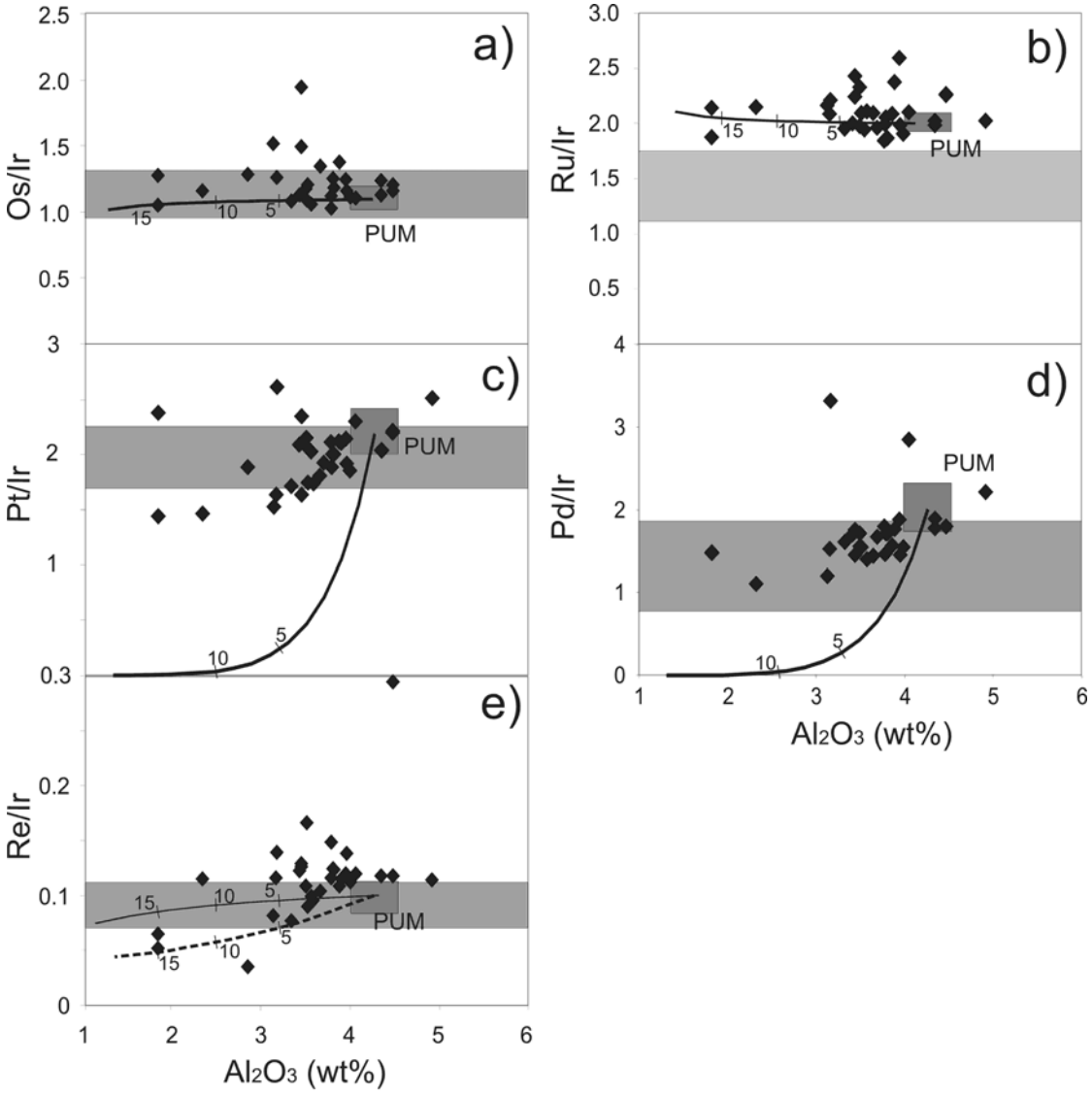

Figure 5.4: HSE ratios vs. Al_2O_3 (wt%); a) Os/Ir; b) Ru/Ir; c) Pt/Ir; d) Pd/Ir; e) Re/Ir; continuous and dashed lines: see Figure 5.1 for details; shaded box: PUM (Becker et al., 2006; shaded bar: range of chondritic ratios (Horan et al., 2003).

5.4.1 Serpentinization as the source of non-chondritic HSE distribution?

All Totalp lherzolite samples are highly serpentinized with H_2O contents of 6.8 to 11.4 wt%. In some previous studies significant uptake of highly radiogenic Os from seawater was suggested to account for chondritic to slightly suprachondritic Os isotope composition of some serpentinized peridotites (Snow and Reisberg, 1995; Walker et al., 1996; Standish et al., 2002). Similar uptake of other HSE from seawater might contribute to elevated concentrations observed in serpentinized peridotites. There are, however, some substantial mass balance problems. HSE concentrations of seawater or meteoric water are extremely low compared to typical HSE concentrations of ultramafic rocks (Weiss and Fresco, 1983; Lee, 1983; Anbar et al., 1996; Sharma et al., 1997). Because of this, unrealistically large amounts of seawater are required to interact with peridotite in order to add sufficient amounts of HSE to cause pronounced HSE anomalies and slightly suprachondritic Os isotope compositions found in some serpentinized mantle peridotites (Martin, 1991; Rehkämper et al., 1999a; Büchl et al., 2002; 2004; Harvey et al., 2006; van Acken et al., 2008).

Correlations of abundances and ratios for some HSE, and $^{187}Os/^{188}Os$ with lithophile fertility indicators such as Al_2O_3 suggest that the observed HSE systematics of peridotites have a primarily igneous origin and the effects of serpentinization may be negligible (this work, Figures 5.1, 5.2, 5.4, Reisberg and Lorand, 1995; Becker et al., 2001; 2006; Luguet et al., 2003; 2004). It is inconceivable that such correlations would be preserved, if the HSE were substantially influenced by hydrothermal or weathering processes, because the aqueous chemistry of the HSE differs substantially from their igneous behaviour (Hodge et al., 1985; Wood, 1987). Furthermore, the degree of serpentinization, approximated by H_2O content, does not correlate with HSE abundances or Os isotope composition. Associated websterites and pyroxenites, which are much less affected by serpentinization, display highly radiogenic Os isotopic composition, correlated enrichments of Pt, Pd and Re (van Acken, 2008; in prep), and highly correlated ratios of Os/Ir, Pd/Ir, Pt/Ir and Re/Ir, similar to what is found in some basaltic magmas (Rehkämper et al., 1999b; Bézos et al., 2005). As in the peridotites, these ratios also correlate with alumina, and thus should reflect igneous, rather than aqueous geochemical processes. Pyroxene-rich veins extending from the Pd- and Re-rich pyroxenites

into the host peridotites (van Acken et al., 2008) also suggests an igneous origin for the observed HSE fractionation in the Totalp peridotites.

5.4.2 Melt Extraction

Mantle peridotites have long been interpreted as residues from partial melting and extraction of basaltic melt. Based on concentrations in oceanic basalts and peridotites, Os, Ir and Ru are considered highly compatible and are enriched in the solid, while Pt, Pd and Re are incompatible to various extents (Morgan et al., 1981; Barnes et al., 1985; Morgan, 1986). Petrographic and geochemical evidence from Totalp peridotites and associated pyroxenites suggests melt infiltration (Müntener et al., 2004; van Acken et al., 2008), which overprinted geochemical signatures established during partial melting events prior to refertilization. In order to understand the degree to which HSE distribution in Totalp peridotites are controlled by partial mantle melting and to quantify the impact of melt-rock interaction during refertilization on the HSE systematics, we compared the observed covariations of HSE concentrations and element ratios with each other and Al_2O_3 by applying different partial melting models to a PUM-type mantle source as representative of fertile mantle peridotite.

Most Totalp lherzolites have lowered concentrations of Pt and Pd compared to PUM, while concentrations of Os, Ir, Ru and Re scatter around PUM values (Table 5.1, Figures 5.1, 5.2). HSE concentrations and covariations with each other are similar to those reported for other oceanic peridotites (Rehkämper et al., 1999a; Luguet et al., 2003; 2004; Lorand et al., 2004) and , with the possible exception of Re, likely reflect their incorporation within sulfide, and thereby absolute sulfide abundance. Inter-element HSE ratios may provide better assessment of HSE redistribution and HSE fractionation during melt-rock interaction (Rehkämper et al., 1999a; Lorand et al., 2000). Pt/Ir and Pd/Ir are chondritic to suprachondritic for most samples, while Os/Ir scatters around chondritic values and Ru/Ir and Re/Ir are suprachondritic for most samples (Figure 5.4), similar to previously reported values for abyssal and ophiolitic peridotites (Rehkämper et al., 1999a; Luguet et al., 2003; 2004). HSE patterns for Totalp peridotites do not show incompatible HSE depletion, as would be expected for simple melt residues (Figure 5.3) and are similar to those reported for refertilized

lherzolites from the Kane Fracture Zone, the Ligurides and the Horoman massif (Rehkämper et al., 1999a; Luguet et al., 2003; 2004). All HSE/Ir ratios with the exception of Ru/Ir show variance from chondritic to suprachondritic values, Pt/Ir and Re/Ir in some samples is subchondritic. Positive covariations of Pt/Ir and Pd/Ir with Al_2O_3, coupled with no significant covariation of Os/Ir and Ru/Ir with Al_2O_3 may indicate incompatible element depletion by partial melting. HSE concentration higher than PUM estimates and extension of covariations beyond PUM (Figure 5.1, 5.2, 5.4) clearly indicates a significant influence of refertilization on the HSE distribution in oceanic lherzolites.

As HSE distribution during partial melting is not fully understood, we compared three different melting models applied to HSE behaviour during partial mantle to the observed HSE signature of Totalp lherzolites. The three models are briefly explained in the following section.

As all HSE partition into sulfides under mantle condition with partition coefficients >1000 (Peach et al., 1990; Fleet et al., 1991; 1999; Bezmen et al., 1994; Sattari et al., 2002), HSE partitioning behaviour can be expected to be controlled by sulfide phases. In the presence of sulfide, HSE fractionation during partial melting in the mantle was shown to be controlled by monosulfide solid solution (mss) – sulfide melt partitioning and subsequent extraction of immiscible sulfide melt along with segregating silicate melt (Bockrath et al., 2004; Ballhaus et al., 2006). While Os, Ir, Ru and Re remain in the solid, Pt and Pd are extracted into the sulfide melt. This model assumes exclusive control of HSE distribution by sulfide phases and does not consider any other residual phases that might host HSE (e. g., alloys, oxides or silicates). Partition coefficients $D_{mss/sulfide\ melt}$ are between 2 – 10 for Os, Ir, Ru and Re and about 0.1 to 0.25 for Pt and Pd (Brenan, 2002; 2008; Bockrath et al., 2004; Mungall et al., 2005; Ballhaus et al., 2006).

It is important to note that the sulfide liquidus is lower than the bulk peridotite liquidus. Sulfide exhaustion occurs at ~ 20% of bulk melting (Ballhaus et al., 2001), and was assumed to be proportional to bulk melting for the melt model. Because of the non-consideration of other phases than sulfides, model results for degrees of melting near sulfide exhaustion become increasingly unreliable and tend to underestimate concentrations of Os, Ir and Ru in the residue, as these elements form highly refractory alloy phases as observed in ophiolites

(Barnes et al., 1985; Bird et al., 1999; Brenan and Andrews, 2001; Meibom et al., 2002; Peregoedova et al., 2004; Walker et al., 2005). Melting trends calculated according to this model are shown as thick lines in Figures 5.1, 5.2 and 5.4.

Solid sulfide-liquid sulfide equilibrium, however, would be inconsistent with the moderate incompatibility of Re during mantle melting as indicated by the Re enrichment in basalts compared to peridotites (Morgan and Lovering, 1967; Hertogen et al., 1980; Morgan et al., 1981; Hauri and Hart, 1997). In order to account for observed moderately incompatible behaviour of Re during partial mantle melting, an additional melting curve (dashed line) was included in figures involving Re, using fractional melting and a Re bulk partition coefficient for melting of fertile spinel peridotite of 0.13, similar to that of Yb (Figure 5.1e), f), 5.2e); Hauri and Hart, 1997, fertile spinel peridotite modes from Pickering-Witter and Johnston, 2000, Yb mineral-melt partition coefficients from Hart and Dunn, 1993 and Kelemen et al., 1993).

Figure 5.2 e) includes a predicted melting curve (dotted line) for residues of partial melting according to the equilibrium partial melting model used by Rehkämper et al. (1999a) and Lorand et al. (1999), which assumes control of HSE distribution by sulfide – silicate partitioning and dissolution of sulfide in separating tholeiitic melt. Under this model, all HSE partition into sulfide and are released into segregating silicate melt as their sulfide host dissolves.

Partial melting trends predicted for Pt and Pd vs. Ir for the mss – sulfide liquid melting model are almost perpendicular to observed correlations in Totalp lherzolites (Figure 5.1 c), d). The majority of samples contain less Ir and Ru than expected for depletion trends, while Os concentrations scatter around the melting trends and are both higher and lower for a given Al_2O_3 (Fig. 5.2 a)-c). Pd, Pt and Re in most samples are overabundant in Totalp peridotites compared to the model predictions and scatter widely (Fig. 5.2 d-e).

The observed scatter in Re vs. Ir, Re vs. Pd and Re vs. Al_2O_3 (Figure 5.1 e), f), 5.3 e) caused by elevated Re concentrations cannot be reproduced to any partial melting trend predicted by either of the applied models. Rhenium concentrations in many Totalp samples are too enriched to account for partial melting residues from both models, assuming PUM model compositions for undepleted mantle, and display wide scatter for a given Al_2O_3 or Ir

concentration (Figure 5.1 e), 5.2 f). In particular observed enrichment of Re to higher values than PUM, as shown by several Totalp samples is incommensurate with depletion of Re during partial melting, as predicted by all melting models and observations from basalts (Roy-Barman and Allègre, 1994; Schiano et al., 1997; Escrig et al., 2005).

When compared to the sulfide – silicate predicted melting trend (Lorand et al., 1999; Rehkämper et al., 1999a), most Totalp samples have lower Pd than predicted by the model (Figure 5.3 c), indicating Pd is not simply controlled by sulfide – silicate equilibria during partial melting.

In summary, concentrations and ratios of HSE in Totalp peridotites are clearly not in accordance with predicted trends by multiple melting models. Refertilization via melt-rock interaction in the lower oceanic lithosphere likely has substantially affected HSE distribution in Totalp lherzolites. In spite of these complications, subchondritic $^{187}Os/^{188}Os$ in depleted Totalp lherzolites (TA2A, TA2B, TA2C, TA7, TA22A2, TA31, TA37; van Acken et al., 2008) indicate a long-term depletion history of at least a few samples.

5.4.3 HSE distribution during melt-rock interaction and lherzolite formation

HSE distribution during melt-rock interaction and refertilization is poorly understood, and contrasting behaviour has been reported in past studies of mantle peridotites. Removal of HSE (Lorand et al., 2000; Becker et al., 2001; Lee, 2002; Büchl et al., 2002; 2004) was observed as well as addition (Lorand, 1989; Lorand et al., 1993; 2000; 2003; Rehkämper et al., 1999a; Schmidt et al., 2000; Becker et al., 2001; Pearson et al., 2004; Luguet et al., 2003; 2004; Ionov et al., 2006) and in some rocks HSE abundances may not be affected at all (Gueddari et al., 1996; Handler and Bennett, 1999).

Field evidence, major and trace element and Os isotope systematics suggest that the Totalp peridotites have undergone significant refertilization after an episode of melt extraction (Müntener et al., 2004; van Acken et al., 2008). Pyroxene-rich veins extending from pyroxenite into the host peridotite, leading to pyroxene enrichment, are observed in the Totalp massif (van Acken et al., 2008) in accord with peridotites adjacent to pyroxenite layers

elsewhere, showing clinopyroxene enrichment compared to peridotites distal from these layers and hints of refertilization for both lithophile elements and HSE (Bodinier et al., 1990; 2004; McPherson et al., 1996; Becker et al., 2001). The most plausible mechanism for addition of incompatible HSE, as apparent in Totalp lherzolites, is addition of sulfide bearing a basaltic, incompatible HSE-enriched signature (Lorand, 1989; Lorand et al., 2000; 2003; Schmidt et al., 2000; Luguet et al., 2003; 2004; Ionov et al., 2006).

While melt generation in the mantle likely occurs at sulfide saturation in the presence of both solid and liquid sulfide (Bockrath et al., 2004; Ballhaus et al., 2006), this is likely not the case for sulfide precipitation at shallower depth. Sulfide solubility in silicate melts increases with decreasing pressure (Wendlandt, 1982; Wallace and Carmichael, 1992; Mavrogenes and O'Neill, 1999; Holzheid and Grove, 2002; O'Neill and Mavrogenes, 2002; Liu et al., 2007). Immiscible sulfide phases present at the stage of melt generation may have been dissolved in silicate melt. Segregation of sulfide upon melt-rock interaction may thus only occur after precipitation silicate minerals, driving the melt to sulfide saturation. Whether HSE were carried along in an immiscible sulfide melt, or dissolved in silicate melt makes no difference for the segregating sulfide, which will carry the melt signature. The sulfides segregated from the melt form only part of the sulfide population of the resulting refertilized peridotite. In situ analyses have revealed large HSE heterogeneity in sulfides from both peridotites (Alard et al., 2000; Luguet et al., 2001; 2004) and pyroxenite (Chapter 3). As rocks representing 'pure' melt composition likely do not exist in the lower lithosphere, melt composition has to be estimated from melting models and basalt compositions.

Addition of sulfides to depleted peridotite during melt-rock interaction with migrating mafic melt bearing a strongly fractionated HSE signature is implied by enrichment of Pt, Pd and Re over compatible HSE compared to predicted melting trends (e.g. Lorand et al., 1993; 2003; Rehkämper et al., 1999a; Alard et al., 2000; Lorand and Alard, 2001; Schmidt et al., 2003; Luguet et al., 2003; 2004; Pearson et al., 2004; Pearson and Nowell, 2004). Incompatible HSE in Totalp peridotites are enriched compared to both melting trends assuming incompatible behaviour during mantle melting based on mss – sulfide melt partitioning (Pt, Pd) or bulk rock incompatibility based on comparisons of concentrations in basalts and peridotites (Re, e.g. Morgan, 1986, Figure 5.1, 5.3). In some peridotites, HSE

concentrations and Os isotopic compositions are higher than primitive mantle estimates (TA3, TA13C, TA20, TA21, TA24A, TA26; Figure 5.1, 5.2, van Acken et al., 2008), thus supporting influx of HSE. In turn, ratios involving incompatible HSE show similar development compared to predicted melting trends from subchondritic to chondritic or even suprachondritic ratios for some samples (TA3, TA13C, TA14, TA15, TA17, and TA21). Osmium, Ir and Ru do not show extensive fractionation from each other, and the observed scatter of IPGE concentrations and Os/Ir and Ru/Ir is accordance with no or only minor addition of these elements from IPGE-poor mafic melts.

For a quantitative model of sulfide segregation from infiltrating melt and subsequent addition of these sulfides to the budget of host peridotite, we adopted the model and parameters by Rehkämper et al. (1999a). They assumed addition of 50 ppm sulfide segregated from each of multiple batches of infiltrating basalt melt to the host peridotite bearing 640 ppm of sulfide. Every batch of melt was assumed to have the same mass as the infiltrated peridotite. HSE partitioning during precipitation is controlled by equilibrium sulfide-silicate partitioning, with partition coefficients $D^{HSE}_{sulfide/silicate}$ according to Fleet et al. (1999, Ni-rich sulfides; $D^{HSE}_{sulfide/silicate}$: Os: 10000; Ir: 50000; Ru: 7000; Pt: 10000; Pd: 10000). Rhenium is assumed to be approximately one order of magnitude less chalcophile (Roy-Barman et al., 1998; Fonseca et al., 2007). Osmium isotopic composition of the melt was approximated by that of associated pyroxenite layers, which represent melt-dominated systems and thus are expected to carry the Os isotopic signature of the melt.

The results of addition of these segregated model sulfides to depleted peridotite are presented in Figure 5.5. Observed HSE signatures in Totalp peridotites are overall consistent with cumulate addition of sulfides with a high-Pt-Pd-Re signature from a basaltic melt in an open melt system to depleted peridotite. Melt-derived sulfides likely originate from several radiogenic endmembers that may represent different melt batches with different histories. Addition of model sulfide from up to 15 batches of mafic melt is consistent with observed HSE signatures, although most Totalp lherzolites can be explained by addition of 5 to 10 batches of sulfides segregated from basaltic melt, in good agreement with Rehkämper et al. (1999a), who found addition of 2 to 10 batches of mafic melt-derived sulfide consistent with HSE signatures from lherzolites from the Horoman peridotite.

Sulfide grains within peridotite samples have been shown to record highly variable HSE concentrations and patterns as well as Os isotope compositions (Alard et al., 2000; Luguet et al., 2001; 2004; 2008; Pearson et al., 2002), resulting in significant small-scale heterogeneity.

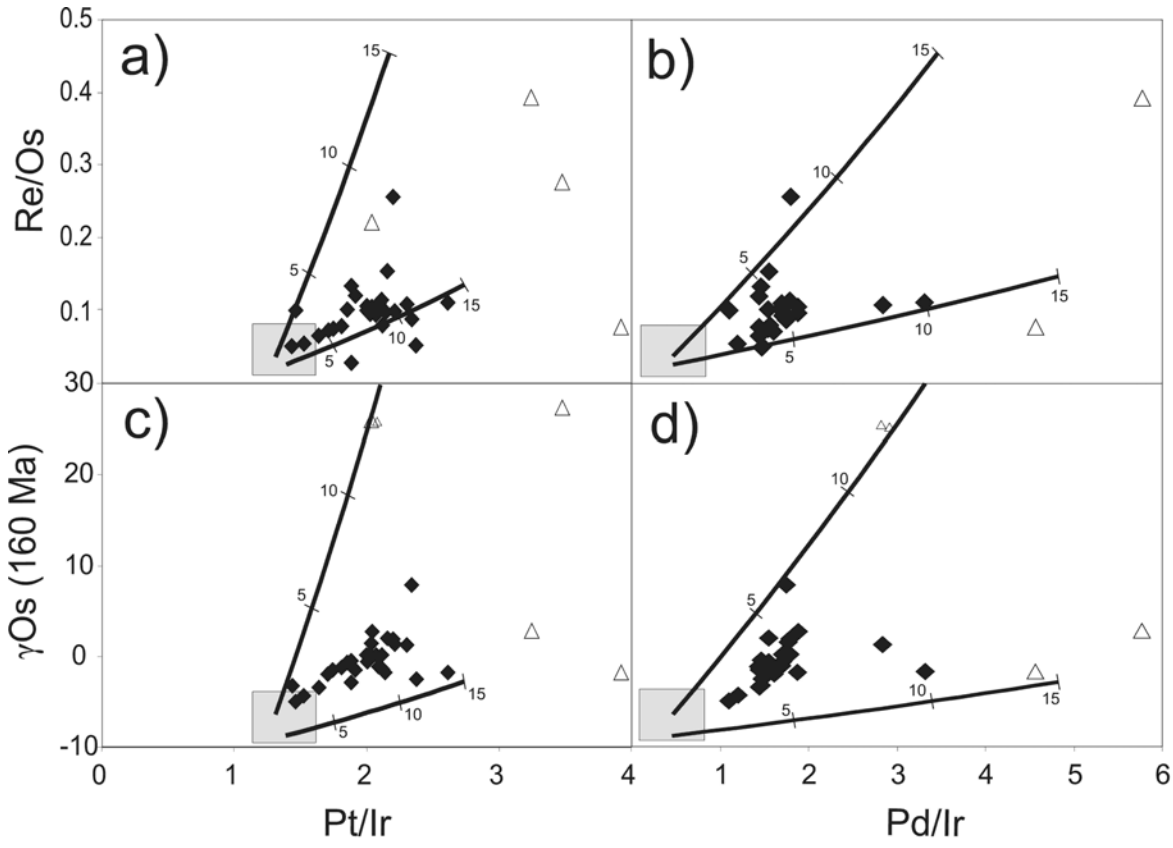

Figure 5.5: CI-chondrite-normalized HSE ratio plots; a) Re/Os vs. Pt/Ir; b) Re/Os vs. Pd/Ir; c) γ_{Os} (160 Ma) vs. Pt/Ir; d) γ_{Os} (160 Ma) vs. Pd/Ir; closed diamonds: Totalp peridotites, open triangle: associated Totalp pyroxenites; lines denotes sulfide addition to depleted peridotite composition (shaded box). Depleted peridotite: $^{187}Os/^{188}Os = 0.120$; 4.5 ppb Os; 4.5 ppb Ir, 4 ppb Pt, 1 ppb Pd; 0.05 ppb Re; upper line melt composition endmember: $^{187}Os/^{188}Os = 2$; 0.011 ppb Os; 0.03 ppb Ir, 0.55 ppb Pt,0.9 ppb Pd, 1 ppb Re, lower line melt composition endmember $^{187}Os/^{188}Os = 0.5$; 0.008 ppb Os; 0.03 ppb Ir, 0.8 ppb Pt, 1.2 ppb Pd; 0.3 ppb Re. Melt endmembers were chosen to provide the entire observed variation. Tick marks on lines correspond to 5, 10 and 15 increments addition of 50 ppm of melt segregated sulfide each to peridotite with 640 ppm sulfide. Ruthenium was not modeled separately, as correlation with Ir indicates almost identical behaviour (Figure 5.1 b).

Variations in HSE bulk distributions in peridotites affected by refertilization may thus represent different proportions of melt- and wall rock-derived sulfide in mixtures of multiple sulfide populations. It has been shown that even in formerly melt dominated systems with little contribution from host peridotite, such as websterites, a diversity of sulfide compositions can coexist, indicating disequilibrium, even at small scales (Chapter 3)

Observed enrichment in Re over other HSE (Figure 5.3) acting compatibly during mss – sulfide melt partitioning possibly hints at Re enrichment in the melt source, such as high Re/Os recycled mafic crust. Because of the highly radiogenic Os isotopic compositions of the melts, we suggest noticeable addition of radiogenic Os has occurred in the peridotites (van Acken et al., 2008, Chapter 3).

In summary, sulfide precipitation during percolative (peridotites) or channellized (pyroxenites) melt flow may result in significant HSE redistribution in residual peridotites in the deep lithosphere as represented by the Totalp ultramafic body. While changes in absolute HSE concentrations are strongly dependent on the absolute amount of sulfide present and may significantly vary between peridotites of similar fertility, HSE ratios may show different responses to refertilization.

Assuming a highly depleted precursor material similar to ophiolitic, abyssal or continental harzburgites (Pearson et al., 2004; Luguet et al., 2003; 2007), Os/Ir_N and Ru/Ir_N are little or not affected by refertilization and scatter around chondritic or slightly suprachondritic values, respectively. Pt/Ir_N tends to increase from subchondritic values as low as 0.5 recorded in depleted harzburgites to approximately chondritic or slightly suprachondritic values of up to 1.4 as recorded in Totalp lherzolites. Apparently, the processes reported here will not lead to substantially increased Pt/Os that may lead to long-term development of radiogenic $^{186}Os/^{188}Os$ in the mantle (Brandon and Walker, 2005). In contrast, Pd/Ir_N is considerably affected and is increased from subchondritic values as low as 0.25 to suprachondritic levels of about 2.5. Re/Ir_N is affected in a similar way by Re addition and can attain values as high as 4.5, with most values recorded in Totalp lherzolites around 1.5 to 2. If the least fertile samples from the Totalp dataset (TA2A and TA22A2) are used as reference, Pt/Ir_N, Pd/Ir_N and Re/Ir_N increase from 0.76, 0.89 and 0.80, respectively, to maximum values of 1.4, 2.5 and 4.5. The

stronger enrichment of Re, relative to Pd and Pt suggests increasing apparent compatibility during sulfide precipitation in these rocks.

HSE ratios such as Pt/It, Pd/Ir, Pd/Pt or Re/Os are clearly susceptible to small-scale redistribution during melt-rock interaction and thus may not be representative of larger (km-size) mantle regions. It is worth noting, however, that the processes described here result in PGE abundances and ratios of PPGE/IPGE (Figure 5.4) that are broadly similar to those reported from many other lherzolites around the world (e. g., Becker et al., 2006).

5.4.4 Rhenium addition

In Totalp lherzolites, linear correlations of Ir with Os and Ru, and, correlations of Ir with Pt and Pd suggest that the variations are controlled by a single phase, likely sulfide, as indicated by petrography. The scatter increases from Pd to Re, which shows considerable scatter and poor correlation with other HSE (Figure 5.1 e, f). Distribution of Re during partial melting and melt-rock interaction is less well constrained than partitioning for other HSE, because of its redox-dependent partitioning behaviour and lower degree of chalcophility (Fonseca et al., 2007; Brenan, 2008). During mss – sulfide melt equilibrium, Re is considered compatible in the residual sulfide (Brenan, 2002; 2008; Ballhaus et al., 2006), however, Re enrichment in basalts, compared to peridotites suggests incompatible behaviour during moderate degrees of mantle melting (Morgan and Lovering, 1967; Hertogen et al., 1980; Morgan et al., 1981; Morgan, 1986).

Less chalcophile partitioning behaviour of Re and resulting incompatibility during melt generation under oxidizing redox conditions (>QFM) may provide an explanation for Re enrichment in basalts (Fonseca et al., 2007; Mallmann and O'Neill, 2007). However, redox conditions in the convecting upper mantle typically are not oxidizing enough (QFM -3 to -1) to allow for this behaviour (e.g. Lee et al., 2003).

A possible explanation for the observed decoupling of Re from other HSE even at reducing conditions typical for oceanic lithosphere may be due to its partitioning behaviour between silicate minerals as observed in experimental studies on Re partitioning. Several studies found Re compatible or moderately incompatible in garnet (Righter and Hauri, 1998, Mallmann and

O'Neill, 2007) or clinopyroxene (Righter et al., 2004; Mallmann and O'Neill, 2007) in the absence of sulfide under reducing conditions (<QFM).

However, there are some problems with this explanation. The abundant presence of sulfides in both Totalp lherzolites and associated pyroxenites suggests sulfide saturation of any melt that circulated, and, by implication, sulfide control over Re partitioning during melt-rock interaction. Infiltrating melts would have to be extremely enriched in Re, which is in accord with derivation from high Re/Os source such as recycled oceanic crust.

Furthermore, the experiments by Righter et al. (2004) and Mallmann and O'Neill (2007) were conducted with Re concentrations exceeding those in real mantle samples by several orders of magnitude, so the obtained partitioning results may not be directly transferred to natural systems, as a dependence of HSE partitioning on absolute HSE concentration has been observed (Fleet et al. 1999).

A comprehensive explanation for the observed enrichment and decoupling of Re from other HSE as observed in Totalp lherzolites clearly requires more detailed knowledge of Re distribution between sulfide and silicate phases in sulfide bearing systems.

5.5 Conclusions

Formation of fertile lherzolites from the Totalp massif is consistent with addition of a basaltic component to depleted peridotite, as proposed by some other studies of peridotite massifs and xenoliths (e.g. Bodinier et al., 1990; Elthon, 1992; Takazawa et al., 1992; Witt-Eickschen et al., 1993; Le Roux et al., 2007). Refertilization likely occurred by precipitation of pyroxenes and spinel from mafic melts that migrated from magma conduits into peridotite wall rock as indicated by diffuse lithology boundaries between pyroxenite layers and peridotite, pyroxene-rich veins and clusters of coarse-grained clinopyroxene.

While compatible HSE (Os, Ir, Ru) seem little affected and are hardly fractionated from each other, as indicated by constant ratios, significant amounts of Pt, Pd and Re may be added to depleted peridotite via precipitation of sulfide from mafic melt, carrying a fractionated HSE signature. Variable initial $^{187}Os/^{188}Os$ of the peridotites reflects variable extent of interaction of the melts with precursor peridotites (van Acken et al., 2008). It is also clear, however, that

at least two different endmember melt compositions must have reacted with depleted peridotites to explain the observed isotopic heterogeneity in the associated websterites and pyroxenites (Chapter 3) and different trends based on the different relative enrichment of Pt, Pd and Re (Figure 5.5). Variable Os isotopic compositions of different melt batches may be a result of different isolation times of mafic material with high Re/Os in the convecting mantle. A good candidate for such old mafic material would be ancient recycled oceanic crust (e.g., Roy-Barman and Allègre, 1994; Schiano et al., 1997).

Although this may comprise a considerable secondary overprint on PPGE and Re concentrations, and lithophile major elements (e. g., Le Roux et al., 2007; van Acken et al., 2008a), the similarity of fertile lherzolite compositions from the present work with typical lherzolites from locales around the world is remarkable (e.g., McDonough and Sun, 1995; Meisel et al., 2001; Becker et al., 2006). This may be interpreted in two ways. Either, many lherzolites have undergone similar refertilization processes (e. g. Bodinier and Godard, 2003). Alternatively, refertilization and partial melting trends would fortuitously produce similar compositions for the most fertile lherzolites. In both explanations, the underlying physical causes for the convergence of fertile peridotite compositions near 4 wt. % Al_2O_3 are not understood.

Acknowledgements

We thank M. Feth, H. Frohna-Binder, K. Hammerschmidt, R.D. Ash, I. Puchtel and M. Fischer-Gödde for technical assistance and R. Fonseca for discussions. This work was partly funded by NSF grant EAR 0309810 to H. B. and R.J.W. and funds from the Freie Universität Berlin.

Table 5.1: Al_2O_3 and HSE concentrations in Totalp peridotites

	Al_2O_3 (wt%)	Os (ppb)	Ir (ppb)	Ru (ppb)	Pt (ppb)	Pd (ppb)	Re (ppb)
TA1	3.70		3.77	7.40	7.25	6.28	
TA2A	2.32	3.90	3.39	7.29	4.96	3.73	0.391
TA2B	3.44	3.24	1.67	3.74	2.73	2.41	0.212
TA2C	3.51	3.94	3.28	6.86	5.72	5.07	0.295
TA3	3.87	5.27	3.84	8.00	8.13	6.01	0.419
TA4	3.57		3.56	7.50	6.17	4.98	0.342
TA5	3.77	2.87	2.82	5.21	5.95	5.04	0.327
TA6	3.50	3.38					0.265
TA7	3.13	5.20	3.47	7.50	5.29	4.16	0.283
TA8	3.89		3.04	7.21	6.39	5.34	0.350
TA9	3.15		2.89	6.02	4.71	4.40	0.336
TA10	3.55	3.33	3.16	6.14	6.38		0.316
TA12	3.42	3.00	2.68	5.35	5.60	4.56	0.329
TA13C	4.05	3.60	3.27	6.86	7.52	9.29	0.390
dupl		3.64					0.391
TA14	3.44	4.33	2.91	7.08	6.81	5.08	0.378
TA15	4.34	3.93	3.49	6.93	7.12	6.57	0.412
dupl		4.02					0.409
dupl		4.34	3.55	7.17	7.22	6.28	
TA16	3.99	3.49	3.15	6.00	5.83	4.87	0.353
TA17	3.16	2.71	2.18	4.82	5.69	7.23	0.300
TA18	3.79	4.10	3.28	6.74	6.56	5.60	0.409
TA19	3.81	4.03	3.46	6.47	6.91	5.90	0.425
TA20	4.92		3.14	6.36	7.87	6.93	0.357
dupl		3.53					0.341
TA21	3.95	3.82	3.08	7.98	6.59	5.78	0.370
TA22A2	1.82	3.41	3.25	6.09	4.66	4.78	0.171
dupl		2.88					0.170
dupl		3.97	3.12	6.69	7.40	4.62	0.204
TA23A	3.65	5.02	3.76	7.88	6.79	5.41	0.390
TA23B	3.49	4.02	3.43	7.99	7.09	5.86	0.375
TA24A	3.78	4.66	4.19	8.34	7.88	6.13	0.622
TA24B	3.50	3.26	3.02	5.96	6.50	4.68	0.501
TA26	3.33	4.60	4.27	8.33	7.28	6.86	0.329
TA31	3.96	4.52	3.92	7.78	7.50	5.66	0.542
TA33A	3.84	3.13					0.255
TA37	2.83	0.204	0.159	1.28	0.299		0.006
TA38	4.47	3.05	2.53	5.71	5.59		0.299
dupl		2.71	2.35	5.33	5.16	4.22	0.695

Chapter 6

Conclusions and Outlook

In the following section, the key results of the presented work are briefly summarized; and a succinct outlook is given.

Refertilization of oceanic lithosphere occurred near the asthenosphere-lithosphere boundary in the Jurassic Pidemont-Liguria Ocean, similar to processes shown for the Lherz ultramafic body (Le Roux et al., 2007). Oceanic peridotites with an origin in the deeper lithospheric mantle are thus not pure residues of polybaric partial melting and melt extraction, but have undergone a more complex multi-stage history. Refertilization likely occurred by cumulate precipitation of pyroxenes, spinel or garnet and sulfides from infiltrating mafic melt. Emplacement of larger peridotite bodies at the ocean floor has been reported from fracture zones and ultra-slow spreading ridge systems (e.g. Dick et al., 2003; Michael et al., 2003; Liu et al., 2008), supporting an origin of the Totalp massif from a very slow-spreading ridge system and the presence of fertile components alongside long-term depleted peridotite in the convecting upper mantle.

Refertilization of oceanic lithosphere by melt-rock interaction may result in significant redistribution of HSE. HSE concentrations in fertile Totalp lherzolites higher than primitive mantle estimates coupled with chondritic to suprachondritic ratios for Pt/Ir, Pd/Ir and Re/Os indicate significant addition of incompatible HSE over compatible HSE. As a consequence, *ratios involving these elements, such as Pd/Ir or Re/Os, may be easily modified, and not be suitable to fingerprint primordial heterogeneities and late accretion signatures or study episodes of partial mantle melting* predating the refertilization events.

Increased concentrations of Pt, Pd and Re in Totalp pyroxenites and lherzolites cannot be reproduced by simple mixing of depleted peridotite and melt. Cumulate precipitation of sulfides from multiple mafic melt batches is a suitable process to explain observed HSE distribution in Totalp mantle rocks. *HSE signatures of Totalp pyroxenites are consistent with formation by pyroxene cumulation in zones of channelized melt flow at high melt/rock ratios, while lherzolite refertilization likely occurred by pyroxene precipitation during porous flow at lower melt/rock ratios.*

The HSE signature of refertilized Totalp peridotites and associated pyroxenite layers thus reflects, with various proportions, both residual sulfides bearing a peridotite HSE signature and sulfides precipitated during multiple melt-rock interaction events carrying a melt signature, in accordance with observed in situ sulfide HSE heterogeneity. Multiple melt batches, and thus possibly multiple refertilization and pyroxenite formation events are indicated by different, highly radiogenic $^{187}Os/^{188}Os$ of Totalp pyroxenites.

Radiogenic $^{187}Os/^{188}Os$ of melt-dominated Totalp pyroxenites indicates a *melt source with long-term enriched Re/Os*. Recycled oceanic crust in the form of eclogitic slices in the convecting mantle ('marble-cake mantle', Allègre and Turcotte, 1986) is a viable source of such melts, given its high Re/Os and lower liquidus compared to ambient mantle peridotite (Yasuda et al., 1994; Yaxley and Green, 1998; Pertermann and Hirschmann, 2003).

Addition of radiogenic Os to depleted peridotite is indicated by suprachondritic initial $^{187}Os/^{188}Os$ in some peridotites and good linear correlations of $^{187}Os/^{188}Os$ with indicators of fertility, such as Al_2O_3 or MgO. Peridotites with subchondritic $^{187}Os/^{188}Os$ occurring alongside peridotites with more radiogenic compositions affirm the presence of material affected by ancient melt extraction events in the convecting oceanic mantle, and local Os isotopic disequilibrium. The *Re-Os isotope system in peridotites is thus less resistant to disturbance* by melt-rock interaction than previously thought (Chesley et al., 1999; Reisberg et al., 2004; Yuan et al., 2007; Pearson et al., 2007). Re-Os model ages (T_{RD} and T_{MA} ages; Shirey and Walker, 1998) should be interpreted with care in the light of possible addition or

removal of both Re and Os; and in respect to their representativeness for larger mantle regions, especially for mantle xenoliths.

Small scale HSE concentration and Os isotope disequilibrium seen in both layered pyroxenite bulk samples and in situ LA-ICP-MS measurement in two Totalp websterites indicate that formation of layered pyroxenites during melt-rock interaction occurs *without equilibration of HSE hosted in sulfide over a distance of a few mm.* This may indicate limited mobility and connectivity of sulfide melts during melt-rock interaction under upper mantle conditions, in accordance with previous in situ studies demonstrating small scale HSE and Os isotope disequilibrium (Luguet et al., 2001; 2004; Pearson et al., 2002; Alard et al., 2002; 2005).

The presence of pyroxenites in the convecting upper mantle, as observed in the Totalp massif, confirms suggestions of several recent studies on oceanic basalts (Lassiter and Hauri, 1998; Lassiter et al., 2000; Sobolev et al., 2005; 2007), that *pyroxenites may form a substantial part of source region of oceanic basalts.* Because of their lower liquidus temperature and preferential melting over wall rock peridotite (Hirschmann and Stolper, 1996; Yaxley and Green, 1998), pyroxenites may contribute extensively to oceanic basaltic volcanism. Pyroxenite layers in the convecting upper mantle might also serve to *bridge the apparent Re-Os isotopic disequilibrium between abyssal peridotites and mid-ocean ridge basalts.* Harzburgitic abyssal peridotites are residues from the highest degrees of melting at the top of the polybaric melting column, and should be in isotopic equilibrium with basalts representing their complementary partial melts. However, MORB display radiogenic $^{187}Os/^{188}Os$ in apparent disequilibrium to associated abyssal peridotites with unradiogenic $^{187}Os/^{188}Os$ (Roy-Barman and Allègre, 1994; Schiano et al., 1997; Brandon et al., 2000; Escrig et al., 2005; Harvey et al., 2006). Contribution of radiogenic $^{187}Os/^{188}Os$ from melting of pyroxenites in the MORB source mantle may provide a solution for this apparent discrepancy.

Along the same lines of thought, estimates of the Re content of the oceanic mantle based on data from extremely depleted abyssal peridotites alone may be biased towards lower Re contents. Mass balance calculation revealed that Re depletion of the upper mantle is not balanced by Re present in the crust, giving rise to the idea of a hidden isolated mantle reservoir to make up for the 'missing' Re. A significant amount of this *'missing' Re* (Martin, 1991; Hauri, 2002) *may be hosted in Re-rich pyroxenite layers or dykes* within the oceanic upper mantle, assuming the presence of pyroxenite layers is representative of lower oceanic lithosphere. The presence of a high-Re component in the form of pyroxenite layers and refertilized peridotite in the convecting mantle is thus established further. A plausible origin for this component may be recycled subducted oceanic crust, with the implication that recycled subducted crust or melts derived thereof may be preserved in the convecting upper mantle.

Suggestions that pyroxenites in the source of plume-related basalts are responsible for the observed high $^{186}Os/^{188}Os$ signature (Luguet et al., 2008) *cannot be entirely confirmed.* Although some pyroxenites, sulfide or alloy grains possess the appropriate elevated Re/Os, Pt/Os and Pt/Re signatures required for the long-term development to radiogenic $^{186}Os/^{188}Os$ while developing only moderately radiogenic $^{187}Os/^{188}Os$, these samples seem to be the exception rather than the rule. From more than 25 bulk pyroxenite samples studied from the Totalp and Beni Bousera (Luguet et al., 2008), only one sample may produce observed ^{186}Os-^{187}Os signature attributed to core-mantle interaction. Mixing of the majority of the samples with depleted mantle, as suggested for the basalt source, cannot generate the observed ^{186}Os enrichment without generating much larger enrichments in ^{187}Os, which are clearly not observed. Sulfides or alloy grains from pyroxenites or eclogites have been shown to potentially develop radiogenic $^{186}Os/^{188}Os$ (Luguet et al., 2008). In Totalp pyroxenites, considerable heterogeneity in respect to sulfide HSE composition was observed. Mixing of sulfide populations from depleted peridotite wall rock on the one hand and precipitates from mafic melt on the other hand has previously been suggested to generate such small-scale heterogeneities (Luguet et al., 2001; 2004; Alard et al., 2002; 2005; Pearson et al., 2002; Powell and O'Reilly, 2007). Bulk rock sulfide compositions thus likely reflect mixtures of

multiple sulfide populations; and HSE signatures of single sulfide grains may not be representative for the bulk rock, let alone larger mantle domains. Based on the available pyroxenite HSE data, pyroxenites may partially contribute to the observed ^{186}Os-^{187}Os signatures observed on Hawaii, Siberia and Gorgona Island (Brandon et al., 1999; 2003; Brandon and Walker, 2005), but is unlikely to be the sole contributor. Based on pyroxenite data, core-mantle interaction cannot be ruled out as a factor controlling the HSE composition of plume-related basalts.

Outlook

While some aspects of melt-rock interaction and refertilization in the lower oceanic lithosphere and its implications for HSE and the Re-Os isotope system have been addressed in the course of this study, a number of challenges remain. Some possible future work is sketched in the following section along with unpublished data from the Totalp massif.

In order to obtain more comprehensive understanding of melt-rock interaction in the mantle, HSE data need to be combined with more traditional lithophile trace elements and isotope systems. Clinopyroxene separates from both Totalp peridotites and pyroxenites were studied for Sr and Nd isotopic composition; and unequivocally point to an origin in the depleted MORB-type mantle (DMM) based on their low $^{87}Sr/^{86}Sr$ around ~0.702 – 0.703 and high $^{143}Nd/^{144}Nd$ ($\varepsilon_{Nd\ (160Ma)}$ ~ 5 – 10). Some pyroxenites show radiogenic $^{87}Sr/^{86}Sr$ of ~ 0.706 coupled with high $^{143}Nd/^{144}Nd$ and extremely radiogenic $^{187}Os/^{188}Os$, possibly reflecting recycling of oceanic crust affected by seawater alteration. Detailed studies of these samples in respect to lithophile trace element concentrations might shed additional light on the matter.

While attempted in this study, in situ determination of $^{187}Os/^{188}Os$ by LA-ICP-MS could not be accomplished on the Totalp pyroxenite samples. In situ $^{187}Os/^{188}Os$ measurements in peridotite samples have been successfully accomplished in the past (Alard et al., 2002; 2005; Pearson et al., 2002; Griffin et al., 2004; Powell and O'Reilly, 2007). Such in situ

measurements on samples from modally layered peridotite – pyroxenite sequences may reveal further evidence for multiple sulfide generations present in mantle pyroxenites and allow further constraints to be put on possible melt sources, high-Re/Os material in the mantle and redistribution of Os during melt-rock interaction. While the sulfide grains in Totalp samples are mostly too small and dissipated, in situ Os isotope studies on peridotites and pyroxenites less affected by serpentinization may provide further clues to a comprehensive understanding of the Os isotope system and broaden its application to mantle processes.

Thorough understanding of HSE distribution during sulfide precipitation from silicate of sulfide melt is hindered by a number of factors. Experimental determinations of partition coefficients are difficult because of sulfide liquid quenching and rapid solid state exsolution and recrystallization. HSE compositions in both peridotite and MORB cover a broad range and reflect sulfide abundance in the respective sample. Obtaining samples representative for larger mantle reservoirs may be another limitation for the understanding of HSE fluxes over larger scales.

To further resolve the current debate about core-mantle interaction and pyroxenites in the source of high $^{186}Os/^{188}Os$ plume-related rocks, pyroxenites from different locations and geological settings need to be studied for HSE concentrations and Os isotopic composition. In addition to this study, detailed HSE and Re/Os studies on pyroxenites are currently available for samples from Beni Bousera, Morocco (Kumar et al., 1996; Pearson and Nowell, 2004; Luguet et al., 2008), Horoman, Japan (Rehkämper et al., 1999a; Saal et al., 2001), Lower Austria (Becker et al., 2004), Eifel, Germany (Schmidt and Snow, 2002), Ural, Russia (Tessalina et al., 2007) and Ronda, Spain (Reisberg et al., 1991). Given the observed heterogeneity and large HSE concentration and Os isotope variation within these pyroxenite sample suites, a comprehensive HSE study of pyroxenites from more locations worldwide may shed further light on the range of pyroxenite HSE and Os isotopes compositions in different mantle environments. Future sampling of pyroxenite layers in geological context with adjacent peridotite or modally layered pyroxene-rich peridotites may further improve our understanding of small-scale redistribution of both lithophile and siderophile trace elements during melt-rock interaction.

Chapter 7

Appendix: Geology and Samples

7.1 Geological Setting

The Totalp ultramafic massif in eastern Switzerland consists of serpentinized spinel lherzolites associated with layered and folded spinel and spinel-garnet clinopyroxenites, spinel websterites, and more rarely spinel orthopyroxenites. The massif forms the northernmost part of the Arosa imbricate zone, which separates the Penninic and Austroalpine units (Figure 7.1; e.g. Schmid et al, 2004). It was emplaced on the ocean floor of the Jurassic Piedmont-Liguria branch of the Tethys Ocean. The Piedmont-Liguria ocean basin underwent a period of spreading from 210 to 160 Ma and attained a maximum width of ~ 500 km (Stampfli and Borel, 2004; Schmid et al., 2004). For a detailed geological overview and a geological map see e.g. Peters and Stettler (1987) and Schmid et al. (2004), for paleogeographical reconstructions see Manatschal and Bernoulli (1998) and Stampfli and Borel (2004).

The ultramafic massif has been tectonically overturned, but is in primary contact with radiolarites and ophicalcitic breccias (Figure 7.2, Weissert and Bernoulli, 1985). From biostratigraphic correlation and $^{39}Ar/^{40}Ar$ dating of phlogopite from pyroxenites, an emplacement age of the body on the seafloor of 160 Ma has been inferred (Weissert and Bernoulli, 1985; Peters and Stettler, 1987). U-Pb ages of 160 ± 1 Ma from zircons in oceanic gabbro from the nearby Platta locality (Schaltegger et al., 2002) suggest coeval magmatism, and thus proximity to an ocean ridge environment at the time of emplacement.

During the Alpine orogeny, the ultramafic body was obducted and tectonically overturned along with surrounding sediments and basaltic and gabbroic rocks (Peters and Stettler, 1987; Müntener et al., 2004; Stampfli and Borel, 2004). The pyroxenites are sometimes folded and concordant or oblique to a high-temperature foliation (Peters, 1963), and occasionally show well-preserved igneous textures (Peters, 1963; Peters and Stettler, 1987; van Acken et al. 2008).

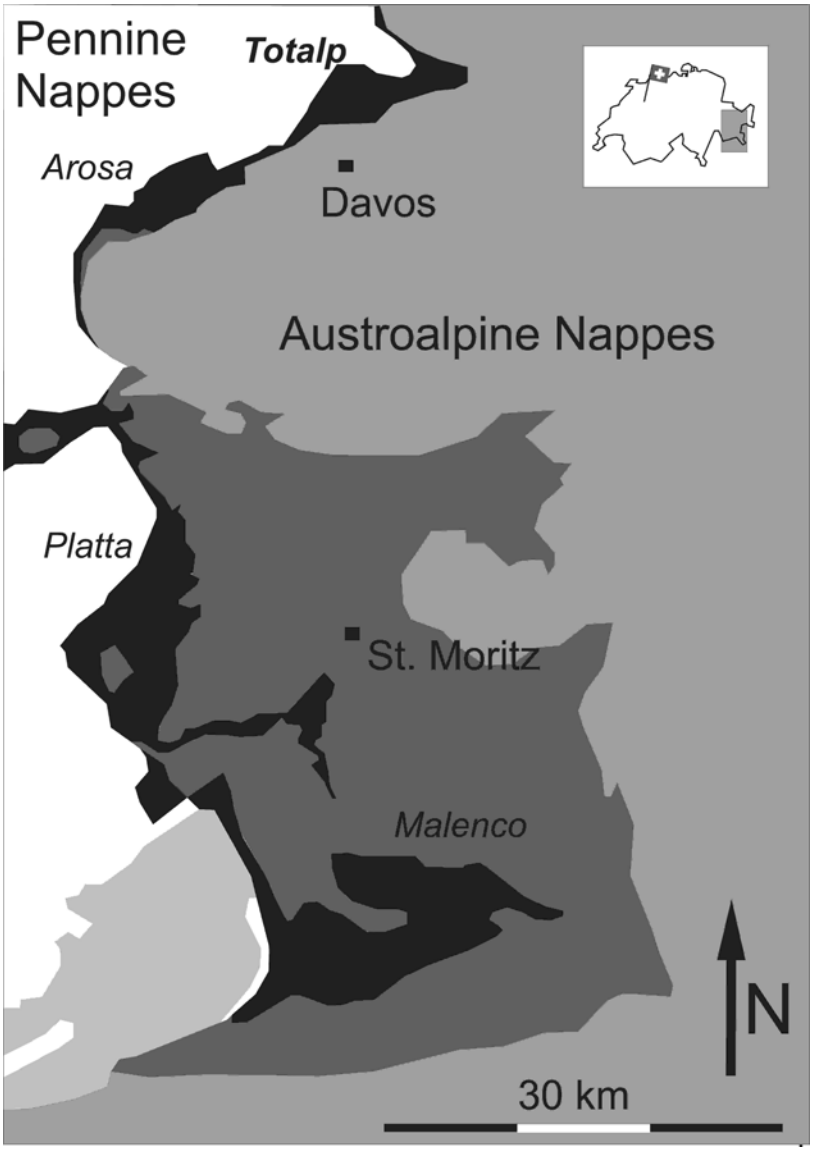

Figure 7.1: Sketch map of southeastern Switzerland, showing the occurrence of ophiolite-bearing units in black, redrawn and simplified after Desmurs et al. (2002) and Müntener et al. (2004)

The presence of spinel in the lherzolites, and spinel and spinel-garnet assemblages in the pyroxenites combined with the absence of plagioclase in both lithologies indicates that the last equilibration occurred in the deeper lithospheric mantle (Peters and Stettler, 1987), followed by rapid uplift. Temperatures between 830 and 975°C and a pressure of 10 ± 3 kbar were

estimated for a last equilibration under spinel lherzolite facies conditions (Peters and Stettler, 1987). The occurrence of garnet in some Totalp pyroxenites indicates higher equilibration pressures for these rocks of up to 15 - 18 kbar (Gasparik, 1984).

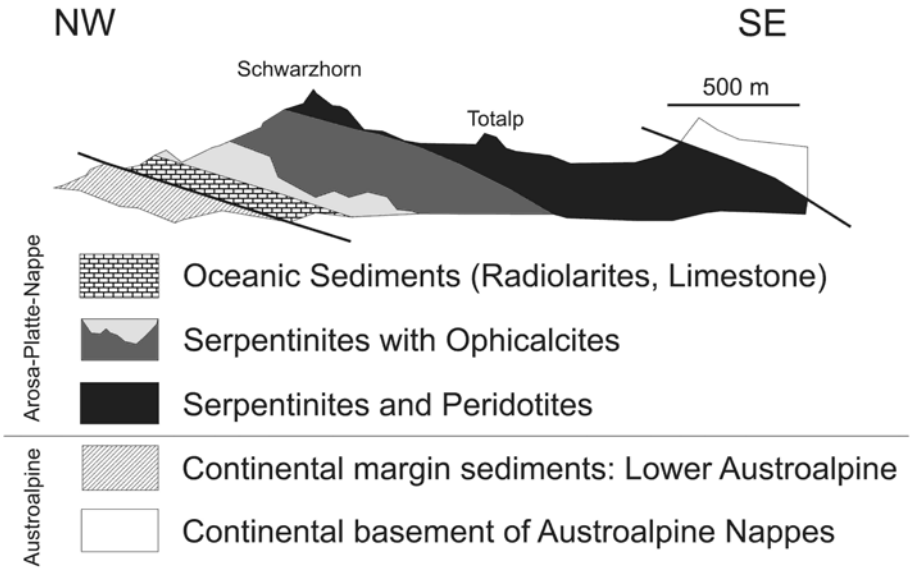

Figure 7.2: Cross section across Totalp imbricate north of Davos showing the tectonically overturned oceanic stratigraphy. Redrawn and simplified after Weissert and Bernoulli (1985)

Evidence for widespread melt-peridotite interaction and refertilization is based on textural evidence, in particular in the transition from pyroxenites to peridotites and in the form of clusters of clinopyroxenes in the peridotites, presumably representing former melt pockets. Additional compositional evidence for addition of clinopyroxene to peridotites is indicated by major element, Sm-Nd and Re-Os isotopic data (Müntener et al., 2004; Piccardo et al., 2004, van Acken et al., 2008).

Following Jurassic seafloor alteration and serpentinization, the rocks underwent a very low grade metamorphic overprint in the course of the Alpine orogeny with peak temperatures of about 100 - 150°C based on stable isotope data (Burkhard and O'Neil, 1988; Früh-Green et al., 1990).

The detailed geologic setting and origin of the Totalp massif is still subject of discussion. Weissert and Bernoulli (1985) suggested an origin from an oceanic fracture zone. Lagabrielle and Lemoine (1997) proposed formation at a very slow-spreading plate margin, not unlike ultra-slow spreading centers like the South-West-Indian ridge or the Arctic Gakkel ridge (Dick et al., 2003; Michael et al., 2003). Several authors advocate an origin in the subcontinental mantle and subsequent tectonic emplacement during the continental rifting/ocean spreading transition by low angle detachment faults similar to that recommended for the southward Platta and Malenco units (Müntener and Hermann, 2001; Desmurs et al., 2002; Müntener et al., 2004).

7.2 Samples

For this study, a number of spinel lherzolites, spinel websterites, spinel- and spinel-garnet clinopyroxenites from pyroxenitic layers from the Totalp massif were studied. Several samples were collected as composite pyroxenite-peridotite samples or comprise profiles across modally layered pyroxenites. Pyroxenite layer thickness varies from few mm up to ca. 0.5 m.

Peridotite samples were collected over a substantial part of the surface area occupied by the ultramafic body. The spinel lherzolites have been serpentinized to various degrees (water content 5.5 – 11.4%, see Supplementary table). Besides serpentine minerals and magnetite, their mineralogy consists mainly of orthopyroxene (opx) and clinopyroxene (cpx). Olivine has been almost completely serpentinized; in the less serpentinized samples, small olivine relics can be found. The original high-temperature textures are still discernable, as fine-grained serpentine forms pseudomorphs after olivine and orthopyroxene. Most peridotites show protogranular textures with anhedral grains that are medium to coarse grained (1 – 5 mm). Some peridotites have porphyroclastic texture with pyroxene and olivine clasts in an anastomozing network of fine-grained serpentine schlieren. Pyroxenes are in general less affected by alteration than olivine, with clinopyroxenes being minimally altered. Cr-poor spinel commonly forms anhedral interstitial grains that show concave embayments towards

larger pyroxene and olivine grains. Spinel is often partially replaced by a secondary magnetite rim. Small sulfide grains can be found scattered throughout the samples, both on grain boundaries and within silicate grains.

The clinopyroxenites and websterites often display protogranular textures and are medium to coarse grained. They comprise anhedral opx, cpx and green or brown spinel. Olivine is

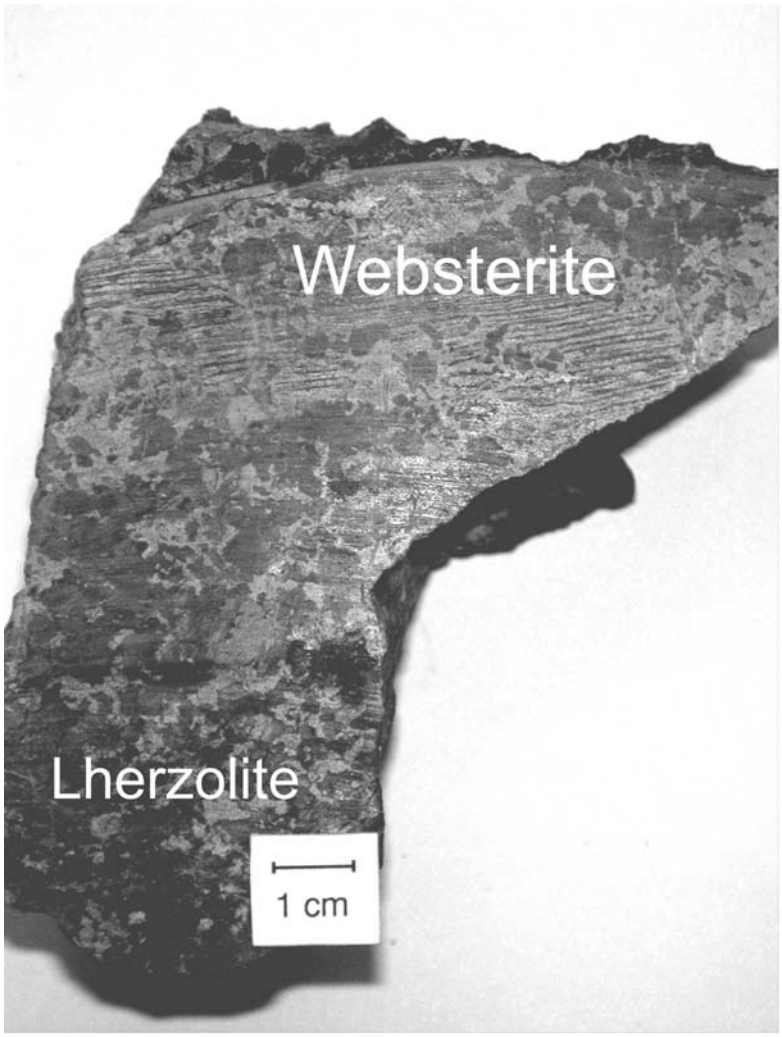

Figure 7.3: Photograph of a hand specimen showing pyroxene-rich veins and igneous textures in the transition region from websterite (top, light-colored) to lherzolite (bottom, dark-colored) in a composite sample (TA11) from the Totalp massif, Eastern Switzerland. The websterite layer at the top contains exsolved pyroxene megacrysts.

common in websterites, may occur in orthopyroxenites and is absent from spinel- and spinel-garnet clinopyroxenites. During serpentinization, olivine has been largely replaced by fibrous, fine-grained serpentine minerals and magnetite. Pyrope-rich garnet occurs in some clinopyroxenite samples. Grain sizes of all minerals are heterogeneously distributed, varying between < 1 mm and megacrysts of several cm of size. Orthopyroxenes and clinopyroxenes are often clustered in cumulate textures, ranging in size from tens of µm to megacrysts and show various degrees of serpentinization. Clinopyroxenes tend to be less altered than orthopyroxenes. Pyroxene exsolution lamellae are common, with kinked exsolution lamellae recording deformation. Notable are megacrystic pyroxenite layers, with individual orthopyroxene grains measuring up to 10 by 15 cm in size (TA22A1). In megacrystic pyroxenes, broad pyroxene exsolution lamellae occur. Exsolution of garnet in clinopyroxene and garnet coronas surrounding spinel are restricted to some Al-rich clinopyroxenites, and likely reflect cooling under deep lithosphere conditions. Embayed spinel, partially altered to magnetite or hematite, occurs preferentially along grain boundaries of cpx. Detailed petrographic descriptions of lithologies occurring in the Totalp massif are given by Peters (1963 and 1968).

Brief headword descriptions of representative samples from this study are given below (ol: olivine; opx: orthopyroxene; cpx: clinopyroxene; spl: spinel; gt: garnet).

TA1: protogranular, px-rich lherzolite, serpentine minerals from ol- and px-alteration from mesh-like textures of fibrous small serpentine grains, spinel altered to Fe-oxide, kinked exsolution bands in pyroxene megacrysts show tectonic stress

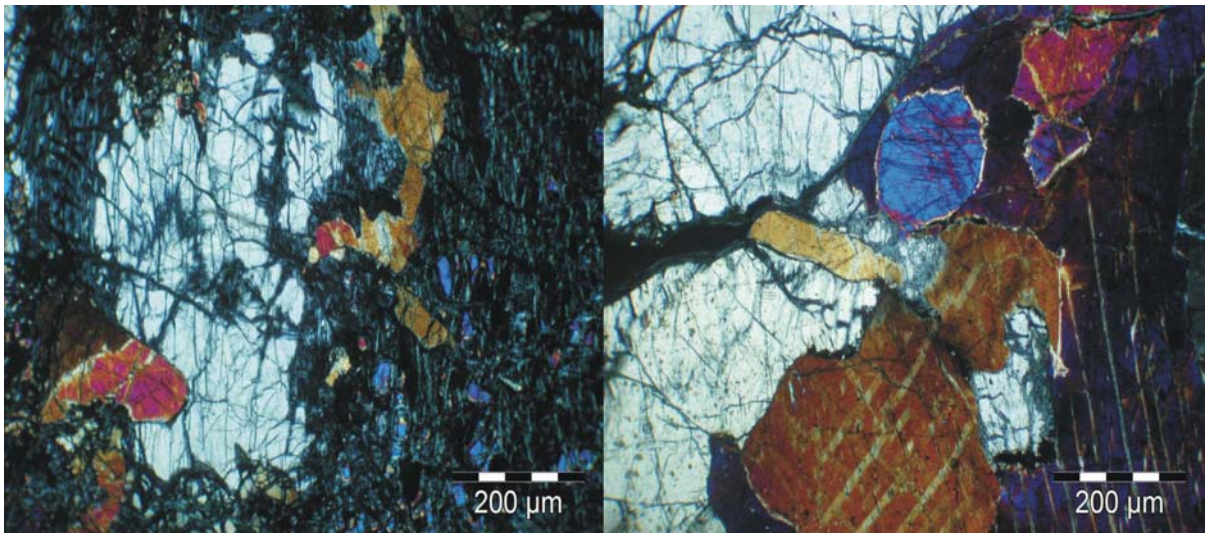

Figure 7.4: thin section microscope images, polarized light, crossed polarizers; left: typical Totalp lherzolite texture, sample TA18; right: pyroxene macro- and megacryst cumulates, websterite sample TA13D

TA2A: protogranular lherzolite; fresh px-megacrysts forming a layer; kinked cleavage shows tectonic stress; ol completely altered; veins of fibrous serpentine throughout the sample

TA2B: protogranular lherzolite; strong serpentinization and opacitisation; few fresh px; serpentine forms mesh pattern

TA3: protogranular lherzolite, relics of ol and px megacrysts; vein network of fibrous serpentine, even cpx partially affected by serpentinization, veins of serpentine minerals possibly reflect fluid flow

TA4: highly serpentinized protogranular, px-rich lherzolite, mesh texture of serpentine, ol completely serpentinized, px only altered along cracks and cleavage

TA7: porphyroclastic lherzolite, completely serpentinized, pyroxene-megacryst contours still recognizable, anastomosing vein network of fibrous serpentine

TA8: porphyroclastic lherzolite, anastomosing vein network of fibrous serpentine minerals, around relics of olivine and pyroxene megacrysts,

TA9: protogranular lherzolite, relics of anhedral ol- and px-megacrysts in a groundmass of fibrous serpentine minerals

TA10: protogranular lherzolite, relics of anhedral ol-megacrysts in a groundmass of fibrous serpentine minerals; well preserved pyroxene megacrysts form a poorly defined layer; serpentine veins crosscut pyroxene megacrysts

TA11: TA11A1 (olivine-websterite) contains orthopyroxene and clinopyroxene megacrysts with sizes up to several cm, containing abundant two-pyroxene exsolution features. While the clinopyroxene appear fresh, orthopyroxene is almost completed serpentinized. In contrast to other samples, no serpentine network has formed here. TA11A2 (spinel olivine-websterite) contains abundant clinopyroxene, orthopyroxene, spinel and relic olivine and displays a protogranular texture. TA11B (porphyroclastic spinel websterite) contains abundant kink-banded orthopyroxene and clinopyroxene megacrysts and minor spinel in a serpentine ground mass.

TA12: protogranular lherzolite, cpx-megacrysts, ol-relics, large fraction of opaque Fe-oxide phase around brown spinel, serpentine displays mesh-like texture, pyroxene megacrysts form a cm-wide layer, spinel altered to Fe-oxide concentrated within that layer

TA13 Sample TA13B (olivine websterite) contains abundant megacrystic orthopyroxene porphyroclasts embedded in medium to coarse-grained clinopyroxene, orthopyroxene and serpentinized olivine. Both orthopyroxene and clinopyroxene show kinked exsolution lamellae. TA13B contains no primary spinel, only Fe-oxide as its alteration products. Sample TA13D (spinel websterite) has a modal composition and coarse-grained porphyroclastic texture similar to TA13B, except that it also contains coarse-grained primary spinel along grain boundaries. Orthopyroxene and clinopyroxene grains are smaller than in sample TA13B.

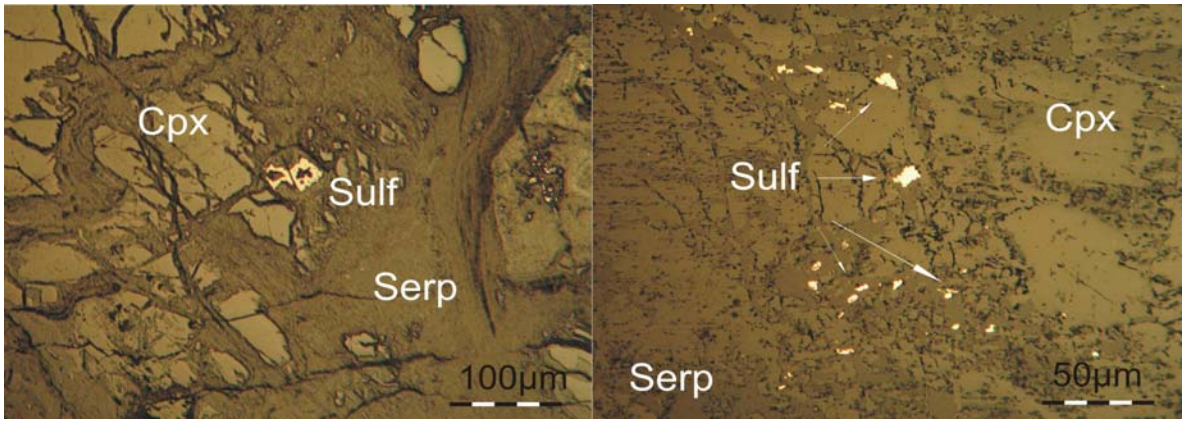

Figure 7.5: thick section reflected light microscope images; left: anhedral sulfide grain in websterite TA11A2; right: disseminated sulfides in wehrlite TA54A

TA14: protogranular; px-rich lherzolite, fibrous serpentine forms mesh texture around fresh pyroxene clasts, spinel altered to Fe-oxide

TA15: protogranular lherzolite; relics of ol and px megacrysts; strongly serpentinized, mesh texture of fibrous serpentine; large amount of opaque phases, spinel altered to Fe-oxide concentrated along pyroxene megacrysts

TA16: protogranular; px-rich lherzolite, comparatively serpentinized to a lesser degree; fibrous serpentine forms mesh texture around fresh pyroxene clasts, spinel altered to Fe-oxide

TA17: pyroxene-poor lherzolite, completely serpentinized, no primary textures recognizable

TA18: protogranular lherzolite; relics of ol and px megacrysts preserved in clusters; strongly serpentinized, mesh texture of fibrous serpentine; spinel completely altered to Fe-oxides

TA20: protogranular lherzolite; relics of ol and px megacrysts in a fibrous serpentine groundmass, mesh texture of serpentine; large amounts of opaque minerals (Fe-oxides?) both as mm-size crystals and on serpentine – pyroxene boundaries

TA21: lherzolite, completely serpentinized, few remaining pyroxene grains concentrated in a layer within a groundmass of fine-grained, fibrous serpentine minerals and sometimes crosscut by serpentine veins

TA22: TA22A1 (websterite) is a coarse-grained pyroxene-rich layer, embedded in the completely serpentinized lherzolite TA22A2, with a few relic clinopyroxene porphyroclasts in a serpentine matrix. The primary texture of the lherzolite is no longer discernable.

TA23A: protogranular px-rich lherzolite with fresh cpx and altered opx, ol completely altered to serpentine, spinel altered to Fe-oxides; fibrous fine-grained serpentine minerals form a network around px relics concentrated in a layer, some px grains crosscut by serpentine veins

TA23B: protogranular lherzolite; megacryst relics of ol and cpx; strongly altered along cracks and cleavage; high content of opaque minerals, mostly spinel altered to Fe oxides

TA24A: protogranular lherzolite with px-megacrysts arranged in clusters; fine-grained fibrous serpentine form a mesh texture around px- and ol relics, serpentine veins between px-and ser-aggregates, partial serpentinization of px along cracks and cleavage

TA24B: lherzolite; primary texture erased by serpentinization, some px-clusters still discernable in a groundmass of fibrous, fine-rained serpentine minerals, few ol relics, spinel partially altered to Fe-oxides

TA26: porphyroclastic lherzolite with px-megacryst layers separated by a groundmass of fibrous fine-grained serpentine minerals, crosscut by serpentine veins indicating fluid flow, spinel partially altered to Fe-oxides

TA54: samples TA54A, B, C1 - C3 and D represent a sequence of wehrlite to garnet olivine-clinopyroxenite layers cut as between 2 and 5 cm-thick slices from a modally zoned pyroxenite; cpx show minor alteration along exsolution lamellae and cleavage, while minor opx and ol are strongly serpentinized near grain boundaries; embayed anhedral spl is almost completely converted to secondary Fe-oxides; TA54A represents a very sulfide rich spl wehrlite layer in contact with lherzolite; gt content increases from TA54B to TA54D, while spl abundance decreases from TA54B through TA54D. All TA54 samples show cumulate textures of pyroxene megacrysts, with serpentinized olivine remnants.

TA55: layered lherzolite – websterite – clinopyroxenite sequence, TA55AB: lherzolite; TA55C ol-websterite; TA55D1: ol-websterite; boundaries between websterite and lherzolite are sharp; layer thickness of TA55C and TA55D1 is approximately 2.5 cm; minor serpentinization along cracks and grain boundaries. Opx-rich sample TA55C does not contain garnet and grades into cpx-rich and garnet-bearing olivine-websterite TA55D1. TA55C contains both orthopyroxene and clinopyroxene along minor olivine and spinel, the latter two partially altered to serpentine minerals, hematite and magnetite. TA55D1 contains less orthopyroxene than TA55C and has been affected more intensively by serpentinization.

TA61: coarse grained protogranular garnet olivine-clinopyroxenite layer, little signs of serpentinization; without clear spatial relation to surrounding serpentinized peridotite; large deformed opx and cpx without pyroxene exsolution features are crosscut by garnet veins, likely representing garnet exsolution along cracks or cleavage.

Appendix Table 7.3.1: Measured major element concentrations in wt%, except where stated otherwise

	SiO_2	TiO_2	Al_2O_3	Fe_2O_3	FeO	MnO	MgO	CaO	Na_2O	K_2O	P_2O_5	H_2O	CO_2	Cr(ppm)	Cr_2O_3	Ni(ppm)	NiO	sum
TA-1	41.8	0.13	3.33	8.12	7.31	0.12	33.0	3.42	0.30	0.01	0.01	8.48	0.12	2304	0.34	1709	0.22	98.59
TA-2A	38.3	0.06	2.00	8.87	7.98	0.10	36.0	1.05	0.07	0.01	0.01	11.36	0.22	1617	0.24	1964	0.25	97.62
TA-2B	40.4	0.12	3.03	7.46	6.72	0.10	33.6	3.20	0.24	0.01	0.01	9.27	0.18	2293	0.34	1779	0.23	97.40
TA-2C	39.7	0.10	3.09	8.05	7.24	0.10	34.5	2.52	0.19	0.01	0.01	10.34	0.19	2426	0.35	1902	0.24	98.51
TA-3	41.3	0.12	3.52	8.09	7.28	0.11	35.6	2.33	0.14	0.01	0.02	7.74	0.20	2695	0.39	1867	0.24	99.01
TA-4	40.5	0.11	3.18	8.12	7.30	0.11	34.9	2.23	0.08	0.01	0.02	8.2	0.22	2339	0.34	1842	0.23	97.48
TA-5	40.0	0.12	3.36	7.94	7.15	0.12	34.6	2.95	0.19	0.01	0.01	8.96	0.13	2176	0.32	1778	0.23	98.15
TA-6	39.6	0.11	3.08	7.95	7.15	0.11	34.3	2.82	0.17	0.01	0.01	9.87	0.15	2183	0.32	1803	0.23	97.94
TA-7	39.2	0.12	2.73	8.17	7.35	0.11	35.7	1.48	0.09	0.01	0.02	11.16	0.15	2601	0.38	1925	0.24	98.69
TA-8	41.3	0.14	3.58	8.28	7.45	0.12	36.1	2.58	0.15	0.01	0.02	6.83	0.21	2719	0.40	1925	0.24	99.08
TA-9	39.1	0.10	2.76	8.37	7.53	0.11	35.2	2.10	0.17	0.01	0.01	10.36	0.17	2049	0.30	1902	0.24	98.12
TA-10	40.8	0.11	3.16	8.57	7.71	0.12	33.8	2.67	0.18	0.01	0.01	8.89	0.18	1801	0.26	1748	0.22	98.14
TA-11A1	41.6	0.31	8.21	5.84	5.25	0.14	24.0	10.7	0.61	0.01	0.01	6.3	0.09	4016	0.59	792	0.10	97.87
TA-11A2	40.7	0.26	8.41	6.56	5.90	0.14	26.7	8.32	0.45	0.01	0.01	7.02	0.11	4022	0.59	999	0.13	98.70
TA-11B	41.1	0.27	7.94	6.48	5.83	0.14	25.9	9.02	0.48	0.01	0.01	7.18	0.10	3685	0.54	1042	0.13	98.68
TA-12	39.9	0.10	3.03	8.44	7.59	0.11	34.6	2.53	0.18	0.01	0.01	10.02	0.14	2293	0.34	1871	0.24	98.81
TA-13B	45.2	0.25	6.57	6.22	5.60	0.14	25.5	9.29	0.55	0.01	0.01	5.59	0.11	3146	0.46	918	0.12	99.40
TA-13C	41.1	0.11	3.62	7.56	6.80	0.10	34.0	2.89	0.21	0.01	0.02	9.69	0.18	1909	0.28	1825	0.23	99.21
TA-13D	43.6	0.20	6.51	6.72	6.05	0.14	28.5	6.30	0.50	0.01	0.01	6.35	0.13	3811	0.56	1327	0.17	99.00
TA-14	40.4	0.11	3.05	8.22	7.39	0.11	34.2	2.81	0.19	0.01	0.01	9.17	0.14	1934	0.28	1833	0.23	98.11
TA-15	41.4	0.14	3.93	7.95	7.15	0.12	33.5	3.45	0.25	0.01	0.01	8.41	0.13	2518	0.37	1719	0.22	99.12
TA-16	40.5	0.11	3.57	8.09	7.28	0.12	33.9	3.24	0.23	0.01	0.01	8.63	0.13	2730	0.40	1750	0.22	98.34
TA-17	39.1	0.12	2.78	7.56	6.80	0.11	34.8	3.22	0.19	0.01	0.01	10.82	0.20	2704	0.40	1893	0.24	98.83
TA-18	40.1	0.14	3.36	7.96	7.16	0.11	33.7	3.11	0.23	0.01	0.02	10.44	0.14	2324	0.34	1793	0.23	99.07
TA-19	38.9	0.13	3.31	7.82	7.04	0.14	33.2	3.20	0.17	0.01	0.01	10.71	0.24	2466	0.36	1874	0.24	97.71
TA-20	40.5	0.16	4.40	8.08	7.27	0.13	32.1	3.91	0.29	0.01	0.01	9.43	0.13	3581	0.52	1633	0.21	99.07
TA-21	40.0	0.13	3.51	8.06	7.25	0.12	33.9	3.07	0.24	0.01	0.02	10.51	0.11	2376	0.35	1774	0.23	99.47
TA-22A1	41.7	0.12	2.88	5.95	5.35	0.13	30.5	6.64	0.32	0.01	0.01	9.29	0.34	4352	0.64	1680	0.21	98.11
TA-22A2	39.1	0.05	1.59	7.51	6.76	0.12	37.2	1.74	0.04	0.01	0.01	10.58	0.50	2007	0.29	1903	0.24	98.18
TA-23A	40.8	0.11	3.28	8.01	7.21	0.12	34.7	2.89	0.22	0.01	0.02	9.69	0.15	2205	0.32	1801	0.23	99.69
TA-23B	40.5	0.12	3.12	7.98	7.18	0.11	34.4	3.05	0.24	0.01	0.02	9.78	0.17	2043	0.30	1799	0.23	99.26
TA-24A	40.9	0.11	3.39	8.37	7.53	0.11	33.9	2.99	0.16	0.01	0.01	9.54	0.14	2241	0.33	1801	0.23	99.30
TA-24B	41.0	0.10	3.12	7.77	6.99	0.11	34.6	2.60	0.20	0.01	0.01	9.46	0.15	2199	0.32	1800	0.23	98.87
TA-25B	37.6	0.11	2.57	8.52	7.67	0.10	35.1	2.37	0.16	0.01	0.01	11.13	0.21	2555	0.37	1883	0.24	97.64
TA-26	40.0	0.12	2.94	8.04	7.23	0.11	34.4	2.76	0.17	0.01	0.01	10.5	0.17	2063	0.30	1831	0.23	98.97
TA-27	40.0	0.10	2.93	8.03	7.23	0.11	34.2	2.58	0.20	0.01	0.01	10.76	0.13	2099	0.31	1778	0.23	98.85
TA-28	39.1	0.13	3.46	7.81	7.03	0.13	33.3	3.00	0.23	0.01	0.01		0.18	3077	0.45	856	0.11	87.12
TA-31	40.4	0.14	3.51	7.86	7.08	0.11	33.5	3.00	0.29	0.01	0.02		0.13	4279	0.63	544	0.07	88.88
TA-33A	39.5	0.12	3.37	7.97	7.17	0.13	33.4	3.02	0.21	0.01	0.02		0.17	4196	0.61	796	0.10	87.85
TA-34B	47.0	0.23	11.0	6.01	5.40	0.13	21.6	11.5	0.68	0.01	0.01	1.23	0.08	1795	0.26	629	0.08	99.20
TA-35	49.7	0.18	7.10	4.65	4.18	0.12	20.2	15.1	0.69	0.01	0.01	1.09	0.08	4510	0.66	542	0.07	99.16
TA-36A	50.2	0.15	7.66	4.25	3.83	0.12	20.0	14.7	0.78	0.01	0.01	0.88	0.08	1379	0.20	381	0.05	98.65
TA-36C	52.1	0.10	6.47	6.51	5.86	0.13	30.3	3.05	0.20	0.01	0.02	0.82	0.08	2097	0.31	1791	0.23	99.66
TA-37	38.9	0.07	2.47	7.54	6.78	0.11	36.1	2.07	0.16	0.01	0.01		0.11	3027	0.44	1782	0.23	87.43
TA-38	40.9	0.16	4.01	7.98	7.18	0.13	32.8	3.64	0.30	0.01	0.02		0.1	2627	0.38	1768	0.22	89.80
TA-40	41.2	0.13	3.67	8.15	7.33	0.12	33.3	3.47	0.27	0.01	0.02		0.1	2597	0.38	1807	0.23	90.26
TA-42	40.6	0.12	2.92	8.32	7.49	0.11	35.8	2.19	0.22	0.01	0.02		0.19	2491	0.36	1673	0.21	90.24
TA-49	43.7	0.23	6.93	5.44	4.89	0.12	26.3	8.74	0.49	0.02	0.01	6.43	0.08	2156	0.32	1762	0.22	98.48
TA-50A	41.8	0.15	4.59	7.49		0.14	32.9	4.15	0.38	0.01	0.01	8.80	0.19	3560	0.52	1761	0.22	100.24
TA-50B	39.9	0.12	3.28	7.84		0.11	34.6	3.00	0.30	0.01	0.01	10.33	0.18	2091	0.31	1771	0.23	99.34
TA-50C	39.6	0.13	3.38	7.73		0.12	34.2	3.00	0.34	0.01	0.01	10.93	0.22	2218	0.32	1877	0.24	99.34
TA-51	46.5	0.14	12.9	5.35	4.82	0.14	15.9	17.7	0.62	0.11	0.01	1.22	0.08	2279	0.33	1813	0.23	100.85
TA-54A	36.1	0.11	7.69	7.86		0.14	30.7	4.64	0.13	0.01	0.01	10.76	0.11	5906	0.86	2920	0.37	98.11
TA-54B	42.5	0.17	11.7	5.45		0.14	21.5	13.3	0.51	0.01	0.01	3.44	0.12	7137	1.04	1493	0.19	98.45
TA-54C1	43.5	0.15	12.3	5.27		0.14	21.2	13.4	0.49	0.01	0.01	3.01	0.08	3347	0.49	754	0.10	99.28
TA-54C2	45.0	0.15	11.5	5.03		0.14	19.8	15.1	0.56	0.02	0.01	2.53	0.11	1629	0.24	629	0.08	99.60
TA-54C3	44.9	0.13	12.8	5.35		0.16	18.4	15.4	0.61	0.07	0.01	1.91	0.11	1502	0.22	679	0.09	99.59
TA-54D	44.5	0.12	12.6	5.46		0.17	17.3	16.9	0.57	0.05	0.01	2.18	0.12	1579	0.23	375	0.05	99.65
TA-55AB	41.3	0.15	6.60	7.48		0.15	30.7	4.37	0.20	0.01	0.01	7.52	0.14	4948	0.72	877	0.11	98.42
TA-55C	49.9	0.16	7.62	6.36		0.14	27.0	6.61	0.42	0.03	0.01	1.15	0.05	3746	0.55	1021	0.13	99.09
TA-55D1	45.4	0.21	12.4	5.76		0.14	21.0	12.4	0.62	0.03	0.01	1.35	0.07	4115	0.60	954	0.12	99.06
TA-55D2	46.0	0.20	11.9	5.71		0.14	20.4	13.1	0.62	0.03	0.01	1.46	0.08	2579	0.38	819	0.10	99.36
TA-55E	45.4	0.17	13.3	5.93		0.16	19.5	13.3	0.61	0.08	0.01	1.34	0.09	2127	0.31	527	0.07	99.55
TA-55F	44.0	0.14	13.2	5.89		0.16	16.4	17.2	0.59	0.04	0.01	1.91	0.16	1262	0.18	555	0.07	99.43
TA-56	45.6	0.13	13.3	5.54	4.98	0.14	15.9	17.2	0.62	0.13	0.01	1.33	0.08	921	0.13	352	0.04	99.65
TA-57	40.1	0.13	3.31	7.97	7.17	0.11	34.4	2.79	0.22	0.01	0.02		0.14	2430	0.36	1777	0.23	89.06
TA-60	45.2	0.21	13.5	6.91	6.22	0.16	16.4	14.3	0.73	0.07	0.01	1.43	0.08	1550	0.23	424	0.05	98.62
TA-61	46.4	0.21	10.7	6.05	5.45	0.12	15.0	18.1	0.94	0.02	0.01	1.51	0.08	1659	0.24	636	0.08	98.97
TA-62	40.7	0.13	3.12	7.62	6.86	0.11	34.6	3.03	0.18	0.01	0.02		0.21	2297	0.34	1870	0.24	89.53

All samples measured at Universität Karlsruhe by H. Becker, except TA50, TA54 and TA55 measured at GFZ Potsdam by R. Naumann

Appendix Table 7.3.2: Volatile content corrected major element concentrations in wt%, except where stated otherwise, Mg# and Cr#

	SiO_2	TiO_2	Al_2O_3	FeO	MnO	MgO	CaO	Na_2O	K_2O	P_2O_5	Cr_2O_3	NiO	Mg#	Cr#	Cr (ppm)	Ni (ppm)
TA-1	46.4	0.15	3.70	8.12	0.13	36.7	3.81	0.3	0.01	0.01	0.37	0.24	0.890	0.064	2560	1899
TA-2A	44.5	0.08	2.32	9.27	0.11	41.9	1.22	0.09	0.01	0.01	0.27	0.29	0.889	0.074	1879	2283
TA-2B	45.9	0.13	3.44	7.64	0.12	38.2	3.64	0.27	0.01	0.02	0.38	0.26	0.899	0.069	2607	2023
TA-2C	45.1	0.11	3.51	8.23	0.12	39.2	2.86	0.22	0.01	0.02	0.40	0.28	0.895	0.072	2757	2162
TA-3	45.4	0.13	3.87	7.99	0.12	39.1	2.56	0.15	0.01	0.02	0.43	0.26	0.897	0.070	2959	2050
TA-4	45.5	0.13	3.57	8.20	0.13	39.2	2.50	0.09	0.01	0.02	0.38	0.26	0.895	0.067	2626	2068
TA-5	45.0	0.14	3.77	8.03	0.13	38.8	3.31	0.21	0.01	0.02	0.36	0.25	0.896	0.060	2443	1996
TA-6	45.0	0.13	3.50	8.13	0.13	39.0	3.21	0.19	0.01	0.01	0.36	0.26	0.895	0.065	2483	2051
TA-7	44.9	0.14	3.13	8.41	0.12	40.8	1.69	0.10	0.01	0.02	0.44	0.28	0.896	0.085	2977	2203
TA-8	44.8	0.15	3.89	8.09	0.13	39.2	2.80	0.16	0.01	0.02	0.43	0.27	0.896	0.069	2954	2092
TA-9	44.6	0.12	3.15	8.60	0.12	40.2	2.39	0.19	0.01	0.01	0.34	0.28	0.893	0.068	2339	2172
TA-10	45.8	0.13	3.55	8.66	0.13	38.0	3.00	0.21	0.01	0.01	0.30	0.25	0.887	0.053	2022	1963
TA-11A1	45.5	0.34	8.97	5.74	0.15	26.2	11.7	0.67	0.01	0.02	0.64	0.11	0.891	0.046	4390	866
TA-11A2	44.4	0.28	9.18	6.44	0.16	29.1	9.09	0.49	0.01	0.01	0.64	0.14	0.890	0.045	4392	1091
TA-11B	45.0	0.30	8.69	6.37	0.15	28.4	9.87	0.52	0.01	0.01	0.59	0.15	0.888	0.043	4032	1140
TA-12	45.0	0.11	3.42	8.57	0.12	39.1	2.85	0.21	0.01	0.02	0.38	0.27	0.890	0.069	2587	2111
TA-13B	48.2	0.27	7.01	5.97	0.15	27.2	9.91	0.59	0.01	0.01	0.49	0.12	0.890	0.045	3357	980
TA-13C	46.0	0.12	4.05	7.61	0.11	38.0	3.23	0.24	0.01	0.02	0.31	0.26	0.899	0.049	2137	2043
TA-13D	47.1	0.22	7.04	6.54	0.15	30.8	6.81	0.54	0.01	0.01	0.60	0.18	0.894	0.054	4119	1434
TA-14	45.5	0.12	3.44	8.33	0.13	38.5	3.17	0.22	0.01	0.02	0.32	0.26	0.892	0.058	2178	2064
TA-15	45.7	0.15	4.34	7.89	0.13	37.0	3.81	0.27	0.01	0.01	0.41	0.24	0.893	0.059	2780	1898
TA-16	45.2	0.13	3.99	8.13	0.14	37.9	3.62	0.25	0.01	0.01	0.45	0.25	0.893	0.070	3048	1954
TA-17	44.6	0.14	3.16	7.74	0.12	39.6	3.66	0.22	0.01	0.01	0.45	0.27	0.901	0.087	3079	2156
TA-18	45.3	0.15	3.79	8.09	0.12	38.1	3.51	0.26	0.01	0.02	0.38	0.26	0.894	0.064	2626	2026
TA-19	44.9	0.15	3.81	8.11	0.16	38.3	3.69	0.20	0.01	0.02	0.42	0.27	0.894	0.068	2842	2160
TA-20	45.3	0.18	4.92	8.12	0.15	35.8	4.37	0.33	0.01	0.02	0.58	0.23	0.887	0.074	4001	1824
TA-21	45.1	0.15	3.95	8.16	0.13	38.1	3.45	0.27	0.01	0.02	0.39	0.25	0.893	0.062	2674	1997
TA-22A1	47.1	0.14	3.26	6.05	0.15	34.5	7.51	0.36	0.01	0.01	0.72	0.24	0.910	0.129	4919	1899
TA-22A2	44.8	0.06	1.82	7.76	0.13	42.7	2.00	0.05	0.01	0.02	0.34	0.28	0.908	0.110	2304	2185
TA-23A	45.4	0.12	3.65	8.02	0.13	38.6	3.22	0.24	0.01	0.02	0.36	0.26	0.896	0.062	2454	2004
TA-23B	45.3	0.14	3.49	8.04	0.12	38.6	3.41	0.27	0.01	0.02	0.33	0.26	0.895	0.060	2288	2014
TA-24A	45.6	0.12	3.78	8.40	0.13	37.8	3.33	0.18	0.01	0.01	0.37	0.26	0.889	0.061	2501	2010
TA-24B	45.9	0.11	3.50	7.84	0.12	38.7	2.91	0.22	0.01	0.01	0.36	0.26	0.898	0.065	2464	2017
TA-25B	43.6	0.13	2.98	8.89	0.12	40.6	2.75	0.18	0.01	0.02	0.43	0.28	0.891	0.089	2961	2182
TA-26	45.3	0.14	3.33	8.19	0.13	39.0	3.12	0.19	0.01	0.01	0.34	0.26	0.895	0.064	2336	2074
TA-27	45.5	0.11	3.33	8.21	0.13	38.9	2.93	0.23	0.01	0.01	0.35	0.26	0.894	0.066	2386	2021
TA-28	45.0	0.15	3.98	8.09	0.15	38.3	3.45	0.26	0.01	0.02	0.52	0.13	0.894	0.080	3539	985
TA-31	45.6	0.15	3.96	7.97	0.12	37.7	3.38	0.32	0.01	0.02	0.70	0.08	0.894	0.107	4821	613
TA-33A	45.1	0.13	3.84	8.18	0.14	38.1	3.44	0.24	0.01	0.02	0.70	0.12	0.892	0.109	4786	908
TA-34B	48.0	0.23	11.3	5.52	0.13	22.0	11.7	0.70	0.01	0.01	0.27	0.08	0.877	0.016	1834	643
TA-35	50.7	0.19	7.25	4.27	0.12	20.6	15.4	0.70	0.01	0.01	0.67	0.07	0.896	0.059	4602	553
TA-36A	51.4	0.15	7.84	3.92	0.12	20.4	15.1	0.80	0.01	0.02	0.21	0.05	0.903	0.017	1412	390
TA-36C	52.7	0.10	6.55	5.93	0.13	30.7	3.08	0.20	0.01	0.02	0.31	0.23	0.902	0.031	2123	1813
TA-37	44.5	0.08	2.83	7.77	0.13	41.3	2.37	0.18	0.01	0.02	0.51	0.26	0.905	0.107	3467	2041
TA-38	45.6	0.18	4.47	8.00	0.15	36.5	4.05	0.34	0.01	0.02	0.43	0.25	0.891	0.060	2929	1971
TA-40	45.7	0.15	4.07	8.13	0.13	36.9	3.85	0.30	0.01	0.02	0.42	0.26	0.890	0.065	2880	2004
TA-42	45.1	0.13	3.24	8.32	0.12	39.7	2.43	0.24	0.01	0.02	0.40	0.24	0.895	0.077	2766	1858
TA-49	47.5	0.25	7.53	5.32	0.13	28.6	9.50	0.53	0.02	0.02	0.34	0.24	0.905	0.030	2344	1916
TA-50A	45.8	0.17	5.03	8.21	0.15	36.0	4.55	0.42	0.01	0.01	0.57	0.25	0.887	0.071	3901	1930
TA-50B	44.9	0.14	3.69	8.83	0.13	38.9	3.38	0.34	0.01	0.01	0.34	0.25	0.887	0.059	2354	1994
TA-50C	44.9	0.14	3.83	8.76	0.13	38.7	3.40	0.39	0.01	0.01	0.37	0.27	0.887	0.060	2515	2128
TA-51	46.7	0.14	13.0	4.84	0.14	16.0	17.8	0.62	0.11	0.01	0.33	0.23	0.855	0.017	2289	1821
TA-54A	41.4	0.12	8.81	9.01	0.15	35.2	5.32	0.15	0.01	0.01	0.99	0.43	0.874	0.070	6770	3347
TA-54B	44.7	0.18	12.3	5.74	0.15	22.6	14.0	0.54	0.01	0.01	1.10	0.20	0.875	0.057	7521	1573
TA-54C1	45.3	0.16	12.8	5.48	0.14	22.0	14.0	0.51	0.01	0.01	0.51	0.10	0.877	0.026	3480	784
TA-54C2	46.4	0.15	11.9	5.19	0.14	20.4	15.5	0.58	0.02	0.01	0.25	0.08	0.875	0.014	1680	649
TA-54C3	46.1	0.13	13.1	5.48	0.17	18.9	15.8	0.63	0.07	0.01	0.22	0.09	0.860	0.011	1539	696
TA-54D	45.7	0.12	12.9	5.61	0.17	17.8	17.3	0.59	0.05	0.01	0.24	0.05	0.850	0.012	1622	385
TA-55AB	45.5	0.16	7.27	8.24	0.17	33.8	4.81	0.22	0.01	0.01	0.80	0.12	0.880	0.068	5452	966
TA-55C	51.0	0.16	7.78	6.50	0.14	27.5	6.75	0.43	0.03	0.01	0.56	0.13	0.883	0.046	3827	1043
TA-55D1	46.5	0.22	12.7	5.90	0.14	21.5	12.6	0.63	0.03	0.01	0.62	0.12	0.867	0.032	4214	977
TA-55D2	47.0	0.20	12.2	5.84	0.15	20.9	13.4	0.63	0.03	0.01	0.39	0.11	0.864	0.021	2636	837
TA-55E	46.2	0.18	13.6	6.04	0.17	19.8	13.5	0.62	0.08	0.01	0.32	0.07	0.854	0.015	2168	537
TA-55F	45.2	0.14	13.6	6.05	0.17	16.8	17.7	0.61	0.04	0.01	0.19	0.07	0.832	0.009	1296	570
TA-56	46.4	0.13	13.6	5.07	0.14	16.2	17.6	0.63	0.14	0.01	0.14	0.05	0.850	0.007	937	358
TA-57	45.1	0.15	3.72	8.06	0.12	38.7	3.14	0.25	0.01	0.02	0.40	0.25	0.895	0.067	2733	1998
TA-60	46.6	0.21	13.9	6.41	0.17	16.9	14.7	0.75	0.07	0.01	0.23	0.06	0.824	0.011	1596	437
TA-61	47.7	0.22	11.0	5.59	0.12	15.4	18.6	0.96	0.02	0.01	0.25	0.08	0.831	0.015	1704	653
TA-62	45.6	0.15	3.49	7.68	0.13	38.7	3.39	0.20	0.01	0.02	0.38	0.27	0.900	0.067	2572	2094

Chapter 8

Appendix: Methods

8.1 Whole rock analyses

Pyroxenite and peridotite samples from the Totalp massif were studied for major element compositions; Re, Os, Ir, Ru, Pt and Pd concentrations and Os isotopic composition.

Some layered pyroxenites were cut using a diamond blade. The cut surfaces were abraded, using sand paper or sintered corundum in order to remove contamination from saw marks. Sample chips for most samples were produced in a ceramic jaw crusher. For a few samples a Mn steel jaw crusher was used. After cleaning with ultrapure water sample chips were powdered in an agate disk mill.

Whole rock major element abundances, H_2O and C contents were determined using XRF, Karl-Fischer titration and CSA at Universität Karlsruhe (for details, see Becker, 1996) and GFZ Potsdam (LECO RC-412-Analyzer (H_2O, CO_2). Reproducibilities (2s) are 2 – 3 % for SiO_2, MgO and FeO, 5 – 8 % for Al_2O_3, and CaO and 10 – 20 % for Na_2O, TiO_2 and MnO. Accuracy was monitored using ultramafic rock standards (DTS, UBN, PCC) that were included with each batch of samples and yielded results within quoted precisions.

For the determination of HSE abundances and Os isotope analysis, between two and three grams of sample powder were spiked with a mixed ^{99}Ru-^{105}Pd-^{191}Ir-^{194}Pt-Spike and a mixed ^{185}Re-^{190}Os spike prior to digestion. Digestion was performed in 2.5 ml conc. HCL and 5 ml conc. HNO_3 in sealed borosilicate glass Carius tubes at 220°C for 24 h followed by digestion at 320 °C to 345°C for 48 h, using the technique outlined elsewhere (Becker et al., 2006).

Osmium separation and analysis followed a modified procedure of Cohen and Waters (1996). After opening of the Carius tubes, the sample solution with the residue was transferred into polypropylene centrifuge tubes using ultrapure water. Three ml of CCl_4 were added to the sample sludge. The mixture was shaken to ensure thorough mixing of CCl_4 with the aqua regia and Os extraction and centrifuged for five minutes. The CCl_4 was transferred into Teflon beakers filled with 4 ml of concentrated, chilled HBr. This procedure was

repeated twice with three and two ml of CCl_4, respectively. The closed beakers containing HBr and CCl_4 were left on a hotplate at ~80°C for two hours to ensure complete Os extraction into the HBr. After cooling, the CCl_4 was removed and discarded; the HBr fraction was dried down. The residue was taken up in conc. HBr, transferred into the lid of a 5 ml conical Teflon beaker and dried down. A microdistillation technique (Birck et al., 1997) was used to clean the Os fraction. The apex of the conical beakers was filled with 12 µl of conc. HBr. Approximately 40 µl of Cr_2O_3/H_2SO_4 solution was added to the dried residue in the screw cap, the beakers screwed tightly shut and placed upside down on a hotplate at ~80°C for several hours. After opening, the HBr drop was dried down, and the sample Os loaded in HBr onto baked Pt filaments (99.995% ESPI) and covered with NaOH-$Ba(OH)_2$ activator solution.

Osmium isotopic ratios were measured as OsO_3^- using negative thermal ionization mass spectrometry (N-TIMS; Völkening et al., 1991; Creaser et al., 1991) at the Freie Universität Berlin (FUB), using a Thermo Electron Triton instrument, and at the University of Maryland (UMD) using a VG Sector-54 and a NBS-designed single collector 68° sector, 12° curvature thermal ionization mass spectrometer. Signals were detected on Faraday cups in static mode or by SEM in pulse counting mode, depending on signal intensity. Target intensities for Faraday cup measurement were 200 mV on mass 240, for SEM measurement 100000 counts on mass 240.

For measurements at FUB, an ion source was used for Pt filament measurements only, to avoid contamination and possible interferences from previous measurement on Re filaments. O_2 pressure during all measurements at FUB and UMD was set to $1* 10^{-7}$ to $1.7 * 10^{-7}$ bar with a bleed valve attached to the ion source chamber. Source and flight tube pressure were monitored throughout the measurement. Heating procedures had to be adapted for each sample, as no uniform current and focus settings could be obtained, likely because of varying filament geometry and discrepancies during loading. The range of filament currents during measurement ranges from 1000 mA to 1450 mA, preventing a uniform heating procedure to be given. Samples were heated with 100 mA per minute to 900 mA. After opening of the analyzer gate valve, heating continued with 50 mA per minute until 1050 mA or until the first signal was recorded. Depending on signal tendencies, some samples were continuously

heating during measurement. For Faraday cup runs, 100 isotope ratios were obtained, for SEM runs, 40 ratios.

All measured ratios were corrected for interferences from isobaric OsO_3^--molecules. Oxygen isotope corrections were made using $^{18}O/^{16}O$ and $^{17}O/^{16}O$ of 0.00204 and 0.00037, respectively. Measured ratios were mass fractionation corrected to a $^{192}Os/^{188}Os$ ratio of 3.08271 (Shirey and Walker, 1998) using an exponential fractionation law. For the low Os samples, $^{187}Os/^{188}Os$ was corrected for spike contribution, which led to a slight increase in $^{187}Os/^{188}Os$ in most samples, and to a substantial increase in samples TA54C1-3 and TA56. Unspiked duplicate measurements of these low oxygen samples replicated the corrected $^{187}Os/^{188}Os$ value.

A Johnson-Matthey Os standard solution was measured along with every batch of samples analyzed. Over the course of several months, measured $^{187}Os/^{188}Os$ of this standard at the FUB using faraday cups was 0.11381±0.00007 (2s, n=29). Measurements with the SEM yielded $^{187}Os/^{188}Os$ of 0.1138±0.0003 (2s, n=5). For the samples run at UMD, the Johnson-Matthey standard yielded $^{187}Os/^{188}Os$ of 0.1138±2 for both the VG Sector 54 (faraday cup runs) and the NBS mass spectrometer (SEM runs). Total procedural blanks were 4.8±2.0 pg for Os with an $^{187}Os/^{188}Os$ of 0.170±0.040. Osmium blank contributions to samples were <2% for Os poor samples TA54C1 and TA56 and <1% for all other samples. Duplicate analyses showed a good reproducibility for Os isotopic composition for most samples of 1% or better. For TA38, reproducibility between duplicates reaches only 2.2%. Duplicate reproduction for low Os pyroxenite samples is as low as 10% for most samples and worse than 20% for TA54C1, but may be significantly affected by uncertainties of the spike $^{187}Os/^{188}Os$ used for correction.

For PGE and Re isotope dilution analyses, one third of the remaining aqua regia fraction was carefully reduced in volume in Teflon beakers, converted to chloride in using first 8 ml 6 M HCl and then 8 ml 0.2 M HCl, and dried down. The samples were then taken up in 10 ml 0.2 M HCl and were loaded onto ion exchange columns that contained 10 ml Eichrom AG50X-8 (100-200 mesh) cation exchange resin. While the PGE and Re passed the resin without interaction, most other elements were retained on the column (Meisel et al. 2003). Care needs to be taken that the columns are not overloaded. 10 ml of 0.2 M HCl were loaded

onto the column for resin pH adjustment. 3ml of sample solution were added and discarded along with the previously added acid. 4.5 ml of sample solution were subsequently loaded and collected. 9 ml of 0.2 M were loaded and collected, the total fraction collected for analysis consisted of 13.5 ml. Smaller collected fractions may result in loss of Re on the column, while larger collected fractions contain Cd and Mo, leading to possible interferences on Ru and Pd. An additional cleanup step was tried for one batch of samples, but resulted in no significant improvement in signal intensity or interference removal. The collected fraction was dried down on a hotplate at ~120°C, taken up in 0.28 M HNO_3 and measured on Element 2 (UMD) or Element XR (FUB) sector field ICP-MS instruments in low-resolution mode, using an Aridus membrane desolvation system. At FUB, Re was analyzed using a cyclonic glass spray chamber. Abundances were determined by isotope dilution.

An analysis typically comprised 400 scans of masses 98, 99, 101, 102, 103, 104, 105, 106, 108, 110, 111, 185, 187, 189, 191, 193, 194, 195, 196, 197, 198 and 199. Isobaric interferences caused by Cd, Os and Hg on Pd, Re and Pt were insignificant in all cases. A mixed Re–Ir–Ru–Pt–Pd in house reference solution with roughly chondritic abundance ratios and ~1ng/g Ir was analyzed multiple times during each analytical session and monitored over the course of several months. Isotopic ratios of samples were corrected for mass discrimination by comparison with the in-house standard ratios with recommended values. For this standard solution, 2 s.d. for ratios used for ID in spiked samples are 2.4% for $^{99}Ru/^{101}Ru$, 2.0% for $^{105}Pd/^{106}Pd$, 3.2% for $^{185}Re/^{187}Re$, 1.8% for $^{191}Ir/^{193}Ir$ and 1.1% for $^{194}Pt/^{195}Pt$. All ratios overlap with the accepted ratios within the 2 s.d. error.

For the measurements at FUB, special care had to be taken concerning the machine setup, Tuning was optimized to signal stability and low oxide rates, with a maximum signal intensity of $1 – 4 * 10^6$ counts. Gas flows and torch position were tuned with a Be-In-U solution, and varied massively over the course of the work. Measurements were conducted in analog mode, using the method PGE_van_Acken_004.met. Rhenium was not measurable with the Aridus desolvation system, for reasons not understood. Results were not reproducible, and intensity on both Re masses was critically low with the Aridus system. All Re measurements using this setup had to be removed from consideration. Similar problems occurred with Ru measurements using either a cyclonic glass spray chamber or the Peltier Scott-type spray

chamber assembly. Massive non-systematic interferences occurred on masses 101 and 102 for both samples and reference solutions, rendering all Ru measurements without the Aridus system unusable. As consequence, all samples were measured at least twice, with the Aridus desolvation system and with a cyclonic spray chamber setup. For the aforementioned reasons, some Re and Ru results were rejected. Iridium, Pt and Pd generally measurements generally were in excellent agreement for Aridus and glassware setups.

Washout time between samples was set between 3 and 5 min. On-peak zeroes for 0.28 M HNO_3 were taken after every 4 – 5 samples to monitor potential memory effects and were insignificant in all cases. Total chemistry blanks run in the course of this study (n = 7) were 7–12 pg for Re, 2.8–6.9 pg for Os, 0.3–7 pg for Ir, 2–20 pg for Ru, 2–440 pg for Pt and 42–420 pg for Pd. Blanks for Pt and Pd were substantially affected by the batch of Carius tubes used. Osmium blanks were reduced by subjecting HNO_3 used for digestion to H_2O_2 prior to distillation. Blanks for Ir, Ru, Pt and Pd were lowered over time by additional acid distillation steps. Performance of the Aridus rinse procedure with 1M HNO_3 and 0.5 M HCl prior to blank measurements resulted in significant improvement of both on-peak and chemistry blanks.

With the exception of Os and Ir in samples TA54C1, TA54D2, TA54D and TA56, blank corrections were negligible or minor (<1%). Due to the high Pt and Pd contents of the samples, even the highest Pt and Pd blanks contributed less than 2%. Duplicates and Reruns of samples showed a typical reproducibility of 2% for Os, 5% for Ir, 5% for Ru, 3% for Pt and 5% for Pd concentrations, similar to typical reproducibilities reported for these elements in peridotites. Reproducibilities are worse for Os, Ir and Ru in TA61 and for Pd in TA13B. Rhenium is strongly variable in duplicates, with reproducibility between 2% (TA11A2; TA13B) and 50% (TA11A1, TA38).

8.2 Electron microprobe

Microprobe analyses of sulfide grains in thick sections for S, Fe, Ni, Co and Cu abundances were conducted using the JEOL 8900 Superprobe at the University of Maryland

with an acceleration voltage of 15 kV and probe current of 50 nA. Multiple spots were analyzed per grain from both cores and rims to ensure internal homogeneity of sulfides for the subsequent LA-ICP-MS. Chalcopyrite was used as calibration standard for Cu, pyrite for Fe and S, and Co and Ni metals.

8.3 Laser-Ablation-ICP-MS

Laser ablation data on the same sulfide grains used for microprobe analysis were obtained using a 213 nm laser ablation (LA) system coupled with an Element-2 ICP-MS at the University of Maryland using He as a carrier gas. The sample gas flow was merged with Ar before injection into the plasma. Baselines were measured for about 60 seconds before ablation. Laser intensity was set to 45% (~2 J/cm^2) with a frequency of 8 Hz. The following masses were measured: ^{57}Fe, ^{59}Co, ^{61}Ni, ^{65}Cu, ^{75}As, ^{101}Ru, ^{103}Rh, ^{105}Pd, ^{185}Re, ^{187}Os, ^{188}Os, ^{190}Os, ^{193}Ir, ^{195}Pt and ^{197}Au. Corrections for Ar compounds were minor for all analyses, except for native Cu grains (see below). For internal standardization, Fe concentrations obtained by electron microprobe were used. As an external standard, polished sections of the iron meteorite Coahuila and a synthetical sulfide bead (Brenan internal standard at UMD) were run four times each with each thick section analyzed by LA. A maximum of twelve spots were analyzed per thick section. External precision as documented by the reproducibility of external standards over the measurement period was better than 2.5 % for all elements Trace element abundances were calculated using LAMTRACE software.

9. References

Alard O., Griffin W. L., Lorand J.-P., Jackson S. E., and O'Reilly S. Y. (2000) Non-chondritic distribution of the highly siderophile elements in mantle sulphides. *Nature* **407**, 891 - 894.

Alard O., Griffin W. L., Pearson N. J., Lorand J.-P., and O'Reilly S. Y. (2002) New insights into the Re-Os systematics of sub-continental lithospheric mantle from in situ analysis of sulphides. *Earth and Planetary Science Letters* **203**, 651 - 663.

Alard O., Luguet A., Pearson N. J., Griffin W. L., Lorand J.-P., Gannoun A., Burton K. W., and O'Reilly S. Y. (2005) *In situ* Os isotopes in abyssal peridotites bridge the isotopic gap between MORBs and their source mantle. *Nature* **436**, 1005 - 1008.

Allègre C. J. and Luck J.-M. (1980) Osmium isotopes as petrogenetic and geological tracers. *Earth and Planetary Science Letters* **48**, 148 - 154.

Allègre C. J. and Turcotte D. L. (1986) Implications of a two-component marble-cake mantle. *Nature* **323**, 123 - 127.

Amossé J., Dablé P., and Allibert M. (2000) Thermochemical behaviour of Pt, Ir, Rh and Ru vs fO_2 and fS_2 in a basaltic melt. Implications for the differentiation and precipitation of these elements. *Mineralogy and Petrology* **68**, 29 - 62.

Anbar A. D., Wasserburg G. J., Papanastassiou D. A., and Andersson P. S. (1996) Iridium in Natural Waters. *Science* **273**, 1524 - 1528.

Asimow P. D. (1999) A model that reconciles major- and trace-element data from abyssal peridotites. *Earth and Planetary Science Letters* **169**, 303 - 319.

Baker M. B. and Beckett J. R. (1999) The origin of abyssal peridotites: a reinterpretation based on primary bulk compositions. *Earth and Planetary Science Letters* **171**, 49 - 61.

Ballhaus C., Tredoux M., and Späth A. (2001) Phase Relations in the Fe-Ni-Cu-PGE-S System at Magmatic Temperature and Application to Massive Sulphide Ores of the Sudbury Igneous Complex. *Journal of Petrology* **42**(10), 1911 - 1926.

Ballhaus C., Bockrath C., Wohlgemuth-Ueberwasser C., Laurenz V., and Berndt J. (2006) Fractionation of the noble metals by physical processes. *Contrib Mineral Petrol* **152**, 667 - 684.

Barnes S.-J., Naldrett A. J., and Gorton M. P. (1985) The origin of the fractionation of platinum-group elements in terrestrial magmas. *Chemical Geology* **53**, 303 - 323.

Barnes S. J. (1993) Partitioning of the platinum group elements and gold between silicate and sulphide magmas in the Munni Munni Complex, Western Australia. *Geochimica et Cosmochimica Acta* **57**, 1277 - 1290.

Beccaluva L., Bianchini G., Coltorti M., Perkins W. T., Siena F., Vaccaro C., and Wilson M. (2001) Multistage evolution of the European lithospheric mantle: new evidence from Sardinian peridotite xenoliths. *Contrib Mineral Petrol* **142**, 284 - 297.

Beccaluva L., Bianchini G., Bonadiman C., Siena F., and Vaccaro C. (2004) Coexisting anorogenic and subduction-related metasomatism in mantle xenoliths from the Betic Cordillera (southern Spain). *Lithos* **75**, 67 - 87.

Becker H. (1996a) Crustal Trace Element and Isotopic Signatures in Garnet Pyroxenites from Garnet Peridotite Massifs from Lower Austria. *Journal of Petrology* **37**(4), 785 - 810.

Becker H. (1996b) Geochemistry of garnet peridotite massifs from lower Austria and the composition of deep lithosphere beneath a Palaeozoic convergent plate margin. *Chemical Geology* **134**, 49 - 65.

Becker H. (2000) Re-Os fractionation in eclogites and blueshists and the implications for recycling of oceanic crust into the mantle. *Earth and Planetary Science Letters* **177**, 287 - 300.

Becker H., Shirey S. B., and Carlson R. W. (2001) Effects of melt percolation on the Re-Os systematics of peridotites from a Paleozoic convergent plate margin. *Earth and Planetary Science Letters* **188**, 107 - 121.

Becker H., Carlson R. W., and Shirey S. B. (2004) Slab-derived osmium and isotopic disequilibrium in garnet pyroxenites from a Paleozoic convergent plate margin (lower Austria). *Chemical Geology* **208**, 141 - 156.

Becker H., Horan M. F., Walker R. J., Gao S., Lorand J.-P., and Rudnick R. L. (2006) Highly siderophile element composition of the Earth's primitive upper mantle: constraints from new data on peridotite massifs and xenoliths. *Geochimica et Cosmochimica Acta* **70**, 4528 - 4550.

Begemann F., Ludwig K. R., Lugmair G. W., Nyquist L. E., Patchett P. J., Renne P. R., Shih C.-Y., Villa I. M., and Walker R. J. (2001) Call for an improved set of decay constants for geochronological use. *Geochimica et Cosmochimica Acta* **65**(1), 111 - 121.

Beyer E. E., Griffin W. L., and O'Reilly S. Y. (2006) Transformation of Archaean Lithospheric Mantle by Refertilization: Evidence from Exposed Peridotites in the Western Gneiss Region, Norway. *Journal of Petrology* **47**(8), 1611 - 1638.

Bezmen N. I., Asif M., Brügmann G., Romanenko I. M., and Naldrett A. J. (1994) Distribution of Pd, Rh, Ru, Ir, Os and Au between sulfide and silicate metals. *Geochimica et Cosmochimica Acta* **58**(4), 1251 - 1260.

Bézos A., Lorand J.-P., Humler E., and Gros M. (2005) Platinum-group element systematics in Mid-Oceanic Ridge basaltic glasses from the Pacific, Atlantic and Indian Oceans. *Geochimica et Cosmochimica Acta* **69**(10), 2613 - 2627.

Birck J.-L., Roy-Barman M., and Capmas F. (1997) Os Isotopic Measurements at the Femtomole Level in Natural Samples. *Geostandards Newsletter*(1), 19 - 27.

Bird J. M., Meibom A., Frei R., and Nägler T. F. (1999) Osmium and lead isotopes of rare OsIrRu minerals: derivation from the core-mantle boundary region? *Earth and Planetary Science Letters* **170**, 83 - 92.

Blichert-Toft J., Albarède F., and Kornprobst J. (1999) Lu-Hf Isotope Systematics of Garnet Pyroxenites from Beni Bousera, Morocco: Implications for Basalt Origin. *Science* **283**, 1303 - 1306.

Blusztajn J., Hart S. R., Ravizza G. E., and Dick H. J. B. (2000) Platinum-group elements and Os isotope characteristics of the lower oceanic crust. *Chemical Geology* **168**, 113 - 122.

Bockrath C., Ballhaus C., and Holzheid A. (2004) Fractionation of the Platinum-Group Elements During Mantle Melting. *Science* **305**, 1951 - 1953.

Bodinier J. L., Guiraud M., Fabriès J., Dostal J., and Dupuy C. (1987) Petrogenesis of layered pyroxenites from the Lherz, Freychinède and Prades ultramafic bodies (Ariège, french Pyrénées). *Geochimica et Cosmochimica Acta* **51**, 279 - 290.

Bodinier J. L., Vasseur G., Vernieres J., Dupuy C., and Fabries J. (1990) Mechanisms of Mantle Metasomatism: Geochemical Evidence from the Lherz Orogenic Peridotite. *Journal of Petrology* **31**(3), 597 - 628.

Bodinier J. L. and Godard M. (2003) Orogenic, Ophiolitic, and Abyssal Peridotites. In *Treatise on Geochemistry, Part 2*, Vol. 2 (ed. K. K. Turekian and H. D. Holland), pp. 103 - 170. Elsevier Ltd.

Bodinier J. L., Menzies M. A., Shimizu N., Frey F. A., and McPherson E. (2004) Silicate, Hydrous and Carbonate Metasomatism at Lherz, France: Contemporaneous Derivatives of Silicate Melt-Harzburgite Reaction. *Journal of Petrology* **45**(2), 299 - 320.

Bodinier J. L., Garrido C. J., Chanefo I., Bruguier O., and Gervilla F. (2008) Origin of Pyroxenite-Peridotite Veined Mantle by Refertilization Reactions: Evidence from the Ronda Peridotite (Southern Spain). *Journal of Petrology* **49**(5), 999 - 1025.

Brandon A. D., Creaser R. A., Shirey S. B., and Carlson R. W. (1996) Osmium Recycling in Subduction Zones. *Science* **272**, 861 - 864.

Brandon A. D., Walker R. J., Morgan J. W., Norman M. D., and Prichard H. M. (1998) Coupled ^{186}Os and ^{187}Os Evidence for Core-Mantle Interaction. *Science* **280**, 1570 - 1573.

Brandon A. D., Norman M. D., Walker R. J., and Morgan J. W. (1999) ^{186}Os-^{187}Os systematics of Hawaiian picrites. *Earth and Planetary Science Letters* **174**, 25 - 42.

Brandon A. D., Snow J. E., Walker R. J., Morgan J. W., and Mock T. D. (2000) ^{190}Pt-^{186}Os and ^{187}Re-^{187}Os systematics of abyssal peridotites. *Earth and Planetary Science Letters* **177**, 319 - 335.

Brandon A. D., Walker R. J., Puchtel I. S., Becker H., Humayun M., and Revillon S. (2003) ^{186}Os-^{187}Os systematics of Gorgona Island komatiites: implications for early growth of the inner core. *Earth and Planetary Science Letters* **206**, 411 - 426.

Brandon A. D. and Walker R. J. (2005) The debate over core-mantle interaction. *Earth and Planetary Science Letters* **232**, 211 - 225.

Brandon A. D., Walker R. J., and Puchtel I. S. (2006) Platinum–osmium isotope evolution of the Earth's mantle: Constraints from chondrites and Os-rich alloys. *Geochimica et Cosmochimica Acta* **70**, 2093 - 2103.

Brandon A. D., Graham D. W., Waight T., and Gautason B. (2007) ^{186}Os and ^{187}Os enrichments and high-^{3}He/^{4}He sources in the Earth's mantle: Evidence from Icelandic picrites. *Geochimica et Cosmochimica Acta* **71**, 4570 - 4591.

Brenan J. M. (2002) Re-Os fractionation in magmatic sulfide melt by monosulfide solid solution. *Earth and Planetary Science Letters* **199**, 257 - 268.

Brenan J. M., McDonough W. F., and Ash R. (2005) An experimental study of the solubility and partitioning of iridium, osmium and gold between olivine and silicate melt. *Earth and Planetary Science Letters* **237**, 855 - 872.

Brenan J. M. (2008) Re-Os fractionation by sulfide melt - silicate melt partitioning: A new spin. *Chemical Geology* **248**, 140 - 165.

Brenan J. M. and Andrews D. (2001) High-temperature stability of laurite and Ru-Os-Ir alloy and their role in PGE fractionation in mafic magmas. *The Canadian Mineralogist* **39**, 341 - 360.

Büchl A., Brügmann G., Batanova V. G., and Hofmann A. W. (2004) Os mobilization during melt percolation: The evolution of Os isotope heterogeneities in the mantle sequence of the Troodos ophiolite, Cyprus. *Geochimica et Cosmochimica Acta* **68**(16), 3397 - 3408.

Büchl A., Brügmann G., Batanova V. G., Münker C., and Hofmann A. W. (2002) Melt percolation monitored by Os isotopes and HSE abundances: a case study from the mantle section of the Troodos Ophiolite. *Earth and Planetary Science Letters* **204**, 385 - 402.

Burkhard D. J. M. and O'Neil J. R. (1988) Contrasting serpentinization processes in the eastern Central Alps. *Contrib Mineral Petrol* **99**, 498 - 506.

Burton K. W., Schiano P., Birck J.-L., and Allègre C. J. (1999) Osmium isotope disequilibrium between mantle minerals in a spinel-lherzolite. *Earth and Planetary Science Letters* **172**, 311 - 322.

Burton K. W., Schiano P., Birck J.-L., Allègre C. J., Rehkämper M., Halliday A. N., and Dawson J. B. (2000) The distribution and behaviour of rhenium and osmium amongst mantle minerals and the age of the lithospheric mantle beneath Tanzania. *Earth and Planetary Science Letters* **183**, 93 - 106.

Burton K. W., Gannoun A., Birck J.-L., Allègre C. J., Schiano P., Clochiatti R., and Alard O. (2002) The compatibility of rhenium and osmium in natural olivine and their behaviour during mantle melting and basalt genesis. *Earth and Planetary Science Letters* **198**, 63 - 76.

Cannat M., Bideau D., and Hébert R. (1990) Plastic deformation and magmatic impregnation in serpentinized ultramafic rocks from the Garrett transform fault (East Pacific Rise). *Earth and Planetary Science Letters* **101**, 216 - 232.

Carlson R. W. (2005) Application of the Pt-Re-Os isotopic systems to mantle geochemistry and geochronology. *Lithos* **82**, 249 - 272.

Carlson R. W. and Irving A. J. (1994) Depletion and enrichment history of subcontinental lithospheric mantle: An Os, Sr, Nd and Pb isotopic study of ultramafic xenoliths from the northwestern Wyoming Craton. *Earth and Planetary Science Letters* **126**, 457 - 472.

Chesley J., Rudnick R. L., and Lee C.-T. (1999) Re-Os systematics of mantle xenoliths from the East African Rift: Age, structure, and history of the Tanzanian craton. *Geochimica et Cosmochimica Acta* **63**(7/8), 1203 - 1217.

Chou C.-L. (1978) Fractionation of siderophile elements in the earth's upper mantle. *Proc. Lunar Planet. Sci. Conf. 9th*, 219 - 230.

Cohen A. S. and Waters F. G. (1996) Separation of osmium from geological materials by solvent extraction for analysy by thermal ionization mass spectrometry. *Analytica Chimica Acta* **332**, 269 - 275.

Creaser R. A., Papanastassiou D. A., and Wasserburg G. J. (1991) Negative thermal ion mass spectrometry of osmium, rhemium and iridium. *Geochimica et Cosmochimica Acta* **55**, 397 - 401.

Dale C. W., Gannoun A., Burton K. W., Argles T. W., and Parkinson I. J. (2007) Rhenium-osmium isotope and elemental behaviour during subduction of oceanic crust and the implications for mantle recycling. *Earth and Planetary Science Letters* **253**, 211 - 225.

Dantas C., Ceuleneer G., Grégoire M., Python M., Freydier R., Warren J., and Dick H. J. B. (2007) Pyroxenites from the Southwest Indian Ridge, 9-16°E: Cumulates from Incremental Melt Fractions Produced at the Top of a Cold Melting Regime. *Journal of Petrology* **48**(4), 647 - 660.

Davies G. R., Nixon P. H., Pearson D. G., and Obata M. (1993) Tectonic implications of graphitized diamonds from the Ronda peridotite massif, southern Spain. *Geology* **21**(5), 471 - 474.

Dawson J. B. (2002) Metasomatism and Partial Melting in Upper-Mantle Peridotite Xenoliths from the Lashaine Volcano, Northern Tanzania. *Journal of Petrology* **43**(9), 1749 - 1777.

Dawson J. B. and Smith J. V. (1992) Olivine-mica pyroxenite xenoliths from northern Tanzania: metasomatic products of upper-mantle peridotite. *Journal of Volcanology and Geothermal Research* **50**, 131 - 142.

Desborough G. A. and Czamanske G. K. (1973) Sulfides in Eclogite Nodules from a Kimberlite Pipe, South Africa, with comments on Violarite Stoichiometry. *American Mineralogist* **58**, 195 - 202.

Desmurs L., Müntener O., and Manatschal G. (2002) Onset of magmatic accretion within a magma-poor rifted margin: a case study from the Platta ocean-continent transition, eastern Switzerland. *Contrib Mineral Petrol* **144**, 365 - 382.

Dick H. J. B. and Sinton J. M. (1979) Compositional layering in alpine peridotites: evidence for pressure solution creep in the mantle. *Journal of Geology* **87**, 403 - 416.

Dick H. J. B., Lin J., and Schouten H. (2003) An ultraslow-spreading class of ocean ridge. *Nature* **426**, 405 - 412.

Downes H. (2007) Origin and significance of spinel and garnet pyroxenites in the shallow lithospheric mantle: Ultramafic massifs in orogenic belts in Western Europe and NW Africa. *Lithos* **99**, 1 - 24.

Downes H. and Dupuy C. (1987) Textural, isotopic and REE variations in spinel peridotite xenoliths, Massif Central, France. *Earth and Planetary Science Letters* **82**, 121 - 135.

Elthon D. (1992) Chemical Trends in Abyssal Peridotites: Refertilization of Depleted Suboceanic Mantle. *Journal of Geophysical Research* **97**(B6), 9015 - 9025.

Ertel W., O'Neill H. S. C., Sylvester P. J., Dingwell D. B., and Spettel B. (2001) The solubility of rhenium in silicate melts: Implications for the geochemical properties of rhenium at high temperatures. *Geochimica et Cosmochimica Acta* **65**(13), 2161 - 2170.

Ertel W., Walter M. J., Drake M. J., and Sylvester P. J. (2006) Experimental study of platinum solubility in silicate melt to 14 GPa and 2273 K: Implications for accretion and core formation in Earth. *Geochimica et Cosmochimica Acta* **70**, 2591 - 2602.

Escrig S., Schiano P., Schilling J.-G., and Allègre C. J. (2005) Rhenium-osmium isotope systematics in MORB from the Southern Mid-Atlantic Ridge (40°-50° S). *Earth and Planetary Science Letters* **235**, 528 - 548.

Fabriès J., Lorand J.-P., and Bodinier J.-L. (1998) Petrogenetic evolution of orogenic lherzolite massifs in the central and western Pyrenees. *Tectonophysics* **292**, 145 - 167.

Fleet M. E., Stone W. E., and Crocket J. H. (1991) Partitioning of palladium, iridium, and platinum between sulfide liquid and basalt melt: Effects of melt composition, concentration, and oxygen fugacity. *Geochimica et Cosmochimica Acta* **55**, 2545 - 2554.

Fleet M. E., Chryssoulis S. L., Stone W. E., and Weisener C. G. (1993) Partitioning of platinum-group elements and Au in the Fe-Ni-Cu-S system: experiments on the fractional crystallization of sulfide melt. *Contrib Mineral Petrol* **115**, 36 - 44.

Fleet M. E., Crocket J. H., and Stone W. E. (1996) Partitioning of platinum-group elements (Os, Ir, Ru, Pt, Pd) and gold between sulfide liquid and basalt melt. *Geochimica et Cosmochimica Acta* **60**(13), 2397 - 2412.

Fleet M. E., Crocket J. H., Liu M., and Stone W. E. (1999) Laboratory patitioning of platinum-group elements (PGE) and gold with application to magmatic sulfide-PGE deposits. *Lithos* **47**, 127 - 142.

Fonseca R. O. C., Mallmann G., O'Neill H. S. C., and Campbell I. H. (2007) How chalcophile is rhenium? An experimental study of the solubility in sulphide mattes. *Earth and Planetary Science Letters* **260**, 537 - 548.

Frey F. A., Suen C. J., and Stockman H. W. (1985) The Ronda high temperature peridotite: Geochemistry and petrogenesis. *Geochimica et Cosmochimica Acta* **49**, 2469 - 2491.

Früh-Green G., Weissert H., and Bernoulli D. (1990) A multiple fluid history recorded in Alpine ophiolites. *Journal of the Geological Society* **147**, 959 - 970.

Gannoun A., Burton K. W., Thomas L. E., Parkinson I. J., van Calsteren P. W., and Schiano P. (2004) Osmium Isotope Heterogeneity in the Constituent Phases of Mid-Ocean Ridge Basalts. *Science* **303**, 70 - 72.

Gannoun A., Burton K. W., Parkinson I. J., Alard O., Schiano P., and Thomas L. E. (2007) The scale and origin of the osmium isotope variations in mid-ocean ridge basalts. *Earth and Planetary Science Letters* **259**, 541 - 556.

Gao S., Rudnick R. L., Carlson R. W., McDonough W. F., and Liu Y.-S. (2002) Re-Os evidence for replacement of ancient mantle lithosphere beneath the North China craton. *Earth and Planetary Science Letters* **198**, 307 - 322.

Garrido C. J. and Bodinier J. L. (1999) Diversity of Mafic Rocks in the Ronda Peridotite: Evidence for Pervasive Melt-Rock Reaction during Heating of Subcontinental Lithosphere by Upwelling Asthenosphere. *Journal of Petrology* **40**(5), 729 - 754.

Garrido C. J., Bodinier J. L., and Alard O. (2000) Incompatible trace element partitioning and residence in anhydrous spinel peridotites and websterites from the Ronda orogenic peridotite. *Earth and Planetary Science Letters* **181**, 341 - 358.

Garuti G., Gorgoni C., and Sighinolfi G. P. (1984) Sulfide mineralogy and chalcophile and siderophile element abundances in the Ivrea-Verbano mantle peridotites (Western Italian Alps). *Earth and Planetary Science Letters* **70**, 69 - 87.

Gasparik T. (1984) Two-pyroxene thermobarometry with new experimental data in the system CaO - MgO - Al2O3 - SiO2. *Contrib Mineral Petrol* **87**, 87 - 97.

Gasparik T. (1987) Orthopyroxene thermobarometry in simple and complex systems. *Contrib Mineral Petrol* **96**, 357 - 370.

Godard M., Bodinier J. L., and Vasseur G. (1995) Effects of mineralogical reactions on trace element redistributions in mantle rocks during percolation processes: A chromatographic approach. *Earth and Planetary Science Letters* **133**, 449 - 461.

Greau Y., Griffin W. L., Alard O., and O'Reilly S. Y. (2008) Petrology and geochemistry of eclogitic sulfides: a new insight on the origin of mantle eclogites? *9th International Kimberlite Conference*, 91KC-A-000126.

Grieco G., Ferrario A., and Mathez E. A. (2004) The effect of metasomatism on the Cr-PGE mineralization in the Finero Complex, Ivrea Zone, Southern Alps. *Ore Geology Reviews* **24**, 299 - 314.

Griffin W. L., Graham S., O'Reilly S. Y., and Pearson N. J. (2004) Lithosphere evolution beneath the Kaapvaal Craton: Re-Os systematics of sulfides in mantle-derived peridotites. *Chemical Geology* **208**, 89 - 118.

Gueddari K., Piboule M., and Amossé J. (1996) Differentiation of platinum-group elements (PGE) and of gold during partial melting of peridotites in the lherzolitic massifs of the Betico-Rifean range (Ronda and Beni Bousera). *Chemical Geology* **134**, 181 - 197.

Handler M. R., Bennett V. C., and Esat T. M. (1997) The persistence of off-cratonic lithospheric mantle: Os isotopic systematics of variably metasomatised southeast Australian xenoliths. *Earth and Planetary Science Letters* **151**, 61 - 75.

Handler M. R. and Bennett V. C. (1999) Behaviour of Platinum-group elements in the subcontinental mantle of eastern Australia during variable metasomatism and melt depletion. *Geochimica et Cosmochimica Acta* **63**(21), 3597 - 3618.

Handler M. R., Bennett V. C., and Carlson R. W. (2005) Nd, Sr and Os isotope systematics in young, fertile spinel peridotite xenoliths from northern Queensland, Australia: A unique view of depleted MORB mantle? *Geochimica et Cosmochimica Acta* **69**(24), 5747 - 5763.

Hart S. R. and Dunn T. (1993) Experimental cpx/melt partitioning of 24 trace elements. *Contrib Mineral Petrol* **113**, 1 - 8.

Hart S. R. and Ravizza G. E. (1996) Os Partitioning Between Phases in Lherzolite and Basalt. In *Earth Processes: Reading the Isotopic Code*, Vol. 95, pp. 123 - 134. American Geophysical Union.

Harvey J., Gannoun A., Burton K. W., Rogers N. W., Alard O., and Parkinson I. J. (2006) Ancient melt extraction from the oceanic upper mantle revealed by Re-Os isotopes in abyssal peridotites from the Mid-Atlantic ridge. *Earth and Planetary Science Letters* **244**, 606 - 621.

Haughton D. R., Roeder P. L., and Skinner B. J. (1974) Solubility of Sulfur in Mafic Magmas. *Economic Geology* **69**(4), 451 - 467.

Hauri E. H. (2002) Osmium isotopes and mantle convection. *Phil. Trans. R. Soc. Lond.* **360**, 2371 - 2382.

Hauri E. H. and Hart S. R. (1993) Re-Os isotope systematics of HIMU and EMII oceanic island basalts from the south Pacific Ocean. *Earth and Planetary Science Letters* **114**, 353 - 371.

Hauri E. H. and Hart S. R. (1997) Rhenium abundances and systematics in oceanic basalts. *Chemical Geology* **139**, 185 - 205.

Hellebrand E., Snow J. E., Dick H. J. B., and Hofmann A. W. (2001) Coupled major and trace elements as indicators of the extent of melting in mid-ocean-ridge peridotites. *Nature* **410**, 677 - 681.

Hellebrand E., Snow J. E., Hoppe P., and Hofmann A. W. (2002) Garnet-field Melting and Late-stage Refertilization in 'Residual' Abyssal Peridotites from the Central Indian Ridge. *Journal of Petrology* **43**(12), 2305 - 2398.

Hellebrand E. and Snow J. E. (2003) Deep melting and sodic metasomatism underneath the highly oblique spreading Lena Trough (Arctic Ocean). *Earth and Planetary Science Letters* **216**, 283 - 299.

Henry P., Azambre B., Miontigny R., Rossy M., and Stevenson R. K. (1998) Late mantle evolution of the Pyrenean sub-continental lithospheric mantle in the light of new 40Ar-39Ar and Sm-Nd ages on pyroxenites and peridotites (Pyrenees, France). *Tectonophysics* **296**, 103 - 123.

Hertogen J., Janssens M.-J., and Palme H. (1980) Trace elements in ocean ridge basalt glasses: implications for fractionations during mantle evolution and petrogenesis. *Geochimica et Cosmochimica Acta* **44**, 2125 - 2143.

Hirschmann M. M. and Stolper E. M. (1996) A possible role for garnet pyroxenite in the origin of the "garnet signature" in MORB. *Contrib Mineral Petrol* **124**, 185 - 208.

Hirschmann M. M., Kogiso T., Baker M. B., and Stolper E. M. (2003) Alkalic magmas generated by partial melting of garnet pyroxenite. *Geology* **31**, 481 - 484.

Hodge V. F., Stallard M., Koide M., and Goldberg E. D. (1985) Platinum and the platinum anomaly in the marine environment. *Earth and Planetary Science Letters* **72**, 158 - 162.

Holzheid A., Sylvester P., O'Neill H. S. C., Rubie D. C., and Palme H. (2000) Evidence for a late chondritic veneer in the Earth's mantle from high-pressure partitioning of palladium and platinum. *Nature* **406**, 396 - 399.

Holzheid A. and Grove T. L. (2002) Sulfur saturation limits in silicate melts and their implications for core formation scenarios for terrestrial planets. *American Mineralogist* **87**, 227 - 237.

Ionov D. A., Bodinier J. L., Mukasa S. B., and Zanetti A. (2002) Mechanisms and Sources of Mantle Metasomatism: Major and Trace Element Compositions of Peridotite Xenoliths from Spitsbergen in the Context of Numerical Modelling. *Journal of Petrology* **43**(12), 2219 - 2259.

Irving A. J. (1974) Geochemical and High Pressure Experimental Studies of Garnet Pyroxenite and Pyroxene Granulite Xenoliths from the Delegate Basaltic Pipes, Australia. *Journal of Petrology* **15**(1), 1 - 40.

Ionov D. A., Shirey S. B., Weis D., Brügmann G., and. (2006) Os-Hf-Sr-Nd isotope and PGE systematics of spinel peridotite xenoliths from Tok, SE Siberian craton: Effects of pervasive metasomatism in shallow refractory mantle. *Earth and Planetary Science Letters* **241**, 47 - 64.

Ito G. and Mahoney J. J. (2005) Flow and melting of a heterogeneous mantle: 1. Method and importance to the geochemistyr of ocean island and mid-ocean ridge basalts. *Earth and Planetary Science Letters* **230**, 29 - 46.

Johnson K. T. M. and Dick H. J. B. (1992) Open System Melting and Temporal and Spatial Variation of Peridotite and Basalt at the Atlantis II Fracture Zone. *Journal of Geophysical Research* **97**(B6), 9219 - 9241.

Johnson K. T. M., Dick H. J. B., and Shimizu N. (1990) Melting in the Oceanic Upper Mantle: An Ion Microprobe Study of Diopsides in Abyssal Peridotites. *Journal of Geophysical Research* **93**(B3), 2661 - 2678.

Jones J. H. and Drake M. (1986) Geochemical constraints on core formation in the Earth. *Nature* **322**, 221 - 228.

Kelemen P. B. (1990) Reaction Between Ultramafic Rock and Fractionating Basaltic Magma I. Phase Relations, the Origin of Calc-alkaline Magma Series and the Formation of Discordant Dunite. *Journal of Petrology* **31**(1), 51 - 98.

Kelemen P. B., Dick H. J. B., and Quick J. E. (1992) Formation of harzburgite by pervasive melt/rock reaction in the upper mantle. *Nature* **358**, 635 - 641.

Kelemen P. B., Shimizu N., and Dunn T. (1993) Relative depletion of niobium in some arc magmas and the continental crust: partitioning of K, Nb, La and Ce during melt/rock reaction in the upper mantle. *Earth and Planetary Science Letters* **120**, 111 - 134.

Kelemen P., Hirth G., Shimizu N., Spiegelman M., and Dick H. J. B. (1997) A review of melt migration processes in the adiabatically upwelling mantle beneath oceanic spreading ridges. *Phil. Trans. R. Soc. Lond.* **355**, 283 - 318.

Kimura K., Lewis R. S., and Anders E. (1974) Distribution of gold and rhenium between nickel-iron and silicate melts: implications for the abundance of siderophile elements on the Earth and Moon. *Geochimica et Cosmochimica Acta* **38**, 683 - 701.

Kinzler R. J. (1997) Melting of mantle peridotite at pressures approaching the spinel to garnet-transition: Application to mid-ocean ridge basalt petrogenesis. *Journal of Geophysical Research* **102**(B1), 853 - 874.

Kinzler R. J. and Grove T. L. (1992) Primary Magmas of Mid-Ocean Ridge Basalts 1. Experiments and Methods. *Journal of Geophysical Research* **97**(B5), 6885 - 6906.

Kogiso T. and Hirschmann M. M. (2001) Experimental study of clinopyroxenite partial melting and the origin of ultra-calcic melt inclusions. *Contrib Mineral Petrol* **142**, 347 - 360.

Kogiso T., Hirschmann M. M., and Frost D. J. (2003) High pressure partial melting of garnet pyroxenite: possible mafic lithologies in the source of ocean island basalts. *Earth and Planetary Science Letters* **216**, 603 - 617.

Kogiso T., Hirschmann M. M., and Pertermann M. (2004) High-pressure Partial melting of Mafic Lithologies in the Mantle. *Journal of Petrology* **45**(12), 2407 - 2422.

Kornprobst J. (1969) Le massif ultrabasique des Beni Bouchera (Rif Interne, Maroc): Etude des péridotites de haute température et de haute pression, et des pyroxénolites, à grenat ou sans grenat, qui leur sont associées. *Contrib Mineral Petrol* **23**, 283 - 322.

Kornprobst J., Piboule M., Roden M. F., and Tabit A. (1990) Corundum-bearing Garnet Clinopyroxenites at Beni Bousera (Morocco): Original Plagioclase-rich Gabbros Recrystallized at Depth within the Mantle? *Journal of Petrology* **31**(3), 717 - 745.

Kumar N., Reisberg L., and Zindler A. (1996) A major and trace element and strontium, neodymium, and osmium isotopic study of a thick pyroxenite layer from the Beni Bousera Ultramafic Complex of northern Morocco. *Geochimica et Cosmochimica Acta* **60**(8), 1429 - 1444.

Lagabrielle Y. and Lemoine M. (1997) Alpine, Corsican and Apennine ophiolites: the slow-spreading ridge model. *Comptes Rendus Acad Sci Paris, Sciences de la terre et des planètes* **325**, 909 - 920.

Lassiter J. C. and Hauri E. H. (1998) Osmium-isotope variations in Hawaiian lavas: evidence for recycled oceanic lithosphere in the Hawaiian plume. *Earth and Planetary Science Letters* **164**, 483 - 496.

Lassiter J. C., Hauri E. H., Reiners P. W., and Garcia M. O. (2000) Generation of Hawaiian post-erosional lavas by melting of a mixed lherzolite/pyroxenite source. *Earth and Planetary Science Letters* **178**, 269 - 284.

Lassiter J. C. (2006) Constraints on the coupled thermal evolution of the Earth's core and mantle, the age of the inner core, and the origin of the $^{186}Os/^{188}Os$ "core signal" in plume-derived lavas. *Earth and Planetary Science Letters* **250**, 306 - 317.

Lee C.-T. (2002) Platinum-group element geochemistry of peridotite xenoliths from the Sierra Nevada and the Basin and Range, California. *Geochimica et Cosmochimica Acta* **66**(22), 3987 - 4005.

Lee C.-T. A., Brandon A. D., and Norman M. (2003) Vanadium in peridotites as a proxy for paleo-fO_2 during partial melting: Prospects, limitations, and implications. *Geochimica et Cosmochimica Acta* **67**(16), 3045 - 3064.

Lee D. S. (1983) Palladium and nickel in north-east Pacific waters. *Nature* **305**, 47 - 48.

Lenoir X., Garrido C. J., Bodinier J. L., and Dautria J.-M. (2000) Contrasting lithospheric mantle domains beneath the Massif Central (France) revealed by geochemistry of peridotite xenoliths. *Earth and Planetary Science Letters* **181**, 359 - 375.

Le Roux V., Bodinier J. L., Tommasi A., Alard O., Dautria J.-M., Vauchez A., and Riches A. J. V. (2007) The Lherz spinel lherzolite: Refertilized rather than pristine mantle. *Earth and Planetary Science Letters* **259**, 599 - 612.

Li C., Barnes S.-J., Makovicky E., Rose-Hansen J., and Makovicky M. (1996) Partitioning of nickel, copper, iridium, rhenium, platinum and palladium between monosulfide solid solution and sulfide liquid: Effects of composition and temperature. *Geochimica et Cosmochimica Acta* **60**(7), 1231 - 1238.

Liu C.-Z., Snow J. E., Hellebrand E., Brügmann G., von der Handt A., Büchl A., and Hofmann A. W. (2008) Ancient, highly heterogeneous mantle beneath Gakkel ridge, Arctic Ocean. *Nature* **452**, 311 - 316.

Liu Y., Samaha N.-T., and Baker D. R. (2007) Sulfur concentration at sulfide saturation (SCSS) in magmatic silicate melts. *Geochimica et Cosmochimica Acta* **71**, 1783 - 1799.Lorand J.-P. (1989) Abundance and distribution of Cu-Fe-Ni sulfides, sulfur, copper and platinum-group elements in orogenic-type spinel lherzolite massifs of Ariège (northeastern Pyrenees, France). *Earth and Planetary Science Letters* **93**, 50 - 64.

Lorand J.-P., Keays R. R., and Bodinier J. L. (1993) Copper and Noble Metal Enrichments Across the Lithosphere-Asthenosphere Boundary of Mantle Diapirs: Evidence from the Lanzo Lherzolite Massif. *Journal of Petrology* **34**(6), 1111 - 1140.

Lorand J.-P., Pattou L., and Gros M. (1999) Fractionation of Platinum-group Elements and Gold in the Upper Mantle: a Detailed Study in Pyrenean Orogenic Lherzolites. *Journal of Petrology* **40**(6), 957 - 981.

Lorand J.-P., Schmidt G., Palme H., and Kratz K.-L. (2000) Highly siderophile element geochemistry of the Earth's mantle: new data for the Lanzo (Italy) and Ronda (Spain) orogenic peridotite bodies. *Lithos* **53**, 149 - 164.

Lorand J.-P. and Alard O. (2001) Platinum-group element abundances in the upper mantle: New constraints from in situ and whole-rock analyses of Massif Central xenoliths (France). *Geochimica et Cosmochimica Acta* **65**(16), 2789 - 2806.

Lorand J.-P., Reisberg L., and Bedini R. M. (2003) Platinum-group elements and melt percolation processes in Sidamo spinel peridotite xenoliths, Ethiopia, East African Rift. *Chemical Geology* **196**, 57 - 75.

Lorand J.-P., Delpech G., Grégoire M., Moine B., O'Reilly S. Y., and Cottin J.-Y. (2004) Platinum-group elements and the multistage metasomatic history of Kerguelen lithospheric mantle (South Indian Ocean). *Chemical Geology* **208**, 195 - 215.

Lorand J.-P., Luguet A., Alard O., Bézos A., and Meisel T. (2008) Abundance and distribution of platinum-group in orogenic lherzolites; a case study in a Fontete Rouge lherzolite (French pyrénées). *Chemical Geology* **248**, 174 - 194.

Loubet M. and Allègre C. J. (1982) Trace elements in orogenic lherzolites reveal the complex history of the upper mantle. *Nature* **298**, 809 - 814.

Luguet A., Alard O., Lorand J.-P., Pearson N. J., Ryan C., and O'Reilly S. Y. (2001) Laser-ablation microprobe (LAM)-ICPMS unravels the highly siderophile element geochemistry of the oceanic mantle. *Earth and Planetary Science Letters* **189**, 285 - 294.

Luguet A., Lorand J.-P., and Seyler M. (2003) Sulfide petrology and highly siderophile element geochemistry of abyssal peridotites: A coupled study of samples from the Kane Fracture Zone (45°W 23°20N, MARK Area, Atlantic Ocean). *Geochimica et Cosmochimica Acta* **67**(8), 1553 - 1570.

Luguet A., Lorand J.-P., Alard O., and Cottin J.-Y. (2004) A multi-technique study of platinum group element systematic in some Ligurian ophiolitic peridotites, Italy. *Chemical Geology* **208**, 175 - 194.

Luguet A., Shirey S. B., Lorand J.-P., Horan M. F., and Carlson R. W. (2007) Residual platinum-group minerals from highly depleted harzburgites of the Lherz massif (France) and their role in HSE fractionation of the mantle. *Geochimica et Cosmochimica Acta* **71**, 3082 - 3097.

Luguet A., Pearson D. G., Nowell G. N., Dreher S. T., Coggon J. A., Spetsius Z. V., and Parman S. W. (2008) Enriched Pt-Re-Os Isotope Systematics in Plume Lavas Explained by Metasomatic Sulfides. *Science* **319**, 453 - 456.

Lundstrom C. C., Gill J., and Williams Q. (2000) A geochemically consistent hypothesis for MORB generation. *Chemical Geology* **162**, 105 - 126.

Mallmann G. and O'Neill H. S. C. (2007) The effect of oxygen fugacity on the partitioning of Re between crystals and silicate melt during mantle melting. *Geochimica et Cosmochimica Acta* **71**, 2837 - 2857.

Manatschal G. and Bernoulli D. (1998) Rifting and early evolution of ancient ocean basins: the record of the Mesozoic Tethys and of the Galicia-Newfoundland margins. *Marine Geophysical Researches* **20**, 371 - 381.

Manatschal G., Müntener O., Lavier L. L., Minshull T. A., and Péron-Pinvidic G. (2007) Observations from the Alpine Tethys and Iberia-Newfoundland margins pertinent to the interpretation of continental breakup. *Geological Society Special Publications* **282**, 291 - 324.

Martin C. E. (1991) Osmium isotope characteristics of mantle-derived rocks. *Geochimica et Cosmochimica Acta* **55**, 1421 - 1434.

Mavrogenes J. A. and O'Neill H. S. C. (1999) The relative effects of pressure, temperature and oxygen fugacity on the solubility of sulfide in mafic magmas. *Geochimica et Cosmochimica Acta* **63**(7/8), 1173- 1180.

McDonough W. F. and Sun S.-S. (1995) The composition of the Earth. *Chemical Geology* **120**, 223 - 253.

Meibom A., Sleep N. H., Page Chamberlain C., Coleman R. G., Frei R., Hren M. T., and Wooden J. L. (2002) Re-Os isotopic evidence for long-lived heterogeneity and equilibration processes in the Earth's upper mantle. *Nature* **419**, 705 - 708.

Meisel T., Biino G. G., and Nägler T. F. (1996a) Re-Os, Sm-Nd, and rare earth element evidence for Proterozoic oceanic and possible subcontinental lithosphere in tectonized ultramafic lenses from the Swiss Alps. *Geochimica et Cosmochimica Acta* **60**(14), 2583 - 2593.

Meisel T., Walker R. J., Irving A. J., and Lorand J.-P. (2001b) Osmium isotopic compositions of mantle xenoliths: A global perspective. *Geochimica et Cosmochimica Acta* **65**(8), 1311 - 1323.

Meisel T., Fellner N., and Moser J. (2003a) A simple procedure for the determination of platinum group elements and rhenium (Ru, Rh, Pd, Re, Os, Ir and Pt) using ID-ICP-MS with an inexpensive on-line matrix separation in geological and environmental materials. *J. Anal. At. Spectrom.* **18**, 720 - 726.

Menzies M. A., Kempton P., and Dungan M. (1985) Interaction of Continental Lithosphere and Asthenospheric Melts below the Geronimo Volcanic Field, U.S.A. *Journal of Petrology* **26**(3), 663 - 693.

Michael P. J., Langmuir C. H., Dick H. J. B., Snow J. E., Goldstein S. L., Graham D. W., Lehnert K., Kurras G., Jokat W., Mühe R., and Edmonds H. N. (2003) Magmatic and amagmatic seafloor generation at the ultraslow-spreading Gakkel ridge, Arctic Ocean. *Nature* **423**, 956 - 961.

Mitchell R. H. and Keays R. R. (1981) Abundance and distribution of gold, palladium and iridium in some spinel ad garnet lherzolites: implications for the nature and origin of precious metal-rich intergranular components in the upper mantle. *Geochimica et Cosmochimica Acta* **45**, 2425 - 2442.

Morgan J. W. and Lovering J. F. (1967) Rhenium and Osmium Abundances in some Igneous and Metamorphic Rocks. *Earth and Planetary Science Letters* **3**, 219 - 224.

Morgan J. W., Wandless G. A., Petrie R. K., and Irving A. J. (1981) Composition of the Earth's upper mantle - I. Siderophile trace elements in ultramafic nodules. *Tectonophysics* **75**, 47 - 67.

Morgan J. W. and Baedecker P. A. (1983) Elemental composition of sulfide particles from an ultramafic xenolith and the siderophile element content of the upper mantle. *Proc. Lunar Planet. Sci. Conf. 14th*, 513 - 514.

Morgan J. W. (1986) Ultramafic Xenoliths: Clues to Earth's Late Accretionary History. *Journal of Geophysical Research* **91**(B12), 12375 - 12387.

Morgan J. W., Walker R. J., Brandon A. D., and Horan M. F. (2001) Siderophile elements in Earth's upper mantle and lunar breccias: Data synthesis suggests manifestations of the same late influx. *Meteoritics and Planetary Science* **36**, 1257 - 1275.

Morishita T., Arai S., Gervilla F., and Green D. H. (2003) Closed-system geochemical recycling of crustal materials in alpine-type peridotite. *Geochimica et Cosmochimica Acta* **67**(2), 303 - 310.

Müntener O. and Hermann J. (2001) The role of lower crust and continental upper mantle during formation of non-volcanic passive margins: evidence from the Alps. In *Non-Volcanic Rifting of Continental Margins: A Comparison of Evidence from Land and Sea*, Vol. 187 (ed. R. C. L. Wilson, R. B. Whitmarsh, B. Taylor, and N. Froitzheim), pp. 267 - 288. Geological Society.

Müntener O., Pettke T., Desmurs L., Meier M., and Schaltegger U. (2004) Refertilization of mantle peridotite in embryonic ocean basins: trace element and Nd isotopic evidence and implications for crust-mantle relationships. *Earth and Planetary Science Letters* **221**, 293 - 308.

Mungall J. E., Andrews D. R. A., Cabri L. J., Sylvester P. J., and Tubrett M. (2005) Partitioning of Cu, Ni, Au and platinum-group elements between monosulfide solid solution and sulfide melt under controlled oxygen and sulfur fugacities. *Geochimica et Cosmochimica Acta* **69**(17), 4349 - 4360.

Murthy V.R. (1991) Early Differentiation of the Earth and the Problem of Mantle Siderophile Elements: A new Approach. *Science* **253**, 303 - 306.

Murthy V.R. and Karato S.-I. (1997) Core formation and chemical equilibrium in the Earth - II: Chemical consequences for the mantle and core. *Physics of the Earth and Planetary Interiors* **100**, 81 - 95.

Niu Y. (1997) Mantle Melting and Melt Extraction Processes beneath Ocean Ridges: Evidence from Abyssal Peridotites. *Journal of Petrology* **38**(8), 1047 - 1074.

O'Hara M. J. (1968) The bearing of phase quilibria studies in synthetic and natural systems on the origin and evolution of basic and ultrabasic rocks. *Earth Science Reviews* **4**, 69 - 133.

O'Neill H. S. C., Dingwell D. B., Borisov A., Spettel B., and Palme H. (1995) Experimental petrochemistry of some highly siderophile elements at high temperatures, and some implications for core formation and the mantle's early history. *Chemical Geology* **120**, 255 - 273.

O'Neill H. S. C. and Mavrogenes J. A. (2002) The Sulfide Capacity and the Sulfur Content at Sulfide Saturation of Silicate Melts at 1400°C and 1 bar. *Journal of Petrology* **43**(6), 1049 - 1087.

Obata M. (1980) The Ronda Peridotite: Garnet-, Spinel-, and Plagioclase-Lherzolite Facies and the P-T-Trajectories of a High-Temperature Mantle Intrusion. *Journal of Petrology* **21**(3), 533 - 572.

Olive V., Ellam R. M., and Harte B. (1997) A Re-Os isotope study of ultramafic xenoliths from the Matsoku kimberlite. *Earth and Planetary Science Letters* **150**, 129 - 140.

Pattou L., Lorand J.-P., and Gros M. (1996) Non-chondritic platinum-group element ratios in the Earth's mantle. *Nature* **379**, 712 - 715.

Peach C. L., Mathez E. A., and Keays R. R. (1990) Sulfide melt-silicate melt distribution coefficients for noble metals and other chalcophile elements as deduced from MORB: Implications for partial melting. *Geochimica et Cosmochimica Acta* **54**, 3379 - 3389.

Peach C. L., Mathez E. A., Keays R. R., and Reeves S. J. (1994) Experimentally determined sulfide melt-silicate melt partition coefficients for iridium and palladium. *Chemical Geology* **117**, 361 - 377.

Pearson D. G., Canil D., and Shirey S. B. (2003) Mantle Samples Included in Volcanic Rocks: Xenoliths and Diamonds. In *Treatise on Geochemistry, Part 2*, Vol. 2 (ed. K. K. Turekian and H. D. Holland), pp. 171 - 225. Elsevier Ltd.

Pearson D. G., Davies G. R., and Nixon P. H. (1993) Geochemical Constraints on the Petrogenesis of Diamond Facies Pyroxenites from the Beni Bousera Peridotite Massif, North Morocco. *Journal of Petrology* **34**(1), 125 - 172.

Pearson D. G., Irvine G. J., Ionov D. A., Boyd F. R., and Dreibus G. E. (2004) Re-Os isotope systematics and platinum group element fractionation during mantle melt extraction: a study of massif and xenolith peridotite suites. *Chemical Geology* **208**, 29 - 59.

Pearson D. G. and Nowell G. N. (2004) Re-Os and Lu-Hf Isotope Constraints on the Origin and Age of Pyroxenites from the Beni Bousera Peridotite massif: Implications for Mixed Peridotite-Pyroxenite Mantle Sources. *Journal of Petrology* **45**(2), 439 - 455.

Pearson N. J., Alard O., Griffin W. L., Jackson S. E., and O'Reilly S. Y. (2002) In situ measurement of Re-Os isotopes in mantle sulfides by laser ablation multicollector-inductively coupled plasma mass spectrometry: Analytical methods and preliminary results. *Geochimica et Cosmochimica Acta* **66**(6), 1037 - 1050.

Peregoedova A., Barnes S.-J., and Baker D. R. (2004) The formation of Pt-Ir alloys and Cu-Pd-rich sulfide melts by partial desulfurization of Fe-Ni-Cu sulfides: results of experiments and implications for natural systems. *Chemical Geology* **208**, 247 - 264.

Pertermann M. and Hirschmann M. M. (2003a) Anhydrous Partial Melting Experiments on MORB-like Eclogite: Phase Relations, Phase Compositions and Mineral-Melt Partitioning of Major Elements at 2-3 GPa. *Journal of Petrology* **44**(12), 2173 - 2201.

Pertermann M. and Hirschmann M. M. (2003b) Partial melting experiments on a MORB-like pyroxenite between 2 and 3 GPa: Constraints on the presence of pyroxenite in basalt source regions from solidus location and melting rate. *Journal of Geophysical Research* **108**(B2), 2125, doi:10.1029/2000JB000118.

Peslier A. H., Reisberg L., Ludden J., and Francis D. (2000) Re-Os constraints on harzburgite and lherzolite formation in the lithospheric mantle: A study of Northern Canadian Cordillera xenoliths. *Geochimica et Cosmochimica Acta* **64**(17), 3061 - 3071.

Peters T. (1963) Mineralogie und Petrographie des Totalpserpentins bei Davos. *Schweizerische Mineralogische und Petrographische Mitteilungen* **43**, 531 - 685.

Peters T. (1968) Distribution of Mg, Fe, Al, Ca and Na in Coexisting Olivine, Orthopyroxene and Clinopyroxene in the Totalp Serpentinite (Davos, Switzerland) and in the Alpine Metamorphosed Malenco Serpentinite (N. Italy). *Contrib Mineral Petrol* **18**, 65 - 75.

Peters T. and Stettler A. (1987) Radiometric age, thermobarometry and mode of emplacement of the Totalp peridotite in the Eastern Swiss Alps. *Schweizerische Mineralogische und Petrographische Mitteilungen* **67**, 285 - 294.

Piccardo G. B., Messiga B., and Vannucci R. (1988) The Zabargad peridotite - pyroxenite association: petrological constraints on evolution. *Tectonophysics* **150**, 135 - 162.

Piccardo G. B., Müntener O., and Zanetti A. (2004) Alpine-Apennine ophiolitic peridotites: new concepts on their composition and evolution. *Ofioliti* **29**(1), 63 - 74.

Piccardo G. B., Zanetti A., and Müntener O. (2007) Melt/peridotite interaction in the Southern Lanzo peridotite: Field, textural and geochemical evidence. *Lithos* **94**, 181 - 209.

Pickering-Witter J. and Johnston A. D. (2000) The effects of variable bulk composition on the melting systematics of fertile peridotitic assemblages. *Contrib Mineral Petrol* **140**, 190 - 211.

Poirier A. (2006) Re-Os and Pb isotope systematics in reduced fjord sediments from Saanich Inlet (Western Canada). *Earth and Planetary Science Letters* **249**, 119 - 131.

Polvé M. and Allègre C. J. (1980) Orogenic lherzolite complexes studied by ^{87}Rb-^{87}Sr: A clue to understand the mantle convection processes? *Earth and Planetary Science Letters* **51**, 71 - 93.

Powell W. and O'Reilly S. Y. (2007) Metasomatism and sulfide mobility in lithospheric mantle beneath eastern Australia: Implications for mantle Re-Os chronology. *Lithos* **94**, 132 - 147.

Quick J. E. (1981) The Origin and Significance of Large, Tabular Dunite Bodies in the Trinity Peridotite, Northern California. *Contrib Mineral Petrol* **78**, 413 - 422.

Rampone E., Piccardo G. B., Vannucci R., and Bottazzi P. (1997) Chemistry and origin of trapped melts in ophiolitic peridotites. *Geochimica et Cosmochimica Acta* **61**(21), 4557 - 4569.

Rampone E., Romairone A., and Hofmann A. W. (2004) Contrasting bulk and mineral chemistry in depleted mantle peridotites: evidence for reactive porous flow. *Earth and Planetary Science Letters* **218**, 491 - 506.

Rampone E., Romairone A., Abouchami W., Piccardo G. B., and Hofmann A. W. (2005) Chronology, Petrology and Isotope Geochemistry of the Erro-Tobio Peridotites (Ligurian Alps, Italy): Records of Late Palaeozoic Lithospheric Extension. *Journal of Petrology* **46**(4), 799 - 827.

Rampone E. and Borghini G. (2008) Melt migration and intrusion in the Erro-Tobbio peridotites (Ligurian Alps, Italy): Insights on magmatic processes in extending lithospheric mantle. *European Journal of Mineralogy* **20**(4), 573 - 586.

Ravizza G., Blusztajn J., and Prichard H. M. (2001) Re-Os systematics and platinum-group element distribution in metalliferous sediments from the Troodos ophiolite. *Earth and Planetary Science Letters* **188**, 369 - 381.

Ravizza G. and Pyle D. (1997) PGE and Os isotopic analyses of single sample aliquots with NiS fire assay preconcentration. *Chemical Geology* **141**, 251 - 268.

Rehkämper M., Halliday A. N., Alt J., Fitton J. G., Zipfel J., and Takazawa E. (1999a) Non-chondritic platinum-group element ratios in oceanic mantle lithosphere: petrogenetic signature of melt percolation? *Earth and Planetary Science Letters* **172**, 65 - 81.

Rehkämper M., Halliday A. N., Fitton G., Lee D.-C., Wieneke M., and Arndt N. T. (1999b) Ir, Ru, Pt, and Pd in basalts and komatiites: New constraints for the geochemical behavior of the platinum-group elements in the mantle. *Geochimica et Cosmochimica Acta* **62**(22), 3915 - 3934.

Reisberg L. C., Allègre C. J., and Luck J.-M. (1991) The Re-Os systematics of the Ronda Ultramafic Complex of southern Spain. *Earth and Planetary Science Letters* **105**, 196 - 213.

Reisberg L. and Lorand J.-P. (1995) Longevity of sub-continental mantle lithosphere from osmium isotope systematics in orogenic peridotite massifs. *Nature* **376**, 159 - 162.

Reisberg L., Zhi X., Lorand J.-P., Wagner C., Peng Z., and Zimmermann C. (2005) Re-Os and S systematics of spinel peridotite xenoliths from east central China: Evidence for contrasting effects of melt percolation. *Earth and Planetary Science Letters* **239**(3 - 4), 286 - 309.

Reisberg L., Rouxel O., Ludden J., Staudigel H., and Zimmermann C. (2008) Re.Os results from ODP Site 801: Evidence for extensive Re uptake during alteration of oceanic crust. *Chemical Geology* **248**, 256 - 271.

Richardson S. H., Shirey S. B., Harris J. W., and Carlson R. W. (2001) Archaean subduction recorded by Re-Os isotopes in eclogitic sulfide inclusions in Kimberley diamonds. *Earth and Planetary Science Letters* **191**, 257 - 266.

Righter K. and Drake M. J. (1997) Metal-silicate equilibrium in a homogeneously accreting earth: new results for Re. *Earth and Planetary Science Letters* **146**, 541 - 553.

Righter K. and Hauri E. H. (1998) Compatibility of Rhenium in Garnet During Mantle Melting and Magma Genesis. *Science* **280**, 1737 - 1741.

Righter K., Walker R. J., and Warren P. H. (2000) Significance of Highly Siderophile Elements and Osmium Isotopes in the Lunar and Terrestrial Mantles. In *Origin of the Earth and Moon* (ed. R. Canup and K. Righter), pp. 291 - 322. University of Arizona Press, Tucson, AZ.

Righter K., Campbell A. J., Humayun M., and Hervig R. L. (2004) Partitioning of Ru, Rh, Pd, Re, Ir, and Au between Cr-bearing spinel, olivine, pyroxene and silicate melts. *Geochimica et Cosmochimica Acta* **68**(4), 867 - 880.

Rivalenti G., Mazzuchelli M., Vannucci R., Hofmann A. W., Ottolini L., Bottazzi P., and Obermiller W. (1995) The relationship between websterite and peridotite in the Balmuccia peridotite massif (NW Italy) as revealed by trace element variations in clinopyroxene. *Contrib Mineral Petrol* **121**, 275 - 288.

Roy-Barman M. and Allègre C. J. (1994) $^{187}Os/^{186}Os$ ratios of mid-ocean ridge basalts and abyssal peridotites. *Geochimica et Cosmochimica Acta* **58**(22), 5043 - 5054.

Roy-Barman M. and Allègre C. J. (1995) $^{187}Os/^{186}Os$ in oceanic island basalts: tracing oceanic rust recycling in the mantle. *Earth and Planetary Science Letters* **129**, 145 - 161.

Roy-Barman M., Luck J.-M., and Allègre C. J. (1996) Os isotopes in orogenic lherzolite massifs and mantle heterogeneities. *Chemical Geology* **130**, 55 - 64.

Roy-Barman M., Wasserburg G. J., Papanastassiou D. A., and Chaussidon M. (1998) Osmium isotopic compositions and Re-Os concentrations in sulfide globules from basaltic glasses. *Earth and Planetary Science Letters* **154**, 331 - 347.

Saal A. E., Takazawa E., Frey F. A., Shimizu N., and Hart S. R. (2001) Re-Os Isotopes in the Horoman Peridotite: Evidence for Refertilization? *Journal of Petrology* **42**(1), 25 – 37

Santos J. F., Schärer U., Gil Ibarguchi J. I., and Girardeau J. (2002) Genesis of Pyroxenite-rich Peridotite at Cabo Ortegal (NW Spain): Geochemical and Pb-Sr-Nd Isotope Data. *Journal of Petrology* **43**(1), 17 - 43.

Sattari P., Brenan J. M., Horn I., and McDonough W. F. (2002) Experimental Constraints on the Sulfide- and Chromite-Silicate Melt Partitioning Behavior of Rhenium and Platinum-Group Elements. *Economic Geology* **97**, 385 - 398.

Schaltegger U., Desmurs L., Manatschal G., Müntener O., Meier M., Frank M., and Bernoulli D. (2002) The transition from rifting to sea-floor spreading within a magma-poor rifted margin: field and isotopic constraints. *Terra Nova* **14**, 156 - 162.

Scherstén A., Elliott T., Hawkesworth C. J., and Norman M. (2004) Tungsten isotope evidence that mantle plumes contain no contribution from the Earth's core. *Nature* **427**, 234 - 237.

Schiano P., Birck J.-L., and Allègre C. J. (1997) Osmium-strontium-neodymium-lead isotopic covariations in mid-ocean ridge basalt glasses and the heterogeneity of the upper mantle. *Earth and Planetary Science Letters* **150**, 363 - 379.

Schmid S. M., Fügenschuh B., Kissling E., and Schuster R. (2004) Tectonic map and overall architecture of the Alpine orogen. *Eclogae Geologicae Helvetiae* **97**, 93 - 117.

Schmidt G., Palme H., Kratz K.-L., and Kurat G. (2000) Are highly siderophile elements (PGE, Re and Au) fractionated in the upper mantle of the Earth? New results on peridotites from Zabargad. *Chemical Geology* **163**, 167 - 188.

Schmidt G. and Snow J. E. (2002) Os isotopes in mantle xenoliths from the Eifel volcanic field and the Vogelsberg (Germany): age constraints on the lithospheric mantle. *Contrib Mineral Petrol* **143**, 694 - 705.

Selby D., Creaser R. A., Stein H. J., Markey R. J., and Hannah J. L. (2007) Assessment of the ^{187}Re decay constant by cross calibration of Re-Os molybenite and U-Pb zircon chronometers in magmatic ore systems. *Geochimica et Cosmochimica Acta* **71**, 1999 - 2013.

Seyler M. and Bonatti E. (1997) Regional-scale melt-rock interaction in lherzolitic mantle in the Romanche Fracture Zone (Atlantic Ocean). *Earth and Planetary Science Letters* **146**, 273 - 287.

Sharma M., Papanastassiou D. A., and Wasserburg G. J. (1997) The concentration and isotopic composition of osmium in the oceans. *Geochimica et Cosmochimica Acta* **61**(16), 3287 - 3299.

Shaw D. M. (1970) Trace element fractionation during anatexis. *Geochimica et Cosmochimica Acta* **34**, 237 - 243.

Shervais J. W. and Mukasa S. B. (1991) The Balmuccia Orogenic Lherzolite Massif, Italy. *Journal of Petrology* Special Lherzolite Issue, 155 - 174.

Shirey S. B. and Walker R. J. (1998) The Re-Os isotope system in cosmochemistry and high-temperature geochemistry. *Annu. Rev. Earth Planet. Sci.* **26**, 423 - 500.

Sinigoi S., Comin-Chiaramonti P., Demarchi G., and Siena F. (1983) Differentiation of Partial Melts in the Mantle: Evidence from the Balmuccia Peridotite, Italy. *Contrib Mineral Petrol* **82**, 351 - 359.

Smith A. D. (2003) Critical evaluation of Re-Os and Pt-Os isotopic evidence on the origin of intraplate volcanism. *Journal of Geodynamics* **36**, 1 - 16.

Smoliar M. I., Walker R. J., and Morgan J. W. (1996) Re-Os ages of Group IIA, IIIA, IVA, and IVB iron meteorites. *Science* **271**, 1099 - 1102.

Snow J. E. and Reisberg L. (1995) Erratum of "Os isotopic systematics of the MORB mantle: results from altered abyssal peridotites". *Earth and Planetary Science Letters* **136**, 723 - 733.

Snow J. E. and Schmidt G. (1998) Constraints on Earth accretion deduced from noble metals in the oceanic mantle. *Nature* **391**, 166 - 169.

Sobolev A. V., Hofmann A. W., Kuzmin D. V., Yaxley G. M., Arndt N. T., Chung S.-L., Danyushevsky L. V., Elliott T., Frey F. A., Garcia M. O., Gurenko A. A., Kamenetsky V. S., Kerr A. C., Krivolutskaya N. A., Matvienkov V. V., Nikogosian I. K., Rocholl A., Sigurdsson I. A., Sushchevskaya N. M., and Teklay M. (2007) The Amount of Recycled Crust in Sources of Mantle-Derived Melts. *Science* **316**, 412 - 417.

Sobolev A. V., Hofmann A. W., Sobolev S. V., and Nikogosian I. K. (2005) An olivine-free mantle source of Hawaiian shield basalts. *Nature* **434**, 590 - 597.

Stampfli G. M. and Borel G. D. (2004) The TRANSMED Transects in Space and Time: Constraints on the Paleotectonic Evolution of the Mediterranean Domain. In *The TRANSMED atlas* (ed. W. Cavazza), pp. 54 - 90. Springer-Verlag.

Standish J. J., Hart S. R., Blusztajn J., Dick H. J. B., and Lee K. L. (2002) Abyssal peridotite osmium isotopic compositions from Cr-spinel. In *Geochemistry Geophysics Geosystems*, pp. 10.1029/2001GC000161. AGU and the Geochemical Society.

Suen C. J. and Frey F. A. (1987) Origins of the mafic and ultramafic in the Ronda peridotite. *Earth and Planetary Science Letters* **85**, 183 - 202.

Takahashi N. (1992) Evidence for melt segregation towards fractures in the Horoman mantle peridotite complex. *Nature* **359**, 52 - 55.

Takazawa E., Frey F. A., Shimizu N., Obata M., and Bodinier J. L. (1992) Geochemical evidence for melt migration and reaction in the upper mantle. *Nature* **359**, 55 - 58.

Takazawa E., Frey F. A., Shimizu N., and Obata M. (1996) Evolution of the Horoman Peridotite (Hokkaido, Japan): Implications from pyroxene compositions. *Chemical Geology* **134**, 3 - 26.

Takazawa E., Frey F. A., Shimizu N., Saal A. E., and Obata M. (1999) Polybaric Petrogenesis of Mafic Layers in the Horoman Peridotite Complex, Japan. *Journal of Petrology* **40**(12), 1827 - 1851.

Takazawa E., Frey F. A., Shimizu N., and Obata M. (2000) Whole rock compositional variations in an upper mantle peridotite (Horoman, Hokkaido, Japan): Are they consistent with a partial melting process? *Geochimica et Cosmochimica Acta* **64**(4), 695 - 716.

Tessalina S. G., Bourdon B., Gannoun A., Capmas F., Birck J.-L., and Allègre C. J. (2007) Complex proterozoic to paleozoic history of the upper mantle recorded in the Urals lherzolite massifs by Re-Os and Sm-Nd systematics. *Chemical Geology* **240**, 61 - 84.

Toramaru A., Takazawa E., Morishita T., and Matsukage K. (2001) Model of layering formation in a mantle peridotite (Horoman, Hokkaido, Japan). *Earth and Planetary Science Letters* **185**, 299 - 313.

van Acken D., Becker H., and Walker R. J. (2008) Refertilization of Jurassic oceanic peridotites from the Tethys Ocean – implications for the Re-Os systematics of the upper mantle. *Earth and Planetary Science Letters* **268**, 171 - 181.

Van der Wal D. and Bodinier J. L. (1996) Origin of the recrystallisation front in the Ronda peridotite by km-scale pervasive porous melt flow. *Contrib Mineral Petrol* **122**, 387 - 405.

Van Orman J. A., Keshav S., and Fei Y. (2008) High-pressure solid/liquid partitioning of Os, Re and Pt in the Fe-S system. *Earth and Planetary Science Letters* **274**, 250 - 257.

Vaselli G., Downes H., Thirlwall M. F., Dobosi G., Coradossi N., Seghedi I., Szakacs A., and Vannucci R. (1995) Ultramafic Xenoliths in Plio-Pleistocene Alkali Basalts from the Eastern Transylvanian Basin: Depleted Mantle Enriched by Vein Metasomatism. *Journal of Petrology* **36**(1), 23 - 53.

Völkening J., Walczyk T., and Heumann K. G. (1991) Osmium isotope ratio determinations by Negative Thermal Ionization Mass Spectrometry. *International Journal of Mass Spectrometry and Ion Processes* **105**, 147 - 159.

Voshage H., Sinigoi S., Mazzuchelli M., Demarchi G., Rivalenti G., and Hofmann A. W. (1988) Isotopic constraints on the origin of ultramafic and mafic dikes in the Balmuccia peridotite (Ivrea Zone). *Contrib Mineral Petrol* **100**, 261 - 267.

Walker R. J., Carlson R. W., Shirey S. B., and Boyd F. R. (1989) Os, Sr, Nd, and Pb isotope systematics of southern African peridotite xenoliths: Implications for the chemical evolution of subcontinental mantle. *Geochimica et Cosmochimica Acta* **53**, 1583 - 1595.

Walker R. J., Morgan J. W., Horan M. F., Czamanske G. K., Krogstad E. J., Fedorenko V. A., and Kunilov V. E. (1994) Re-Os isotopic evidence for an enriched mantle source for the Noril'sk-type, ore-bearing intrusions, Siberia. *Geochimica et Cosmochimica Acta* **58**(19), 4179 - 4197.

Walker R. J., Hanski E., Vuollo J., and Liipo J. (1996) The Os isotopic composition of Proterozoic upper mantle: evidence for chondritic upper mantle from the Outokumpu ophiolite, Finland. *Earth and Planetary Science Letters* **141**, 161 - 173.

Walker R. J., Morgan J. W., Beary E. S., Smoliar M. I., Czamanske G. K., and Horan M. F. (1997) Applications of the ^{190}Pt-^{186}Os isotope system to geochmistry and cosmochemistry. *Geochimica et Cosmochimica Acta* **61**(22), 4799 - 4807.

Walker R. J., Prichard H. M., Ishiwatari A., and Pimentel M. (2002) The osmium isotopic composition of convecting upper mantle deduced from ophiolite chromites. *Geochimica et Cosmochimica Acta* **66**(2), 329 - 345.

Wallace P. and Carmichael I. S. E. (1992) Sulfur in basaltic magmas. *Geochimica et Cosmochimica Acta* **56**, 1863 - 1874.

Walter M. J., Newsom H. E., Ertel W., and Holzheid A. (2000) Siderophile Elements in the Earth and Moon: Metal/Silicate Partitioning and Implications for Core Formation. In *Origin of the Earth and Moon* (ed. R. Canup and K. Righter), pp. 265 - 289. University of Arizona Press, Tucson, AZ.

Walter M. J. (2003) Melt Extraction and Compositional Variability in the Lithosphere. In *Treatise on Geochemistry, Part 2*, Vol. 2 (ed. K. K. Turekian and H. D. Holland), pp. 363 - 394. Elsevier Ltd.

Weiss H. V. and Fresco J. (1983) Platinum group elements in seawater. I. Palladium. *Can. J. Chem.* **61**, 734 - 736.

Weissert H. and Bernoulli D. (1985) A transform margin in the Mesozoic Tethys: evidence from the Swiss Alps. *Geologische Rundschau* **74**(3), 665 - 679.

Wendlandt R. F. (1982) Sulfide saturation of basalt and andesite melts at high pressures and temperatures. *American Mineralogist* **67**, 877 - 885.

Witt-Eickschen G., Seck H. A., and Reys C. (1993) Multiple Enrichment Processes and their Realtionships in the Subcrustal Lithosphere Beneath the Eifel (Germany). *Journal of Petrology* **34**(1), 1 - 22.

Witt-Eickschen G., Kaminsky W., Kramm U., and Harte B. (1998) The Nature of Young Vein Metasomatism in the Lithosphere of the West Eifel (Germany): Geochemical and Isotopic Constraints from Composite Mantle Xenoliths from the Meerfelder Maar. *Journal of Petrology* **39**(1), 155 - 185.

Witt-Eickschen G. and Kramm U. (1998) Evidence for the multiple stage evolution of the subcontinental lithospheric mantle beneath the Eifel (Germany) from pyroxenite and composite pyroxenite/peridotite xenoliths. *Contrib Mineral Petrol* **131**, 258 - 272.

Witt-Eickschen G., Seck H. A., Mezger K., Eggins S. M., and Altherr R. (2003) Lithospheric Mantle Evolution beneath the Eifel (Germany): Constraints from Sr-Nd-Pb Isotopes and Trace Element Abundances in Spinel Peridotite and Pyroxenite Xenoliths. *Journal of Petrology* **44**(6), 1077 - 1095.

Wood S. A. (1987) Thermodynamic calculations of the volatility of the platinum group elements (PGE): The PGE content of fluids at magmatic temperatures. *Geochimica et Cosmochimica Acta* **51**, 3041 - 3050.

Woodland A. B., Kornprobst J., McPherson E., Bodinier J. L., and Menzies M. A. (1996) Metasomatic interactions in the lithospheric mantle: petrologic evidence from the Lherz massif, French Pyrenees. *Chemical Geology* **134**, 83 - 112.

Xu Y. (2002) Evidence for crustal componets in the mantle and constraints on crustal recycling machanisms: pyroxenite xenoliths from Hannuoba, North China. *Chemical Geology* **182**, 301 - 322.

Yasuda A., Fujii T., and Kurita K. (1994) Melting phase relations of an anhydrous mid-ocean ridge basalt from 3 to 20 GPa: Implications for the behavior of subducted oceanic crust in the mantle. *Journal of Geophysical Research* **99**(B5), 9401 - 9414.

Yaxley G. M. and Green D. H. (1998) Reactions between eclogite and peridotite: mantle refertilisation by subduction of oceanic crust. *Schweizerische Mineralogische und Petrographische Mitteilungen* **78**, 243 - 255.

Curriculum Vitae
David van Acken

der digitalen Version der Dissertation liegt aus Datenschutzgründen kein Lebenslauf bei

for reasons of privacy protection, a CV is not included in the electronic version of the thesis

Danksagung

Viele Menschen haben zu dieser Dissertation beigetragen und mich in dieser Zeit unterstützt. An dieser Stelle möchte ich allen danken.

Meinen Eltern, für den Rückhalt und die Unterstützung während des Studiums und während der Promotionszeit.

Besonderer Dank gilt Prof. Dr. Harry Becker, der mir die Möglichkeit dieser Promotion gegeben hat, mich während der letzten Jahre immer mit Kritik und Anregungen unterstützt hat, und der bei Problemen stets ansprechbar war. Ich danke vor allem für die Möglichkeit, im Rahmen des Projektes Teile der Arbeit an der University of Maryland vorzubereiten, und für die vielen Konferenzen, an denen er mir eine Teilnahme ermöglichte. Ich habe in den letzten Jahren viel von ihm lernen dürfen.

Dr. Konrad Hammerschmidt danke ich für Hilfe und Troubleshooting in allen TIMS-Angelegenheiten, für ständige Ansprechbarkeit und Diskussionsbereitschaft, sowie für guten Rat und Anregungen in jeder Labor- und Lebenslage.

Dr. Frank Wombacher danke ich für Unterstützung, Diskussionen, Ermutigung und Katastrophenmanagement im ICP-MS-Labor.

Monika Feth danke ich für Unterstützung und Hilfe in Chemielabor und Massenspektrometerlabor, und natürlich für Unmengen an Kaffee, Tee, Keksen und Kuchen.

Prof. Dr. Mark Handy danke ich für Diskussionen während und nach dem Geländeaufenthalt bei Davos, währenddessen ich viel über die Geologie des Totalpmassivs und der angrenzenden Lithologien gelernt habe. Dr. Uwe Wiechert danke ich für Diskussionen und Anregungen.

Dr. Dorothee Mertmann, Dr. Ekkehard Scheuber, Dr. Christoph Dobmeier und Dr. Thomas Taute für die Unterstützung und Planung während der Lehrveranstaltungen zur 'Erde I'. Im selben Zuge gilt auch Dank den Tutoren Susanne Schneider, Christina von Nicolai, Daniel Rupp, Alja Schmidt und Felina Schütz, die mit mir zusammen die Studentenmassen mit dem Grundwissen der Geologie versorgt haben (hoffentlich).

Für die Anfertigung von Dünn- und Dickschliffen möchte ich Wolfgang Michaelis und Christiane Behr danken. Für die Wartung der Stahlbomben und (teilweise rabiate) Problembehebung im Umgang mit Ihnen danke ich Dietrich Lange und Achim Hess. Bei Computerproblemen jedweder Art standen Bernd Treczka und Martina Grundmann mit Hilfe zur Seite. Für die Hilfe bei den RFA-Analysen am GFZ Potsdam danke ich Dr. Rudolf Naumann und Andrea Gottsche. Weitere technische Unterstützung kam von Seiten von Dr. Ralf Milke (BSE-Scans) und Dr. Bernhard Pracejus (Auflichtmikroskopie). I also thank the late Dr. T.S. Brewer for providing S analyses for a batch of samples.

Big thanks go to all the people at the Department of Geology at the University of Maryland. During my two stays there, I learned a lot about mass spectrometry and geochemistry. Thanks to Rich Walker and Igor Puchtel for their support doing TIMS analysis, Bill McDonough and Richard Ash for their support with ICP-MS and LA-ICP-MS and Phil Piccoli for his help with the electron microprobe. Rich Walker and Bill McDonough provided valuable comments which significantly improved the manuscripts comprising this thesis. Thanks to Sandy Romeo and Dorothy Brown for their work in organizing my two stays at UMD. Thanks to Roberta Rudnick, Sonja Aulbach, Ralf Halama and Tetsuya Yokoyama for interesting discussions and to Dusty Aeiker, Rick Arevalo and Mario Luong for help with data processing with LAMTRACE. Thanks to all UMD geology grad students there for their kind support, help in the lab, whenever needed, and an introduction into American grad student life: Rick Arevalo, Nick Geboy, Jenise Honesto, Tom Ireland, Dave Johnston, Ryan Kerrigan, Adam Mansur, Michael Mengason, Barry Reno, Kate Scheiderich, and the rest of the crew.

Dank gilt auch meinen Mitdoktoranden des Institutes und Diplomanden und studentischen Hilfskräften der Arbeitsgruppe; für Diskussionen, Hilfe bei verschiedensten Labortätigkeiten

und viele sonstige Kleinigkeiten: Mario Fischer-Gödde, Susanne Schneider, Kristina Hippe, Florian Fußeis, Wiebke Bäro, Janine Lahr, Anika Schmidt, Christian Meyer und Corinna Wutzke.

Für die Unterstützung meiner Arbeit mit REE-Spurenelementdaten durch seine BSc-Arbeit danke ich Marc Weynell.

For discussions at various conferences, which clarified aspects of the work or improved its focus, I wish to thank G. Brügmann, L. Reisberg, T. Meisel, D.G. Pearson, A. Luguet, J.-P. Lorand, C.-Z. Liu, S.-J. Barnes, V. Le Roux, O. Müntener, P. Luffi and G. Manatschal.

Großer Dank gilt der Deutschen Mineralogischen Gesellschaft, die mir mit einem Reisestipendium die Präsentation eines Teils meiner Ergebnisse beim AGU Fall Meeting 2007 in San Francisco ermöglichte.